

THE STUDY OF CONSTITUTIVE RELATIONSHIPS OF MULTI-PHASE FLOW FOR
GEOLOGICAL CARBON SEQUESTRATION

by

Hiroko Mori

Copyright by Hiroko Mori 2013

All Rights Reserved

A thesis submitted to the Faculty and the Board of Trustees of the Colorado School of Mines in partial fulfillment of the requirement for the degree of Master of Science (Hydrology).

Golden, Colorado

Date _____

Signed: _____
Hiroko Mori

Signed: _____
Dr. Tissa H. Illangasekare
Thesis Advisor

Golden, Colorado

Date _____

Signed: _____
Dr. David A. Benson
Professor and Division Director
Hydrologic Science and Engineering

ABSTRACT

To develop effective strategies for safely storing CO₂ in deep geological formations, it is necessary to understand the fundamental processes that contribute to stable entrapment in naturally heterogeneous subsurface formations. However, controlled experiments to generate data at all scales of interest are not feasible, and it is challenging to use supercritical CO₂ (scCO₂) in laboratory settings. Therefore, numerical modeling will be an essential tool for properly characterizing the capillary trapping of scCO₂ in saline aquifers as well as improving the understanding of complex processes in multiphase flow systems.

To produce an effective numerical model to simulate scCO₂ behavior, it is essential to have reliable constitutive relationships such as the capillary pressure (P_c) – saturation (S_w) and relative permeability (k_r) – saturation (S_w) relationships. Although previous studies have used constitutive models to derive constitutive relationships, the accuracy of the constitutive models for various fluids and porous media remains uncertain. Therefore, this research project developed column experiments to derive constitutive relationships by using surrogate fluids instead of scCO₂ and brine and to investigate the applicability of the constitutive models. Having the surrogate fluids makes it more feasible and cost effective to run the experiments because they can be conducted at ambient conditions. Next, the results of an intermediate tank experiment conducted to explore trapping mechanisms of scCO₂ and a numerical simulation using TOUGH2 T2VOC, using the derived constitutive relationships, were compared to verify the applicability of the derived constitutive relationships. Establishing the applicability of surrogate fluids to both measure P_c – S_w and k_r – S_w relationships and producing accurate constitutive relationships will allow researchers to develop a greater understanding of the multiphase flow system and the trapping mechanisms of scCO₂ in saline aquifers.

Leverett scaling, the entry pressure scaling method, and the dielectric sensor method were used to obtain the P_c – S_w relationships. Both scaling methods use P_c – S_w relationships from an air/water system in which data was collected in previous studies. All three methods yielded similar curves for the P_c – S_w relationship. However, the entry pressure scaling method shows a slightly higher entry pressure value compared to other two methods. Moreover, the irreducible saturation and residual saturation for the Soltrol 220/ Glycerol – water mixture differed from the

air/water systems. Therefore, the study required measuring these two saturations independently from the scaling methods.

The long column method and the hydrostatic method were used to measure the k_r – S_w relationships. The experimentally obtained k_r – S_w relationships differed greatly from the constitutive model k_r – S_w relationships such as the van Genuchten – Mualem model. It can be concluded that the van Genuchten – Mualem model cannot be used for this test fluid and sand. Also, the result demonstrated that it is important to measure the k_r – S_w relationships independently from the constitutive models. Moreover, the results did not show any hysteresis behavior.

Lastly, the experimentally obtained constitutive relationships were applied to the numerical model to investigate the applicability of measured constitutive relationships and to examine the impact of constitutive relationships on the two-phase flow system. The simulation which used the experimentally obtained constitutive relationships better replicated the tank experiment compared to the one using the constitutive models without investigating the accuracy of its model. However, the numerical model could not reproduce the movement of the front of the plume because of the inappropriate entry pressure value. Overall, the study demonstrated the impact of the constitutive relationships on the two-phase flow system and the importance of having the applicable constitutive relationships to obtain a better numerical model.

TABLE OF CONTENTS

ABSTRACT.....	iii
TABLE OF CONTENTS.....	v
LIST OF FIGURES	viii
LIST OF TABLES	xi
ACKNOWLEDGEMENT	xiii
CHAPTER 1 – INTRODUCTION.....	1
1.1 Motivation.....	1
1.2 Problem description	4
1.3 Research objectives and goals	5
1.4 Thesis outline	6
CHAPTER 2 – LITERATURE REVIEW	8
2.1 The basic concepts of multiphase flow related to capillary trapping of CO ₂	8
2.1.1 Interfacial tension.....	8
2.1.2 The wetting and non-wetting phase	9
2.1.3 Capillary pressure	10
2.1.4 Darcy’s law	12
2.1.5 Relative permeability.....	13
2.2 Experimentally determined constitutive relationships.....	15
2.2.1 Experimental methods to derive the $P_c - S_w$ relationships.....	15
2.2.2 Experimental methods to derive the $k_r - S_w$ relationships.....	16
2.2.3 Scaling method of the $P_c - S_w$	16
2.3 Constitutive models	18
2.3.1 $P_c - S_w$ Models	19
2.3.2 $k_r - S_w$ Models.....	20

2.4 Impact of the quality of constitutive relationships on numerical models	22
2.5 Use of surrogate fluids	23
2.6 Numerical Models.....	23
2.7 Summary of literature reviews.....	24
2.8 Research Scope	24
2.8.1 Task 1: $P_c - S_w$ curve measurements	25
2.8.2 Task 2: $k_r - S_w$ curve measurement	26
2.8.3 Task3: Modeling	27
CHAPTER 3 – TEST MATERIALS.....	29
3.1 Selection of Surrogate Fluids.....	29
3.2 Selection of Test Sands.....	31
CHAPTER 4 – $P_c - S_w$ CURVE MEASUREMENT.....	34
4.1 Description of the $P_c - S_w$ measurement.....	34
4.1.1 Leverett scaling.....	34
4.1.2 Entry Pressure Scaling Method.....	35
4.1.3 Dielectric Sensor Method	37
4.2 Experimental results of the $P_c - S_w$ relationship.....	40
4.2.1 Leverett Scaling results.....	41
4.2.2 Entry pressure scaling results.....	42
4.2.3 Dielectric sensor results	44
4.2.4 Discussion of the $P_c - S_w$ relationships obtained with different methods.....	46
CHAPTER 5 – DETERMINATION OF $K_R - S_w$ RELATIONSHIPS.....	49
5.1 Description of $k_r - S_w$ measurement.....	49
5.1.1 The van-Genuchten – Mualem Model	49
5.1.2 The Long Column Method.....	50

5.1.3 Hydrostatic Method	52
5.2 The results of the $k_r - S_w$ relationship	56
5.2.1 The results of the long column method.....	57
5.2.2 The result of the hydrostatic method	58
5.2.3 Discussion of the $k_r - S_w$ relationship derived from two different methods.....	60
CHAPTER 6 – MODELING	63
6.1 The constitutive relationships in TOUGH2 T2VOC	63
6.2 Tank experiment	65
6.2.1 Design of intermediate tank experiment	65
6.2.2 Numerical modeling of intermediate tank experiment	67
6.3 Modeling results and discussions.....	70
6.3.1 Result of steady state condition	70
6.3.2 The simulation results of Soltrol 220 injection.....	71
CHAPTER 7 – CONCLUSIONS AND RECOMMENDATIONS	77
7.1 Summary	77
7.2 Findings of the applicability of the constitutive relationships	78
7.3 Findings of the constitutive relationships impacts on the two-phase flow system.....	81
7.4 Contribution to the onsite investigations	81
7.5 Recommendation to the future study	82
CHAPTER 8 – REFERENCES	83
APPENDIX A – The result of Capillary pressure for all sands.....	89
APPENDIX B – The results of relative permeability test	94
APPENDIX C – The comparison of the contour maps	96

LIST OF FIGURES

Figure 1.1	Time scale of CO ₂ trapping in a saline aquifer [<i>Metz et al.</i> , 2005]	2
Figure 2.1	Comparison between water wet and oil wet system [<i>Crain</i> , 2013].....	9
Figure 2.2	Capillary Pressure- Saturation Curve	10
Figure 2.3	Capillary Trapping [<i>Juanes et al.</i> 2006].....	11
Figure 2.4	Relative Permeability	14
Figure 2.5	Comparison between the van Genuchten model and the Brooks and Corey model [<i>Kosugi</i> , 2007].....	20
Figure 3.1	Comparisons of the numerical simulations for the scCO ₂ /brine and Soltrol 220/Glycerol-water system	32
Figure 4.1	CENCO-DuNOüY TENSIOMETER.....	35
Figure 4.2	Entry Pressure Method	37
Figure 4.3	Calibration of sensor.....	39
Figure 4.4	Experimental setup of dielectric sensor method.....	40
Figure 4.5	Methodology to calculate the capillary pressure	40
Figure 4.6	α -mixing model compared with the experimental data	45
Figure 5.1	Experimental setup of Long Column Experiment.....	51
Figure 5.2	Hydrostatic Method.....	54
Figure 5.3	Comparison of the relative permeability for Glycerol-water mixture of 8:2 and 5:5 for Accusand #30/40.....	59
Figure 5.4	The non-wetting phase relative permeability for Accusand #30/40.....	60
Figure 5.5	Comparison between the relative permeability data of Soltrol 220/Glycerol-water and liquid CO ₂ /brine systems.....	61
Figure 6.1	Comparison between fittedcurve and van Genuchten – Mualem model.....	64
Figure 6.2	Design of the tank [<i>Trevisan et al.</i> , 2013]	66
Figure 6.3	Saturation points taken from X-ray system [<i>Trevisan et al.</i> , 2013]	66

Figure 6.4	Schematic of the tank	67
Figure 6.5	Extent of tank	68
Figure 6.6	Steady state conditions	70
Figure 6.7	Representative saturation points of X-ray system.....	71
Figure 6.8	Result of saturation point A.....	73
Figure 6.9	Result of saturation point B.....	73
Figure 6.10	Result of saturation point C.....	74
Figure 6.11	Result of saturation point D.....	74
Figure 6.12	Result of saturation point E.....	75
Figure 6.13	Cumulative mass of Soltrol 220	75
Figure A.1	Accusand #12/20	89
Figure A.2	Accusand #20/30	90
Figure A.3	Accusand #30/40	91
Figure A.4	Accusand #40/50	92
Figure A.5	Accusand #50/70	93
Figure B.1	Relative permeability of Accusand #40/50.....	94
Figure B.2	Relative permeability of Accusand #50/70.....	95
Figure C.1	0.2 hour from injection	96
Figure C.2	0.45 hour from injection	97
Figure C.3	0.77 hour from injection	98
Figure C.4	1.03 hour from injection	99
Figure C.5	1.30 hour from injection	100
Figure C.6	1.55 hour from injection	101
Figure C.7	1.95 hour from injection	102
Figure C.8	2.33 hour from injection	103

Figure C.9	2.66 hour from injection	104
Figure C.10	3.18 hour from injection	105
Figure C.11	3.56 hour from injection	106
Figure C.12	4.13 hour from injection	107

LIST OF TABLES

Table 1.1	Current and planned large-scale CO ₂ injection projects [<i>Friedmann, 2013</i>].....	3
Table 2.1	Permeability Models	21
Table 3.1	Dimensionless numbers of the scCO ₂ and brine system under typical reservoir conditions [<i>Nordbotten et al., 2005</i>]	30
Table 3.2	Comparison between fluid properties of surrogate fluids system and scCO ₂ -brine system [<i>Schroth et al., 1995; Nordbotten et al., 2005; Cheng, 2008</i>]	30
Table 3.3	van Genuchten model parameters for water and air fitted by <i>Smits and Limsuwat</i> [2009]	33
Table 3.4	Hydraulic Properties of Accusands by <i>Schroth et al.</i> [1998], and <i>Smits and Limsuwat</i> [2009]	33
Table 4.1	Interfacial Tensions	42
Table 4.2	Summary of results obtained with entry pressure scaling method.....	43
Table 4.3	The difference between entry pressure measurement from out mass and visual determination.....	44
Table 4.4	Comparison of S_i and S_r value between air/water and Soltrol 220/Glycerol-water system.....	45
Table 4.5	Fitted van Genuchten parameters for the P_c - S_w relationships for the Soltrol 220/Glycerol-water mixture system.....	47
Table 4.6	Fitted van Genuchten parameters for the P_c - S_w relationships for the Soltrol 220/Glycerol-water mixture system by using the residual/irreducible saturation obtained from the air/water system	48
Table 5.1	Properties of Glycerol-water mixture.....	56
Table 5.2	Capillary number.....	56

Table 6.1 Material parameters for the model69

ACKNOWLEDGMENTS

The present study on ‘The study of constitutive relationships of multi-phase flow for geological carbon sequestration’ was accomplished during my master courses at Center for Experimental Study of Subsurface Environmental Processes (CESEP), Colorado School of Mines. I would like to thank all those who have helped me with this study.

I would like to express my sincere gratitude to my supervisor, Professor Tissa H. Illangasekare for providing me this precious study opportunity as a Master student in his laboratory and great help towards the successful completion of this study.

I also would like to express my deepest appreciation to my committee members, Professor Kathleen M. Smits and Professor Yu-Shu Wu, and my non-voting committee members Dr. Toshihiro Sakaki, and Dr. Abdullah Cihan for their elaborated guidance, considerable encouragement and invaluable discussion that make my research of great achievement and my study life unforgettable. Special thanks to Toshihiro Sakaki for continuous guidance on lab experiments and thesis writing.

Also, I received generous support from my lab mates, Ariel Esposito, Elif Agartan, Luca Trevisan, and Michael Plampin. Especially, I would like to give special thanks to Luca Trevisan for giving me many suggestions and collaborative work with my thesis.

I am very grateful to the National Science Foundation, Department of Energy, and Japan Student Services Organization for making my Master’s study possible by the financial support.

I also thank Yi Xiong for providing me great support with TOUGH2 T2VOC model and Ryan D. Hort for helping me to revise my thesis.

Finally I would like to extend my indebtedness to my family and friends for their endless love, understanding, support, and encouragement throughout my study.

CHAPTER 1 – INTRODUCTION

This chapter provides the general description of the carbon sequestration problem and the motivation for the project, and research goals. In addition, the outline to the thesis is given.

1.1 Motivation

Many studies have linked the production of carbon dioxide (CO₂) from fossil fuel combustion to changes in the Earth's climate [*Benson and Surles, 2006*]. The Intergovernmental Panel on Climate Change (IPCC) has suggested that by the beginning of the next century, the Earth's temperature could rise approximately 1.1– 6.4 °C [*IPCC, 2007*] due to the combustion of fossil fuels.

The IPCC suggested that Geological Carbon Sequestration and Storage (GCSS) is a promising large-scale carbon mitigation strategy for long and midterm CO₂ storage [*IPCC, 2005*]. In GCSS, CO₂ is captured from the flue gas of thermal power plants or large industries. The captured CO₂ is concentrated and converted into supercritical fluid [*Benson and Surles, 2006; Elliot and Celia, 2012*]. Supercritical CO₂ (scCO₂) is then injected into saline aquifers or depleted oil and gas reservoirs under impermeable cap rocks to prevent the leakage of CO₂ [*Juanes et al., 2006*]. *Bachu et al.* [1994] reported that saline aquifers are the best site for disposal of CO₂ because of their availability in the proximity of thermal power plants or large industries which generate CO₂, and their ability to dissolve CO₂ so that it could be stored almost indefinitely. Moreover, the potential storage capacity in saline aquifers in the United States is estimated to be in the range of 1,700 – 20,000 Gt of CO₂, while depleted oil and gas reservoirs are also good disposal sites for CO₂; however, the capacity is about 316 Gt of CO₂ which is limited compared to saline aquifers [*Benson and Surles, 2006; Plasynski, 2011; Elliot and Celia, 2012*].

Typically, CO₂ is stored at about 800 meters deep in a supercritical state which is above the critical point. In CO₂, the critical point occurs at the critical temperature of 31.1°C, and the critical pressure of 7.38 MPa. Beyond the critical point, CO₂ has a higher density compared to the gaseous state and has a lower density and a lower viscosity than brine [*Doughty and Pruess, 2004; Bachu and Bennion, 2008*]. Generally, four mechanisms of trapping that contributes to

sequestration are identified: capillary trapping (residual trapping), dissolution, mineralization and structural trapping [Flett *et al.*, 2004; Kumar *et al.*, 2005; Juanes *et al.*, 2006]. The structural trapping and the capillary trapping are the first trapping mechanisms to occur after injecting liquid scCO₂. Storing the scCO₂ underneath the thick impermeable layer of rock, which prevents the leakage of scCO₂ from sequestration reservoirs, is called the structural trapping [Benson and Cole, 2008]. Capillary trapping occurs after injection stops and the brine starts to move into the pores within the plume of scCO₂. The scCO₂ becomes residual at the tail of the plume and gets immobilized in formations [Benson and Cole, 2008]. Capillary trapping has more benefits over structural trapping, such as higher security for storage and enhancements of the dissolution and mineralization processes, as the scCO₂ stays in the pore [Wildenschild *et al.*, 2011]. The second process is the dissolution process when the scCO₂, which has been trapped inside the pores grain, starts to dissolve in brine. The last process is mineralization during which the dissolved scCO₂ starts to react with the rocks and makes carbonated minerals. Both the dissolution and mineralization steps require a few hundred ~ a few thousand years of time scales to occur.

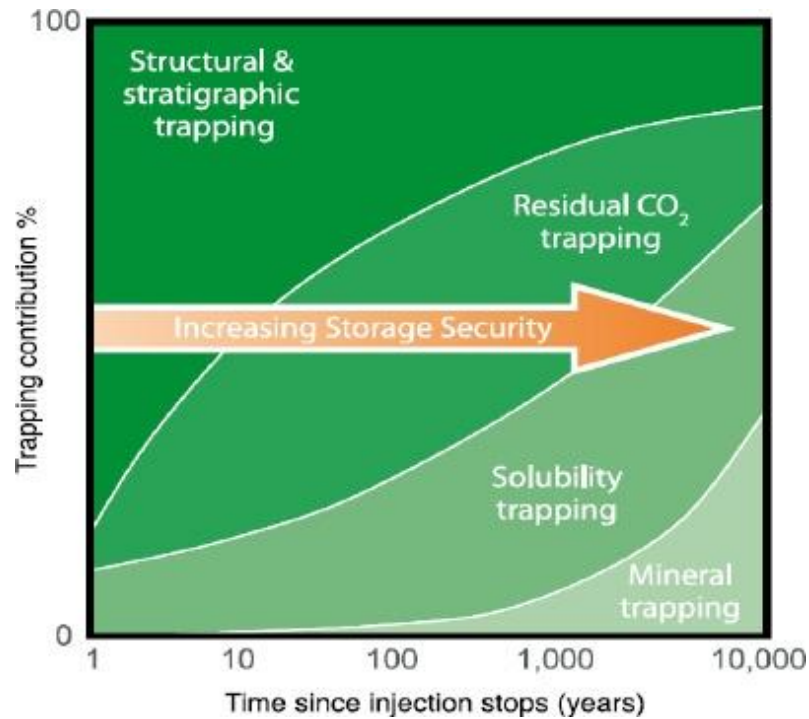


Figure 1.1 Time scale of CO₂ trapping in a saline aquifer [Metz *et al.*, 2005]

Several studies have been reported on site investigations of the effectiveness of scCO₂ trapping by injecting scCO₂ into saline aquifers [Torp and Gail, 2003; Chadwick *et al.*, 2012].

One of the well known GCSS sites is Sleipner in the North Sea. Sleipner site has been established as the first commercial application of a CO₂ storage, and nearly 14 Mt of CO₂ have been injected in deep saline aquifers since 1996 [Chadwick *et al.*, 2012]. The results from the site indicated that GCSS has high potential to mitigate the greenhouse effect. Also, several methods to monitor the behavior of injected CO₂ were developed at this site [Torp and Gail, 2003; Chadwick *et al.*, 2012]. The other well known large-scale injection sites are Weyburn in Canada, In Salah in Algeria. Also, there are many planned injection sites and Table 1.1 shows the list of the current and pending large-scale CO₂ injection projects [Friedmann, 2013].

Table 1.1 Current and planned large-scale CO₂ injection projects [Friedmann, 2013]

Site	Location	Reservoir class	Start date
Sleipner	Norway	Saline Fm.	1996
Weyburn	Canada	EOR	2000
In Salah	Algeria	Sandstone	2004
Snohvit	Norway	Saline Fm.	2008
Cranfield	USA	Saline Fm. And EOR	2009
FutureGen 2.0	USA	Saline Fm.	2016
ZeroGen	Australia	EOR	2018
GreenGen	China	EOR	2015
HECA	USA	EOR	2016
Gorgon	Australia	Saline Fm.	2013
SaskPower Boundary Dam	Canada	EOR	2016
Hauneng Shidongkou	China	Saline Fm.	2016
Shenhua DCL/Majiata	China	Saline Fm.	2013
Archer-Daniels Midland	USA	Saline Fm.	2013
TCEP	USA	EOR	2017

The on-site investigations helped to understand the scCO₂ and brine system. Also, having the knowledge of this two-phase flow behavior will help to characterize, to model and to acquire the knowledge of the effective storage mechanisms of CO₂.

1.2 Problem description

Despite a broad range of studies on GCSS, many uncertainties still remain on the effectiveness of trapping mechanisms to control CO₂ storage [*Schnaar and Diguilio, 2009*]. Some insights can be gained from field investigations, although the heterogeneity of the aquifer formations is complex and limits the understanding of all the factors that contribute to effectiveness of carbon sequestration. In order to advance our understanding of scCO₂ behavior in saline aquifers, it is necessary to understand the fundamental processes that contribute to stable entrapment in naturally heterogeneous subsurface formations. Therefore, it is essential to understand and capture the complex multiphase flow behavior of scCO₂ in brine formations in models that can be used in site-specific analysis.

Understanding the two-phase flow behavior of scCO₂ and brine is necessary for the study of effective trapping mechanisms of CO₂. Various studies have suggested that constitutive relationships may be the most important parameters characterizing the behavior of multiphase flow systems [*Doughty and Pruess, 2004; Flett et al., 2004; Juanes et al., 2006*]. Constitutive relationships are the intrinsic relationships between two parameters relating to a particular system. In this case, the system is the two-phase flow of scCO₂ and brine in the formation. There are various constitutive relationships in the study of the multi-phase flow and this project mainly focuses on the relationships between capillary pressure (P_c) and saturation (S_w) and the relationships between the relative permeability (k_r) and saturation (S_w). However, for two-phase flow system of scCO₂ and brine, it is difficult to develop these relationships in ambient laboratory settings because of the high pressures required to maintain CO₂ in a liquid supercritical state. Moreover, some studies [*Klute and Dirksen, 1986; Dane et al., 1992; Demond and Roberts, 1993*] indicated that experimental methods to derive constitutive relationships of the $k_r - S_w$ are not well replicated and the measurement ranges are restricted by constraints of laboratory experimental settings such as pressure, temperature, and scale.

Due to the difficulty of measuring the $k_r - S_w$ relationship, many researchers have predicted the $k_r - S_w$ relationships from the constitutive models such as Brooks and Corey – Burdine [*Burdine, 1953; Brooks and Corey, 1964*] and van Genuchten – Mualem [*Mualem, 1976; van Genuchten, 1980*] models. The constitutive models are the empirically derived equations which describe the constitutive relationships. They are used not only to define the $k_r -$

S_w relationships but also are used to define the $P_c - S_w$ relationship such as van Genuchten [van Genuchten, 1980] and Brooks and Corey [Brooks and Corey, 1964] models. To define the $k_r - S_w$ relationships, the van Genuchten or Brooks and Corey models are fitted to experimental data of the $P_c - S_w$ relationships [Burdine, 1953; Brooks and Corey, 1964; Mualem, 1976; van Genuchten, 1980]. The advantages of using constitutive models to derive the $k_r - S_w$ relationship are that they can be used to estimate $k_r - S_w$ relationships without direct experimental measurement [Chen et al., 1999]. However, the applicability of these constitutive models is still uncertain because of the simplifying assumptions that are used to obtain models like Mualem [1976] and Burdine [1953] models. Some studies [Fischer and Celia, 1999; Tuller and Or, 2002; Abdullah et al., 2009] suggested that these constitutive models oversimplify the geometries of the pore and it would result in discrepancies between the $k_r - S_w$ relationships derived from the constitutive models and the experimental data. Thus, evaluating the adequacy of these constitutive models in different circumstances using accurate experimental data is critical for better understanding the multiphase flow system and trapping mechanisms of $scCO_2$ in saline aquifers [Chen et al., 1999].

1.3 Research objectives and goals

For a reliable numerical model simulation of $scCO_2$ behavior, it is essential to have reliable $P_c - S_w$ and $k_r - S_w$ relationships [Ostrom and Lenhard, 1998; Dane et al., 1998; Doughty and Pruess, 2004; Flett et al., 2004; Juanes et al., 2006; Liu et al., 2010]. Therefore, the goal of the research presented in this thesis is to develop method to obtain accurate constitutive relationships for $scCO_2$ and brine systems in deep geologic sequestration. Having accurate constitutive relationships will increase the quality of numerical modeling for simulating the $scCO_2$ behavior in saline aquifers. Previous studies [Dane et al., 1998; Chen et al., 1999; Flett et al., 2004; Juanes et al., 2006] used the constitutive models to characterize $P_c - S_w$ and $k_r - S_w$ relationships or to derive these relationships experimentally. Mainly, this project aims to improve the ability to model $scCO_2$ and brine systems using the reliable constitutive relationships.

One practical way to obtain constitutive relationships for simulating $scCO_2$ behavior is to use surrogate fluids in place of $scCO_2$ to avoid laboratory test conditions that require high pressures to keep the CO_2 in supercritical liquid state. Studies of Shook et al. [1992] and Gharbi

et al. [1998] indicated that the dimensionless numbers could be used to evaluate the performance of immiscible flow systems for different reservoir conditions, and properties of the fluids [Garmeh and Johns, 2010]. Fluid pairs for laboratory test under ambient conditions were selected in a way to have same dimensionless numbers as for actual reservoir conditions. This research uses these selected surrogate fluids to obtain the $P_c - S_w$ and $k_r - S_w$ relationships experimentally at ambient conditions. Using this approach, experiments can be conducted using surrogate fluids at ambient conditions yet still capturing scCO₂ behavior in deep formations. The advantages of using surrogate fluids are that it can simplify the experimental setups and significantly reduce cost by not requiring high pressure settings. To achieve this research goal, this project focuses on the following objectives by conducting the experiments with these selected surrogate fluids.

1. Measure the $P_c - S_w$ and $k_r - S_w$ relationships separately and include hysteresis behavior.
2. Compare the experimentally obtained $k_r - S_w$ relationships with van Genuchten – Mualem model to investigate its applicability for the test sand and fluids.
3. Apply the experimentally determined and constitutive models based $k_r - S_w$ relationships in a multiphase model to predict the movement of a multiphase plume recorded in a tank experiment. The comparison will suggest which approach is more accurate.

The intent of this study is to validate the constitutive relationships for the numerical models which simulate the trapping mechanisms of scCO₂. Also, the study includes evaluating the applicability of constitutive relationships measured in test sands and fluids to the properties of actual scCO₂/brine systems. Establishing the applicability of surrogate fluid for measuring these $P_c - S_w$ and $k_r - S_w$ relationships and producing relevant constitutive relationships will allow researchers to develop a greater understanding of the multiphase flow properties and trapping mechanisms of scCO₂ in saline aquifers.

1.4 Thesis outline

This thesis consists of seven chapters and three appendices. Introduction to the problem along with the motivation of the study and the research objectives are provided in Chapter 1.

Literature reviews of the concepts of multiphase flow, two-phase constitutive relationships, and the application of the constitutive relationships to the numerical models are presented in Chapter 2. This review with identification of the research tasks that need to meet the goals of this study. Chapter 3 presents the materials and the discussion of using surrogate fluids. Chapter 4 and 5 discuss the experimental methods and the results of constitutive relationships derived from the constitutive models and experiments for both $P_c - S_w$ and $k_r - S_w$ relationships. Chapter 6 shows the design of numerical model along with comparisons between the numerical model results and the actual experimental results of the tank experiments [Trevisan *et al.*, 2013]. The last chapter 7 gives the conclusions of this project and the suggestions for future work. Appendix A presents the experimental results of the $P_c - S_w$ results of 5 different Accusands and the Appendix B presents the experimental results of the $k_r - S_w$ relationships of 3 different Accusands. Appendix C shows the pictures of the tank experiments.

CHAPTER 2 – LITERATURE REVIEW

Chapter 1 provided the introduction of this research project and objectives of this study. This chapter reviews past studies of the two-phase flow constitutive models and the experimental methods to derive constitutive relationships. This chapter also includes how the constitutive relationships will affect the reliability of numerical models. In addition, the theory of the multi-phase flow of carbon sequestration is reviewed.

2.1 The basic concepts of multiphase flow related to capillary trapping of CO₂

Coal beds, oil/gas reservoir, and saline aquifers are major storage sites for geological carbon sequestration. Especially, saline aquifers have more advantages compared to other sites because of high storage capacity, accessibility to the generator of the CO₂, and long retention periods [Benson and Surlles, 2006]. Therefore, this literature review focuses on understanding multi-phase flow system of the geological carbon sequestration in saline aquifers that are fully saturated with brine. Understanding the basic physical concepts of multiphase flow is important for analyzing the two-phase system of scCO₂ and brine. Mostly, this section reviews basic concepts of two-phase immiscible flows which relates to the capillary trapping of scCO₂.

2.1.1 Interfacial tension

Fetter [1999] described the interfacial tension as “the amount of work necessary to separate a unit area of one substance from another”. The water-wet and the oil-wet system are defined by the contact angle θ between the wetting fluid and the grain surface. From Young’s [1805] equation, the contact angle is the term of the balance force between three phases and it can be written as follows:

$$\cos \theta = \frac{\sigma_{gs} - \sigma_{ls}}{\sigma_{lg}} \quad (2.1)$$

The three interfacial force σ [M L/T²] described in equation (2.1) are gas-solid σ_{gs} , liquid-solid σ_{ls} , and liquid-gas σ_{lg} . When the contact angle between the wetting phase and the sand grain is less than 90°, it is called the water-wet system, while, in the oil wet system, the contact

angle is over 90° [Fetter, 1999]; see Figure 2.1 for the diagram of the contact angle between the water-wet and oil-wet system.

In the case for carbon sequestration, there are three components with two phases: scCO_2 , brine (aqueous phases) and solid substrate (solid phase). Previous studies have noted that the interfacial tensions in CO_2 /brine/rock minerals systems changes with pressure and temperature [Chalbaud *et al.*, 2009; Espizona and Santamarina, 2010]. Interfacial forces between the brine and scCO_2 , and the scCO_2 and rock mineral are sensitive to the temperature and pressure changes [Espizona and Santamarina, 2010]. Also, the study of Chalbaud *et al.* [2009] determined that the salinity of the brine affects the interfacial tensions between the brine and scCO_2 while, the interfacial tensions between the rock mineral and the brine are stable with pressure changes [Espizona and Santamarina, 2010].

2.1.2 The wetting and non-wetting phase

There are two possible sub-surface conditions applicable to two-phase flow, oil-wet and water-wet. Fig 2.1 shows schematic water-wet and oil-wet system [Crain, 2013]. Fetter [1999] provided definitions for wetting and non-wetting systems. The wetting fluids coat the surface of the grain whereas the non-wetting fluids have the lowest adhesive attraction to the solid surface. Naturally, the aquifer is water-wet because the primary condition of the formation is fully saturated with brine or water; therefore, for the carbon sequestration problem, the scCO_2 is considered to be the non-wetting phase and brine to be the wetting phase.

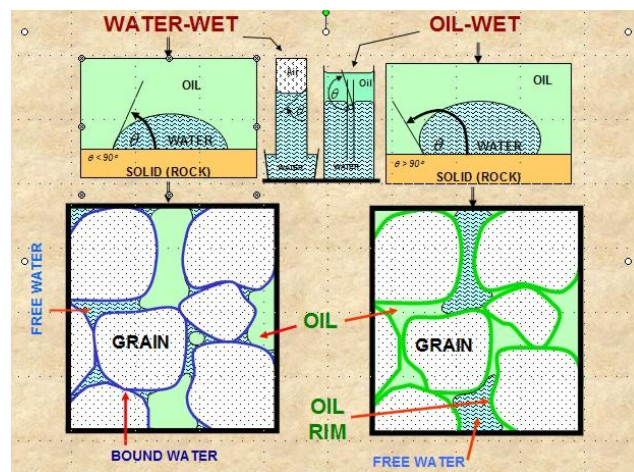


Figure 2.1 Comparison between water wet and oil wet system [Crain, 2013]

When scCO_2 is injected to the saline aquifer, in the earlier stage of placement the liquid scCO_2 is immiscible to the brine. The scCO_2 is less dense than water so it flows on top of the aquifer [Juanes *et al.* 2006]. Immiscible or partially miscible fluids that stay as a separate phase and are lighter than water are referred to as light non-aqueous phase liquids (LNAPLs) while, non-aqueous phase fluids that with densities greater than water is called a dense non-aqueous phase liquids (DNAPLs). The scCO_2 in the presence of brine behaves as a LNAPL.

2.1.3 Capillary pressure

The differences between the pressure of the non-wetting phase P_{nw} and the wetting phase P_w is called the capillary pressure P_c and it can be define as following equation:

$$P_c = (P_{nw} - P_w) \quad (2.2)$$

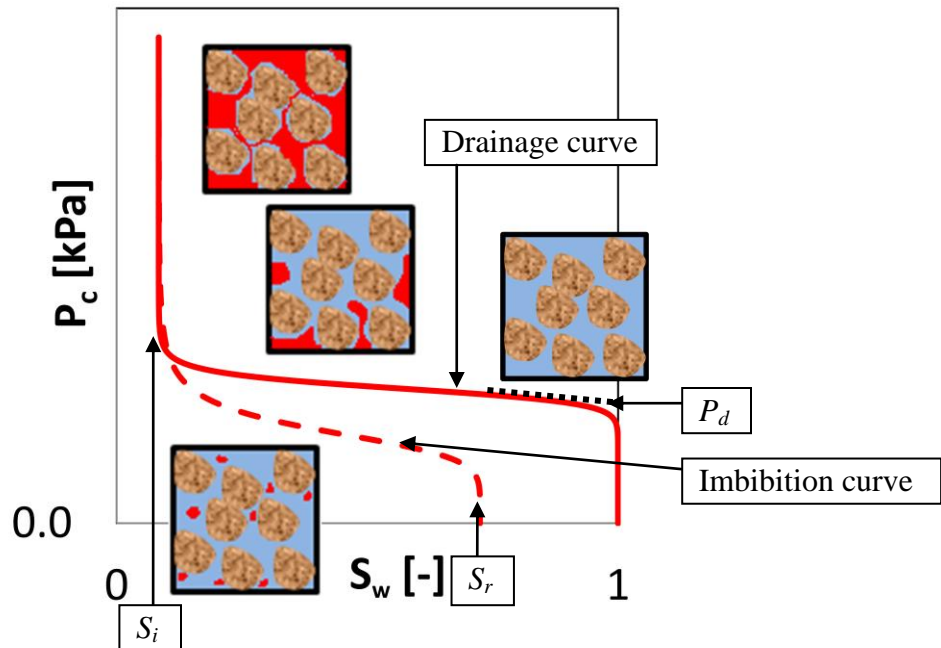


Figure 2.2 Capillary Pressure- Saturation Curve

In the porous medium, the capillary pressure is a function of saturation as shown in Figure 2.2. Before injecting the non-wetting phase, a domain is fully saturated with the wetting phase; therefore, the saturation of the wetting phase is 1.0. During the injection of the non-wetting phase, the wetting phase is slowly displaced by the non-wetting phase and the saturation of the wetting phase decreases. At the same time, the P_c starts to increase. This process is referred to drainage

and the line on the plot of capillary pressure vs. saturation given in Figure 2.2 is called the drainage curve. At the end of the drainage cycle, the saturation of the wetting phase reaches the irreducible wetting fluid saturation (S_i). The saturation of the wetting phase cannot be reduced lower than S_i due to the trapped wetting fluid inside the pore. The S_i is difficult to measure experimentally so often this S_i is selected as the saturation at the maximum P_c which the experimental system is able to reach. The difficulty in measuring the S_i value is a result of when the capillary pressure increases with the decrease of wetting fluid saturation by a very small amount, it never reaches a steady saturation value. Other important parameter associated with drainage is the entry pressure (P_d). The P_d is the capillary pressure at the non-wetting phase starts to enter the soil pores displacing the wetting phase. After the capillary pressure builds up to P_d , the saturation starts to decrease from the initial saturation of 1.0.

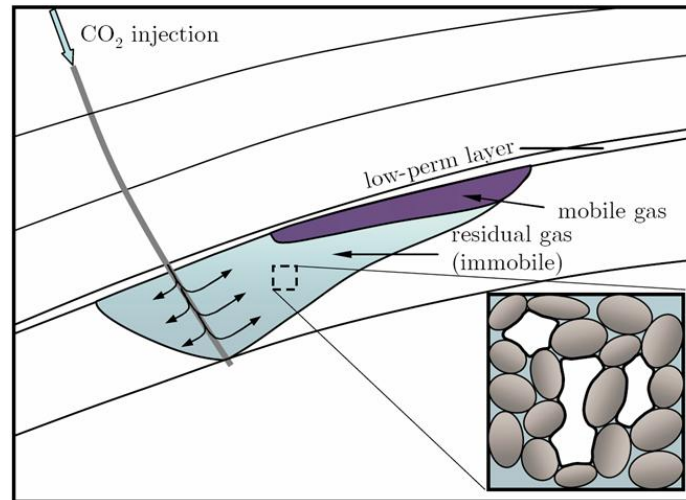


Figure 2.3 Capillary Trapping [Juanes et al. 2006]

The capillary trapping mechanisms of the non-wetting fluid in a two-phase system can be described from the drainage and imbibition curves. In the case of scCO₂ – brine system, when scCO₂ is injected through a well into the saline formation overlain by an impermeable cap-rock. Before the injection, the formation is fully saturated with brine. The scCO₂ moves laterally away from the well due to the pressure gradient created by the injection. The buoyancy force makes the scCO₂ migrates upwards. Consequently, scCO₂ begins to accumulate underneath of impermeable cap rock and slowly migrates under the cap rocks. While the scCO₂ plume migrates along with the groundwater, the drainage and imbibitions processes occur simultaneously. Drainage occurs at the front of scCO₂ plume when it imbibes the saline aquifer and reduces the

wetting fluid saturation. Also, some of the brine remains in the formation in an irreducible state. Whereas the imbibitions process happens at the tale of scCO₂ plume while scCO₂ drains and brine imbibes and traps some of the scCO₂ at residu al saturation (S_r). This is due to the capillary forces and the amount of trapped scCO₂ is highly dependent on the pore geometry [Friedmann, 2013]. This is the basic mechanisms of how the scCO₂ is trapped inside of the pore [Fetter, 1999; Flett et al., 2004]. From the studies of Krevor et al. [2012], Juanes et al. [2006] and Hesse et al. [2008] proposed that large amount of CO₂ can be stored in the formation by capillary trapping.

2.1.4 Darcy's law

The Darcy's law [Darcy, 1856] is based on the Poiseuille's equation that it assumes the porous media is made from the bundle of channels which has different radius.

The following equation is defined as Darcy's law:

$$q = -K_s \frac{dh}{dl} \quad (2.3)$$

where, q is the velocity of the fluid [L/T] $\frac{dh}{dl}$ is the head gradient [-] and K_s is the saturated hydraulic conductivity [L/T].

The Poiseuille's equation is derived from Navier-Stokes equation thus the Darcy's law is based on the assumptions that the fluid is continuous and incompressible. This equation can be extended for the two-phase flow system. The following equation shows extensions of Darcy's law for the wetting phase flow in the presence of the non-wetting fluid.

$$q_w = - \frac{k_{rw} k_i \rho_w}{\mu_w} \frac{dh_w}{dl} \quad (2.4)$$

Where, k_r is the relative permeability [-], k_i is the intrinsic permeability [L²], ρ is the density [M/L³] and μ is the viscosity [M/T/L]. The subscript w refers to the wetting fluid.

Also, Darcy's law for the non-wetting phase flow in the presence of the wetting fluids can be expressed as

$$q_{nw} = - \frac{k_{rnw} k_i \rho_{nw}}{\mu_{nw}} \frac{dh_{nw}}{dl} \quad (2.5)$$

where the subscript nw refers to the non-wetting fluid.

From equation (2.4) and (2.5), the unsaturated hydraulic conductivity of the wetting and the non-wetting fluid can be written as

$$K(S_w) = \frac{k_{rw}k_i\rho_w}{\mu_w} = k_{rw}K_{sw} \quad (2.6)$$

$$K(S_{nw}) = \frac{k_{rnw}k_i\rho_{nw}}{\mu_{nw}} = k_{rnw}K_{snw} \quad (2.7)$$

2.1.5 Relative permeability

The permeability is influenced by several factors such as the effective porosity, pore size, structure, pore-size distribution, isotropy, and effective saturation. Assume that the media is isotropic and the pore geometry is consistent, the only factor which can change the permeability of the fluid is the effective saturation [Corey, 1994]. Changes in the effective saturation will reduce or raise the volumetric flow of the particular fluid per unit total area which is perpendicular to the fluid flow [Oliveira and Demond, 2003].

The definition of relative permeability is the ratio of intrinsic permeability at given saturation $k_i(S_w)$ and the intrinsic permeability of the porous media k_i . The following equation defines the relative permeability for the wetting phase:

$$k_{rw} = \frac{k_i(S_w)}{k_i} \quad (2.8)$$

Also, it can be expressed as the effective permeability at given saturation $K(S_w)$ to the absolute permeability of the fluid at fully saturated condition K_S :

$$k_{rw} = \frac{K(S_w)}{K_S} \quad (2.9)$$

Figure 2.4 shows the typical relative permeability curves. During the drainage process, the relative permeability value of the wetting phase becomes 0 at the irreducible saturation while the non-wetting phase becomes close to 1.0. In this condition, only the non-wetting phase can flow in the porous media. During the imbibitions process, the relative permeability value of the non-wetting phase becomes 0 at the residual saturation and the wetting phase increases close to 1.0.

However, the small volume of non-wetting fluid is remained inside of the pore as the residual state due to the capillary forces; therefore, the saturation of the wetting phase does not reach to 1.0. At the residual saturation, only the wetting phase can flow [Fetter, 1999]. The equations (2.8) and (2.9) are also applicable to the non-wetting phase.

The general trends were found regards to the relative permeability curve for hydrocarbon/water systems [Carig, 1971; Lake, 1989; Dullien, 1992; Krevor et al. 2012]. Krevor et al. [2012] suggested that capillary number $N_c = \frac{v\mu}{\sigma}$ which has larger value than 10^{-6} has the impact on the relative permeability curves. Usually, the capillary number for the carbon sequestration is $N_c \ll 10^{-6}$; therefore, the viscosity and capillarity does not have any effects on the relative permeability in this case.

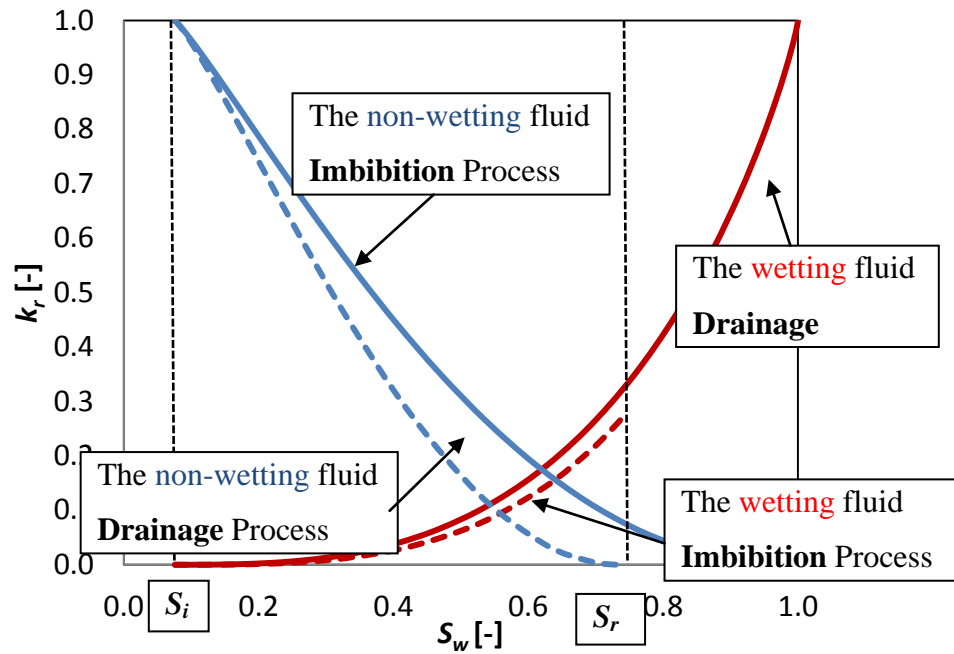


Figure 2.4 Relative Permeability

Relative permeability is a function of the saturation of the fluid, porous medium, temperature and interfacial tension, and capillary number [Bennion and Bachu, 2006; Shen et al., 2006]. Shen et al. [2006] have studied relative permeability with change in interfacial tensions and found relative permeability curves is susceptible to the difference in interfacial tensions. Also, the study by Nakornthap and Evans [1986] proved that there are relationships between the temperature and the relative permeability. Commonly the typical reservoir condition of carbon

sequestration, the capillary number is below 10^{-6} ; therefore, often the changes in capillary numbers do not have an effect on the relative permeability as demonstrated by *Krevor et al.* [2012].

2.2 Experimentally determined constitutive relationships

Reliable constitutive relationships are an important factor to understand the behavior of two-phase flow system [*Dane et al.*, 1998]. Especially, the constitutive models for the relative permeability and saturation relationships have many advantages compared to experimental methods to derive $k_r - S_w$ relationships. Often these models predict the $k_r - S_w$ relationships by fitting the constitutive models of $P_c - S_w$ relationships to experimentally derived $P_c - S_w$ data. However, the reliability of $k_r - S_w$ constitutive relationships is sometimes uncertain [*Demand and Roberts*, 1993; *Dane et al.*, 1998]. Therefore, in some cases, it is essential to compare $k_r - S_w$ constitutive models with experimental data to examine the accuracy of each model [*Chen et al.*, 1999].

2.2.1 Experimental methods to derive the $P_c - S_w$ relationships

Chen et al. [1999] developed a multi-step outflow method combined with the constitutive models for characterizing the capillary pressure-saturation relationship for air-water, oil-water, and air-oil systems. They evaluated the results with seven different constitutive models for two different core samples. The $P_c - S_w$ relationships from the constitutive models and the experimental method were compared. From the analysis, they concluded that van Genuchten-Mualem, Lognormal distribution-Mualem, Brutsaert-Burdine, and Gardner-Mualem models successfully described experimental data. Although they contributed to understanding the accuracy of each model, they neglected hysteresis in their analysis and limited the applicability of their analysis to multi-phase flow.

Krevor et al. [2012] measured the capillary pressure of mercury-air systems using a Micrometrics Autopore IV for four different core samples and modified the characteristic curve of the water-CO₂ system. Like *Chen et al.* [1999], they only investigated drainage processes. To the author's knowledge, some of these studies which neglect the hysteresis behavior will affect

the accuracy of the constitutive models for two-phase flow system.

2.2.2 Experimental methods to derive the $k_r - S_w$ relationships

Understanding the relative permeability of both the wetting and non-wetting phases is critical for carbon sequestration research because the study need to consider the non-wetting phase oppose to air-water system which often neglects the air phase [Dane *et al.*, 1998]. Previous studies used different methods to obtain the permeability of the air-water system experimentally [Burdine, 1953; Corey, 1994].

Dane et al. [1998] developed a technique to measure the non-wetting phase relative permeability using the hydrostatic method. They claim that this method is applicable for both drainage and imbibition processes. However, they only presented the data for the drainage process. *Bachu and Bennion* [2008] obtained more than 20 relative permeability tests for the CO₂ and brine system by changing the pressure and salinity of core samples. They used the coreflood experiments [Bennion and Bachu, 2005] to measure both the wetting and non-wetting relative permeability, while they avoided measuring the imbibition process. *Krevor et al.* [2012] tested four different sandstone rocks to investigate the relative permeability by applying a modified core flooding experiment [Perrin and Benson, 2009]. However, they did not measure the relative permeability during imbibition to simplify the problem. Moreover, the experiments of their study were not able to obtain the maximum saturation of CO₂ which refers to the irreducible saturation of the wetting phase. This is because the experimental setup could not make the capillary pressure high enough to make the core sample to reach the irreducible saturation. Therefore, they have concluded that this experimental method cannot measure the whole relative permeability curve.

2.2.3 Scaling method of the $P_c - S_w$

Many of the conceptual models related to soil physics used the assumption that the pore geometry can be represented as a bundle of straight and cylindrical tubes. However, this simplification is sometimes irrelevant. For the theory of the Leverett scaling, this assumption was neglected and the definition that the same curvature and capillary pressure can be observed

at the same horizontal level for all interfaces between two fluids was used. Interfacial curvature gives the pressure differences between the two fluids which called the capillary pressure and the capillary pressure is the driving force which causes the fluid flow under the action of capillarity.

In his study, he discovered that interfacial curvature multiplied by a factor that is the property of the porous media corresponding to the dimensionless function $J_{(S_{ew})}$. The relationship between this dimensionless function and saturation leads to the generalized curvature – saturation plots for all clean unconsolidated sands [Leverett, 1941]. Moreover, this dimensionless function can be expressed as the relationships between the two arbitrary systems [Chen *et al.*, 1999].

$$J_{(S_{ew})} = \frac{P_{c,1}}{\sigma_1} \left(\frac{k_1}{\phi_1} \right)^{1/2} = \frac{P_{c,2}}{\sigma_2} \left(\frac{k_2}{\phi_2} \right)^{1/2} \quad (2.10)$$

where P_c is the capillary pressure [M/L/T²], σ is the interfacial tension [M L/T²], k is the intrinsic permeability [L²] and ϕ is the porosity [-]. The subscripts denote the sands or fluid pairs. When one uses the same sand matrix, the porosity and the intrinsic permeability will be the same so that equation (2.10) becomes,

$$P_{c,1} = \frac{\sigma_1}{\sigma_2} P_{c,2} \quad (2.11)$$

Equation (2.11) can predict the unknown $P_c - S_w$ relationship for a fluid pair from the known $P_c - S_w$ relationship for a different fluid pair using the ratio of interfacial tension values of each fluid pair. The interfacial tension of air-water system is 73 dynes/cm at 20 °C and for CO₂-brine system is in the range of 20-60 dynes/cm which is mostly depends on the salinity and the temperature [Bachu and Bennion, 2009; Chalbaud *et al.*, 2009].

Lenhard and Parker [1987] and Busby *et al.* [1995] proved by comparing the scaled and experimentally measured $P_c - S_w$ relationships, Leverett scaling can be applicable to various types of fluids and porous media. Also, Chen *et al.* [1999] utilized Leverett scaling to compare the $P_c - S_w$ relationships with the measured data and they concluded that Leverett scaling can predict the air-oil and oil-water systems from the known $P_c - S_w$ relationship of air-water systems. However, this theory cannot be applied in some cases. Hofstee *et al.* [1997] found the non spreading non aqueous phase liquids (NAPLs) are invalid for Leverett scaling. Non spreading NAPLs are a NAPL which has high interfacial tensions with negative spreading coefficient

[Wilkins *et al.*, 1995]. Also, *Demon and Roberts* [1991] suggested that at lower interfacial tensions, there would be more gaps between the irreducible saturation of wetting phase of the scaled curve and the experimentally derived curve. These findings are not relevant to this study; therefore, these concerns can be neglected.

2.3 Constitutive models

As mentioned in earlier, various multi-phase flow studies suggest that constitutive relationships are the most important input parameters of models that simulate the behavior of multiphase flow system [Oostrom and Lenhard, 1998; Dane *et al.*, 1998; Doughty and Pruess, 2004; Flett *et al.*, 2004; Juanes *et al.*, 2006 and Liu *et al.*, 2010]. These studies highlight the impracticability of obtaining the constitutive relationships in the field. In addition, developing these relationships in the laboratory is problematic due to the nature of the soils (heavy silt and clay contents) as well as changing the properties of the soils with lab investigations. This becomes even more complicated in the case of carbon sequestration due to the high pressures needed to develop the relationships in order to maintain CO₂ in a supercritical state. Experimental methods have several disadvantages in that the experiments are lengthy, difficult to reproduce and restricted by experimental setups [Dane *et al.*, 1992; *Demon and Roberts*, 1993; Klute and Dirksen, 1986].

Due to the difficulties, the constitutive models are a more popular option to determine constitutive relationships of $P_c - S_w$ and $k_r - S_w$. Constitutive models derive the $k_r - S_w$ relationships by fitting the parameters to experimentally obtained data of $P_c - S_w$; therefore, the relationships between relative permeability and saturation can be obtained without conducting experiments [Chen *et al.*, 1999]. Furthermore, the scaling method uses the existing data of the $P_c - S_w$ to predict the unknown $P_c - S_w$ relationships of different soil matrix and/or fluid properties. The following paragraphs compare several popular constitutive models of the capillary pressure (P_c) – saturation (S_w) and the relative permeability (k_r) – saturation (S_w) for two-phase systems.

2.3.1 $P_c - S_w$ Models

The most popular constitutive models of the $P_c - S_w$ relationships are the *van Genuchten* [1980] and *Brooks and Corey* [1964] models. The *van Genuchten* [1980] model describes the empirical relationships between the saturation of the wetting fluid and the matric potential.

$$S_{ew} = \frac{1}{[1 + (\alpha h_c)^n]^m} \quad (2.12)$$

where α [1/L] and n [-] are empirical parameters, S_{ew} is the effective saturation of wetting phase [-], h_c is the matric potential [L] and $m = 1 - 1/n$ [-]. The effective saturation is defines as,

$$S_{ew} = \frac{S_w - S_r}{1 - S_r} \quad (2.13)$$

The *Brooks and Corey* [1964] model developed from the empirical observations that the wetting phase saturation as a power function of h_e [ML/T²] with an exponent λ [-] which is correlated to the non-wetting fluid entry pressure and the pore size distribution, respectively:

$$S_{ew} = \left(\frac{h_e}{h_c}\right)^\lambda \quad (2.14)$$

Equation (2.14) has the limitation that h_c has to be greater than h_e . When $h_c \leq h_e$, the S_{ew} is equal to 1.0.

Comparing these two models at high capillary pressures, one can see that the van Genuchten model and the Brooks and Corey model become similar and Figure 2.5 shows that the van Genuchten model approaches the Brooks and Corey model asymptotically at low water content. Therefore, at the low saturation, the van Genuchten model can be replicate as

$$S_{ew} \approx \left(\frac{1}{\alpha h_c}\right)^{mn} \quad (2.15)$$

where $1/\alpha = h_e$ and $\lambda = m \times n$. However, these two models have significant differences in the low h_c range.

With respect to the Brooks and Corey model, the water content starts to decrease after it reaches the displacement head. For the van Genuchten model, the water content decreases before the displacement head and the van Genuchten model represents smooth curve for the $P_c - S_w$ relationships. Because, van Genuchten [1980] indicated the importance of the model to be

depicted as a smooth curve in order to apply numerical models [Kosugi, 2007].

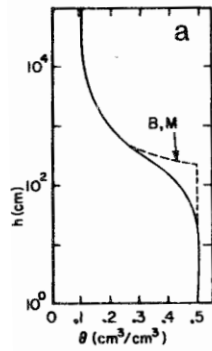


Figure 2.5 Comparison between the van Genuchten model and the Brooks and Corey model [Kosugi, 2007]

2.3.2 $k_r - S_w$ Models

The most typical prediction model of the $k_r - S_w$ relationships is *Mualem* [1976] and *Burdine* [1953] and both models were developed from the Hagen-Poiseuille equation and pore size distribution derived from the $P_c - S_w$ relationships. The equations of *Mualem* [1976] and *Burdine* [1953] model are as follows.

Mualem [1976]:

$$k_{rw} = S_{ew}^\eta \left[\frac{\int_0^{S_e} \frac{dS_e}{h_c}}{\int_0^1 \frac{dS_e}{h_c}} \right]^2 \quad (2.16)$$

$$k_{rn} = (1 - S_{ew})^\eta \left[\frac{\int_{S_e}^1 \frac{dS_e}{h_c}}{\int_0^1 \frac{dS_e}{h_c}} \right]^2 \quad (2.17)$$

Burdine [1953]:

$$k_{rw} = S_{ew}^2 \left[\frac{\int_0^{S_e} \frac{dS_e}{h_c^2}}{\int_0^1 \frac{dS_e}{h_c^2}} \right] \quad (2.18)$$

$$k_{rn} = (1 - S_{ew})^2 \left[\frac{\int_{S_e}^1 \frac{dS_e}{h_c^2}}{\int_0^1 \frac{dS_e}{h_c^2}} \right] \quad (2.19)$$

Table 2.1 shows the $k_r - S_w$ relationship of the different combinations of the van Genuchten and the Brooks and Corey models with Mualem and Burdine model. *Kosugi* [2007] pointed out that there are not many studies described about whether the Mualem model is superior to the other models, although he concluded that typically the Mualem model fits better than the Burdine model. Also, *Chen et al.* [1999] studied the applicability of all models listed in Table 2-1 to the experimental data. They concluded that the van Genuchten and van Genuchten – Mualem models are better than Brooks and Corey and Brooks and Corey – Burdine models to characterize the $P_c - S_w$ and the $k_r - S_w$ relationships from the evaluation of the model’s accuracy, uniqueness, and parameter uncertainties.

Table 2.1 Permeability Models

	Mualem	Burdine
Van Genuchten	van Genuchten - Mualem model $k_{rw} = S_{ew}^\eta \left[1 - \left(1 - S_{ew}^{\frac{1}{m}} \right)^m \right]^2$ $k_{rn} = (1 - S_{ew})^\eta \left[1 - S_{ew}^{\frac{1}{m}} \right]^{2m}$	van Genuchten - Burdine model $k_{rw} = S_{ew}^2 \left[1 - \left(1 - S_{ew}^{\frac{1}{m}} \right)^m \right]$ $k_{rn} = (1 - S_{ew})^2 \left[1 - S_{ew}^{\frac{1}{m}} \right]^m$
Brooks and Corey	Brooks and Corey - Mualem model $k_{rw} = S_{ew}^{\eta+2+2\lambda}$ $k_{rn} = (1 - S_{ew})^\eta \left[1 - S_{ew}^{1+\frac{1}{\lambda}} \right]$	Brooks and Corey -Burdine model $k_{rw} = S_{ew}^{3+\frac{2}{\lambda}}$ $k_{rn} = (1 - S_{ew})^2 \left[1 - S_{ew}^{1+\frac{2}{\lambda}} \right]$

Corey [1994] found the $k_r - S_w$ relationships show little hysteresis behavior. Usually, the $k_r - S_w$ relationships of the non-wetting phase shows more hysteresis compared to the $k_r - S_w$ relationships of the wetting phase. From the Brooks and Corey – Burdine model, if the pore size distribution index is about 2.0, the model can be rewritten as,

$$k_{rw} = S_{ew}^4 \quad (2.20)$$

However, for the uniform pore-size grains, the exponent of the S_{ew} becomes more likely to 3.0 which correspond to Irmay equation [Irmay, 1954]. Hausenberg and Zaslavsky [1963] proved Irmay equation from the experiments of the uniform grain sized sands. Commonly, the Brooks and Corey – Burdine model is suitable for the soil materials and porous rocks [Corey, 1994].

2.4 Impact of the quality of constitutive relationships on numerical models

The accuracy of constitutive relationships significantly affects the accuracy of numerical model simulations. It is well known that hysteresis for both $P_c - S_w$ and $k_r - S_w$ relationships play a significant role in the modeling of multiphase flow [Lenhard, 1992; Holtz, 2002; Doughty and Pruess, 2004; Juanes et al., 2006; Kamaruddin et al., 2011].

Several studies neglected the effect of hysteresis in order to simplify the problem. Juanes et al. [2006] investigated the injection and storage of scCO₂ in a saline aquifer. They performed the numerical simulation of a reservoir to evaluate the processes of scCO₂ trapping. However, they used previously obtained relative permeability data for brine-nitrogen systems and neglected hysteric behavior. They found the hysteresis of the relative permeability plays an important role for the migration of scCO₂. Without considering the hysteresis behavior, they observed no scCO₂ was found to be residual state in the aquifer and the plume of scCO₂ was found below the cap rock. In addition, Doughty and Pruess [2004] considered how formation heterogeneity impacts the capacity of CO₂ storage and investigated on the influence of their model parameter settings. The simulation of numerical model show the significant differences between using the relative permeability of the work from Holtz [2002] and the one from the van Genuchten and Brooks and Corey model. The residual saturation by a factor of two by using the relative permeability value obtained from Holtz [2002] as compared to the constitutive models and this led to significant effects on the storage and mobility of CO₂. Lenhard [1992] and Kamaruddin et al. [2011] also mentioned that neglecting hysteresis induces errors to the model and leads to the discrepancies between what is found in the numerical model and the actual subsurface flow system.

2.5 Use of surrogate fluids

Shook et al. [1992] and *Gharbi et al.* [1998] determined that dimensionless numbers, such as capillary number, bond number, viscosity ratio, and density ratio, can be used to characterize two-phase flow system.

There are several carbon sequestration studies that have been conducted using surrogate fluids. *Pentland et al.* [2010] investigated the residual saturation of the non-wetting phase by changing the initial saturation. They used the brine and n-octane as the analog fluids of brine and scCO₂, respectively. The n-octane was selected because it has a similar density as scCO₂. Also, *Aminzadeh et al.* [2012] selected n-octane as the surrogate of scCO₂. *Pentland et al.* [2010] showed the residual saturation of scCO₂ in their experiment matched with the results of *Spiteri et al.* [2008]. *Spiteri et al.* [2008] investigated the residual hydrocarbon saturation as a function of the initial saturation and found relationships between the two. With this, the study of *Pentland et al.* [2010] seems to be applicable to simulate the behavior of scCO₂ and brine system. However, the interfacial tensions between n-octane and brine are slightly higher than the actual interfacial tension of scCO₂ and brine system. Moreover, both studies did not consider any other hydraulic properties of the scCO₂ dimensionless numbers which characterize the two-phase flow system. Therefore, uncertainty still remained that n-octane and water can be used as the surrogate of the scCO₂ and brine.

2.6 Numerical Models

Various models such as TOUGH2, STOMP, and ECLIPSE [*Falta et al.*, 1995; *Juanes et al.*, 2006; *Schnaar and Digiulio*, 2009] have been used to study about carbon sequestration. In this study, TOUGH2 T2VOC was selected to simulate system requires to model two-phase flow system of surrogate fluids. TOUGH2 T2VOC is a general-purpose simulation program for three phase system consisting of air, water, and a volatile organic compound (VOC) including the calculation for heat transfer. T2VOC is a module for three-phase flow and was designed to simulate such as the NAPL migration, the evaporation and diffusion of VOC, and air stream injection to remove the VOC or NAPL from the contaminated aquifers. In this study, the air phase can be neglected due to there is no air phase. ECO2N is a TOUGH2 module for scCO₂/brine; therefore it often used for the carbon sequestration research. The code uses an

integral finite difference method and is developed at Lawrence Berkeley National Laboratory [Falta *et al.*, 1995].

2.7 Summary of literature reviews

This chapter showed the review of the constitutive relationships of two-phase flow such as the capillary pressure (P_c) – saturation (S_w) and the relative permeability (k_r) – saturation (S_w), which are essential to understand two-phase flow behavior. Especially, the literature review focused on the experimental methods to derive these constitutive relationships and showed the list of the constitutive models. Also, the review presented how the quality of constitutive relationships results in a limitation in our understanding of the two-phase flow system.

This project mainly focuses on the carbon sequestration into the saline aquifer; therefore, this study needs to consider the two-phase flow behavior of scCO₂ and brine. In order to model the two-phase flow system, it is important to have relevant constitutive relationships which can characterize the two-phase flow behavior. From this literature review, it can be said that there are many studies that relied on the constitutive models without evaluating the accuracy of the model for the studying system. Moreover, the studies which tried to compare the constitutive models to the experimental data, the comparison were often based on the drainage cycle and neglected the imbibition process. Before investigating the scCO₂ behavior in saline aquifers, it is important to measure the constitutive relationships independently from the constitutive models and examine the accuracy of the obtained constitutive models.

2.8 Research Scope

The literature review showed that the constitutive relationships are one of the important model input parameters which improves the accuracy of the model which leads to better understanding of two-phase flow system of scCO₂ and brine. To investigate the applicability of the existing constitutive models, it is important to measure the constitutive relationships without using the constitutive models and compare the two.

Surrogate fluids of scCO₂ and brine are used to make the experiments more feasible to conduct and they can be run under ambient conditions. The methods to identify the $P_c - S_w$ and k_r

– S_w relationships for the surrogate fluids are not well established; therefore, it is necessary to investigate the measurements methods to derive these constitutive relationships for the surrogate fluids. It should be noted that developed methods which characterize the $P_c - S_w$ and $k_r - S_w$ relationships are applicable for ambient condition, so these methods cannot be applied to actual $scCO_2$ and brine system which needs high pressure for the maintenance of CO_2 in supercritical state. Also the laboratory facilities in which this work was performed are not appropriate for such experiments.

This project focuses on three experimental tasks with the goal of deriving reliable material parameters that would be used in developing model for investigating the behavior of $scCO_2$ in deep geological formations. These tasks include evaluating multiple methods for experimentally deriving the $P_c - S_w$ and $k_r - S_w$ relationships in surrogate fluid systems. A numerical model (TOUGH2 T2VOC) was used to simulate a tank experiment to investigate the applicability of the constitutive relationships obtained from the experiments to a tank experiment. Also, the numerical model is used to examine the impact of constitutive relationships on the two-phase flow system. In addition, the tank experiment results are compared with the simulation results to examine the applicability of constitutive relationships obtained from constitutive models and experimental methods.

2.8.1 Task 1: $P_c - S_w$ curve measurements

The applicable methods for experimentally characterizing the $P_c - S_w$ and $k_r - S_w$ relationship for the surrogate fluids and test sands have yet to be determined. This work seeks to examine various methods for measuring the $P_c - S_w$ relationships. As noted in section 2.3.3, Leverett scaling can be used to predict the $P_c - S_w$ relationship for the other fluid combination by using the $P_c - S_w$ relationship for the particular fluids. However, scaling method does not consider changes in the irreducible saturation and residual saturation. Therefore, two other methods have been developed in order to observe the differences in these saturations. This research compares the $P_c - S_w$ relationships derived from Leverett scaling, the entry pressure scaling method, and the dielectric sensor method while observing differences in irreducible saturation and residual saturation among each method. Also, hysteresis behaviors of $P_c - S_w$ relationships were investigated

1) Leverett scaling: Leverett scaling was used to predict the relationships of $P_c - S_w$ curve for the other system by using the $P_c - S_w$ relationship for the particular fluids. Previously, *Sakaki and Illangasekare* [2007] developed $P_c - S_w$ relationships for air /water system by using Tempe cells. From equation (2.10), the for the same soil/sand matrix, the equation can neglect the porosity and the permeability terms, thus the only unknown factor is the interfacial tensions. In this study, the interfacial tensions for air/water and surrogate fluids of scCO₂/brine are measured by using a CENCO-DuNOüY TENSIO METER. By comparing interfacial tensions in air/water and surrogate fluids of scCO₂/brine systems, a scaling factor can be determined to scale the $P_c - S_w$ relationships of air/water to surrogate fluids of scCO₂/brine.

2) Entry pressure scaling measurement: The second method is the entry pressure scaling method. This method is similar to Leverett scaling except that it uses the differences in displacement head pressure between an air-water system and surrogate fluids of scCO₂/brine system instead of interfacial tensions. The differences in displacement head pressure are applied as a scaling factor for deriving the $P_c - S_w$ relationship for the surrogate fluids of scCO₂/brine system from the previously determined air/water phase $P_c - S_w$ relationship.

3) Dielectric sensor method: The third method is to use dielectric sensors to measure phase saturation while the injection head and draining head differences were measured to obtain the $P_c - S_w$ relationship. The most important feature of this method is that the irreducible saturation and residual saturation of the surrogate fluids of scCO₂/brine system can be measured. In addition to the $P_c - S_w$ relationship, van Genuchten model is fitted to the experimentally obtained $P_c - S_w$ relationship from the dielectric sensor method and obtained the van Genuchten parameters of α and m .

2.8.2 Task 2: $k_r - S_w$ curve measurement

The van Genuchten – Mualem model is a common method to predict $k_r - S_w$ relationship. The model uses the fitted van Genuchten model to the experimentally obtained $P_c - S_w$ relationship from the dielectric sensor method. However, the applicability of this model is sometimes uncertain due to the many simplifying assumptions that are made in the model. Therefore, in addition to using the van Genuchten – Mualem model, this study uses two other methods to characterize the $k_r - S_w$ relationship for test sands and fluids, one which measures the

wetting phase and one that measures the non-wetting phase. These two alternative methods are described below. Results of experimentally obtained $k_r - S_w$ relationship are compared with the van Genuchten – Mualem model. Also, during the experiments, hysteresis behaviors of $k_r - S_w$ relationships are considered.

1) Long column method: The long column method was developed by *Corey* [2002] to measure relative permeability for the wetting fluid. The principle of this method is to have uniform saturation throughout the column and the head gradient is equal to one at the steady state condition. The saturation can be changed by adjusting the inflow rate of the wetting phase and non-wetting phase fluids. Before starting experiment, the saturated hydraulic conductivity of the system is measured. Flow rate of the wetting fluid is applied to Darcy's law and calculate the unsaturated conductivity of the system. The relative permeability can be calculated from the ratio of unsaturated conductivity to saturated hydraulic conductivity instead of using the effective permeability to absolute permeability.

2) Hydrostatic method: The hydrostatic method was developed by *Dane et al.* [1998]. This method can measure the $k_r - S_w$ relationships for the non-wetting phase. The principle of this method is to have the uniform capillary pressure and saturation throughout the column at the steady state condition. The setup of this column is to have the hydrophilic ceramic cylinder is glided to both end ridges of Teflon cylinder and the sand is packed inside of the ceramic cylinder. At the steady state condition, only the non-wetting phase can flow inside of the column while the wetting phase is at rest. The relative permeability can be measured by using the outflow mass of the non-wetting phase.

2.8.3 Task3: Modeling

The last task is to investigate the applicability of the $P_c - S_w$ and $k_r - S_w$ relationships obtained from the experimental methods and constitutive models to tank experiment. Results of tank experiment are used to compare a numerical model which simulated the tank experiment. Primary, this tank experiment is conducted to investigate the trapping mechanisms of $scCO_2$ and the saturation of $scCO_2$ in the tank experiments are measured by using an X-ray system [*Trevisan et al.*, 2013]. In this project, TOUGH2 T2VOC is used to model the behavior of $scCO_2$ in the tank experiment. The $P_c - S_w$ and $k_r - S_w$ relationships from the experimental methods and

constitutive models are applied separately to the TOUGH2 T2VOC and are compared to see which constitutive relationships replicate the behavior of scCO₂ well.

CHAPTER 3 – TEST MATERIALS

The surrogate fluids of scCO₂ and brine were selected from the study of *Trevisan et al.* [2013]. Surrogate fluids can properly represent the constitutive relationships of the scCO₂/brine system. The advantage of using surrogate fluids is that they are more practical than using the scCO₂-/brine system because they have less limitation in the laboratory set up and are more cost effective.

3.1 Selection of Surrogate Fluids

The surrogate fluids were chosen based on dimensionless numbers which express the ratio of the difference forces. Previous studies, such as *Shook et al.* [1992] and *Gharbi et al.* [1998] have found the following dimensionless numbers can be used to characterize two immiscible fluid flows in similar porous medium:

Bond Number N_B [-],

$$N_B = \frac{\Delta\rho g k}{\sigma} \quad (3.1)$$

where $\Delta\rho$ is the density differences of two immiscible fluids [M/L³], g is the acceleration due to gravity [M/T²], k is the permeability of the porous medium and σ is the interfacial tension of two immiscible fluids [M L/T²].

Capillary Number N_C [-],

$$N_C = \frac{\mu_{nw} u_T}{\sigma} \quad (3.2)$$

where μ_{nw} is the viscosity of non-wetting phase fluid [L²/M/T] and u_T is the fluid flow [L³/T].

Viscosity ratio [-],

$$\text{Viscosity ratio} = \frac{\mu_{nw}}{\mu_w} \quad (3.3)$$

where the subscript w corresponds to wetting phase fluid and n_w is non-wetting phase fluid.

Density ratio [-],

$$\text{Density ratio} = \frac{\rho_{nw}}{\rho_w} \quad (3.4)$$

Table 3.1 shows these four dimensionless numbers under typical reservoir conditions for carbon sequestration studies.

Table 3.1 Dimensionless numbers of the scCO₂ and brine system under typical reservoir conditions [Nordbotten et al., 2005]

Dimensionless numbers [-]	Typical Reservoir conditions
N_B	$\sim 10^{-3}$
N_C	$\sim 10^{-8} - 10^{-9}$
Viscosity ratio	$\sim 0.2 - 0.05$
Density ratio	$\sim 0.2 - 0.7$

In order to use surrogate fluids with the same dimensionless numbers under typical reservoir conditions of the scCO₂-brine system, a 8:2 mixture by weight of Glycerol and water and Soltrol 220 dyed with sudan IV were selected as the analog fluids of brine and scCO₂, respectively. In the following chapters, unless stated, the Soltrol 220 refers to the one dyed in sudan IV and the Glycerol-water mixture corresponds to the one mixed 8:2 ratio by weight.

Table 3.2 Comparison between fluid properties of surrogate fluids system and scCO₂-brine system [Schroth et al., 1995; Nordbotten et al., 2005; Cheng, 2008]

	Soltrol 220	Glycerol/water mixture	scCO ₂	Brine
ρ [g/cm ³]	0.79	1.21	0.270 – 0.730	0.95 – 1.23
μ [mPa s]	3.90	60.9	0.023 – 0.061	0.20 – 1.58
μ_{nw}/μ_w [-]	0.06		0.026 – 0.20	
ρ_{nw}/ρ_w [-]	0.66		0.220 – 0.75	
σ [dyne/cm]	17.3 – 21.0		20.0 – 60.0	
N_c [-]	$10^{-6} - 10^{-7}$		$10^{-5} - 10^{-8}$	
N_B [-]	$10^{-6} - 10^{-7}$		$10^{-7} - 10^{-8}$	

The Glycerol and water mixture $C_3H_5(OH)_3$ was chosen that it has the ability to change density and viscosity by controlling the fraction of Glycerol and water mixture. In this study, the empirical formula from the study of *Cheng* [2008] was used to calculate density and viscosity of the Glycerol and water mixture at ambient conditions. Soltrol 220 is an isoparaffin solvent that is made of a mixture of C13 to C17 alkanes, manufactured by Chevron Phillips Chemical Company. Soltrol 220 is a LNAPL and at ambient condition, it has a very low volatility and solubility. Also, it is less hazardous than other LNAPLs; therefore, it has been commonly used for multiphase flow studies [*Cary et al.*, 1989; *Lenhard*, 1992 and *Schroth et al.*, 1995]. By comparing the dimensionless numbers of the $scCO_2$ -brine system, the mixture of the 80 % of Glycerol and 20 % of water by weight was selected as the surrogate of the brine. In this research, the water refers to de-ionized water. Table 3.2 shows fluid properties and dimensionless numbers of the $scCO_2$ -brine system and surrogate fluids.

Cihan et al. [2011] have conducted a simulation of two-phase flow by using COMSOL. At first he used the hydraulic properties of $scCO_2$ /water to simulate the two-phase flow system, and then used the properties of Soltrol 220/Glycerol-water mixtures to compare the results. Changes in density due to the dissolution of $scCO_2$ were considered in the model, although at this time scale, the dissolution process has not happened. For the Soltrol 220/Glycerol-water system, the model assumed that surrogate fluids are incompressible and the non-wetting phase is insoluble to the wetting phase. Figure 3.1 shows that identical two-phase flow behavior can be obtained by using the fluids which have the same dimensionless numbers. This model simulation results validated that Soltrol 220 and Glycerol-water mixture can be prepared as the analog fluids of $scCO_2$ and brine, respectively. Therefore, conceptually, the $scCO_2$ mobilization in saline aquifers can be analyzed by studying the multiphase flow system of these surrogate fluids. For future work, it is recommended to simulate with the TOUGH2 T2VOC model to replicate the $scCO_2$ /brine system with Soltrol 220/Glycerol-water system.

3.2 Selection of Test Sands

For test sands, five different sieve sized Accusands, manufactured by Unimin Corporation Le Sueur, Minnesota, US were used. The sieved sizes are #12/20, #20/30, #30/40, #40/50, #50/70, respectively. The common features of Accusands are that they have high purity,

low organic content and the grain shape is rounded [Schroth *et al.*, 1995]. The uniformity coefficients of these five sands are approximately 1.2, the grain density is 2.66 g/cm^3 , and its composition is 99.8 % quartz. Tables 3.3 and 3.4 show the properties and the van Genuchten parameters of the water retention functions of the five different Accusands [Smits and Limsuwat, 2009].

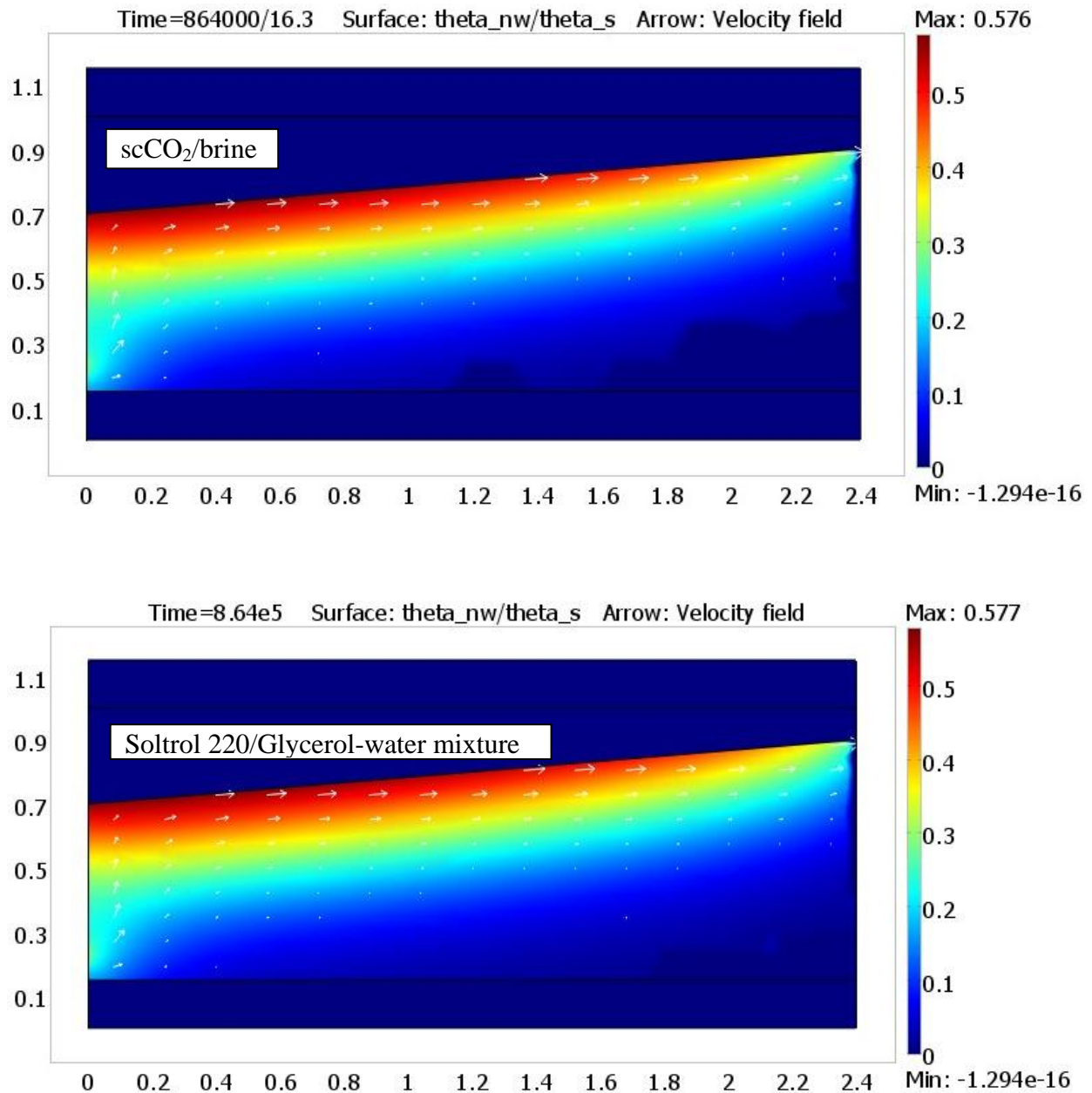


Figure 3.1 Comparisons of the numerical simulations for the scCO₂/brine and Soltrol 220/Glycerol-water system

Table 3.3 van Genuchten model parameters for water and air fitted by *Smits and Limsuwat* [2009]

Accusand		Residual Water Content [-]	Maximum Water Content [-]	α [1/cm]	n [-]	m [-]
#12/20	drain	0.017	0.312	0.10	9.21	0.89
	imbibition	0.017	0.258	0.11	6.00	0.83
#20/30	drain	0.027	0.330	0.07	15.68	0.94
	imbibition	0.027	0.235	0.14	5.10	0.80
#30/40	drain	0.028	0.334	0.06	17.81	0.94
	imbibition	0.028	0.242	0.09	6.50	0.85
#40/50	drain	0.029	0.335	0.04	10.18	0.90
	imbibition	0.029	0.272	0.08	4.20	0.76

Table 3.4 Hydraulic Properties of Accusands by *Schroth et al.* [1998], and *Smits and Limsuwat* [2009]

Accusand	Porosity [-]	d_{50} [mm]	Uniformity coefficient [-]	hydraulic conductivity (water) [cm/s]	intrinsic permeability [cm ²]	Displacement pressure Head of water [cm]
#12/20	0.318	1.040	1.231±0.043	0.376	3.83E-06	7.1
#20/30	0.320	0.750	1.190±0.028	0.230	2.34E-06	12.0
#30/40	0.325	0.524	1.207±0.008	0.106	1.08E-06	16.1
#40/50	0.334	0.358	1.200±0.018	0.052	5.30E-07	19.4
#50/70	0.340	0.270	-	0.029	2.96E-07	34.0

CHAPTER 4 – $P_c - S_w$ CURVE MEASUREMENT

In order to investigate the applicability of constitutive relationship, several experiments and numerical modeling were conducted. This section describes the methods to obtain the constitutive relationship of the $P_c - S_w$. Leverett scaling is applicable for the various porous media and combinations of fluids. However, whether or not Leverett Scaling is accurate enough to characterize the $P_c - S_w$ relationships is still controversial because the scaling factor shifts only the y-axis directions and the theory assumes that the irreducible saturation and residual saturation are constant for the same porous medium. One of the objectives of this project is to modify the existing methods to characterize the $P_c - S_w$ curve for the test materials. In order to verify that the modified methods are sufficient to characterize the $P_c - S_w$ relationships, three different methods were conducted and the results were compared for the five test sands.

4.1 Description of the $P_c - S_w$ measurement

Five different Accusands classified by the sieve sizes as #12/20, #20/30, #30/40, #40/50 and #50/70 were tested to obtain $P_c - S_w$ relationships for Soltrol 220/Glycerol-water system. The following paragraphs show the theories and methods of the experimental setup of the measurements for $P_c - S_w$ relationships. The $P_c - S_w$ relationships were determined by three different methods: Leverett scaling, the entry pressure scaling method and the dielectric sensor method. Details of these methods and corresponding experimental setups are given below.

4.1.1 Leverett scaling

Leverett scaling is used to obtain the $P_c - S_w$ curve and to compare the results with two other methods which is the entry pressure scaling method and the dielectric sensor method. A description of Leverett scaling method is described in section 2.3.3. In this study, the only unknown parameter in equation (2.11) is the interfacial tension of Glycerol/water mixture 8:2 by weight and Soltrol 220 dyed in sudan IV. The interfacial tension between Soltrol 220/Glycerol-water (80:20) was not found in the literature, although some of the interfacial tensions data were found for Soltrol220 and Glycerol phase in the study of *Schroth et al.* [1995], *Chen et al.* [1999], and *Fisher and Morrow* [2006]. Before taking the measurement of interfacial tension, to get an

idea of the interfacial tension value of Soltrol 220/Glycerol-water (80:20), these data were examined.

The interfacial tension is measured using CENCO-DuNOÜY TENSIOMETER and DyNOÜY ring which is referred to as the ring method. The method to measure the interfacial tension is described in the study of *Schroth et al.* [1995]. They stated that the interfacial tensions change with time due to the contamination effect at the interface of fluids, although these changes are neglected in this project to simplify the problem and also, the interfaces between Soltrol 220 and Glycerol-water mixture should be the same because Soltrol 220 is immiscible to Glycerol-water mixture. The test was repeated three times and the average value was used. Besides measuring the Glycerol/water mixture 8:2 by weight and Soltrol 220 dyed in sudan IV, several interfacial tensions of other fluid mixtures were measured to study to see which factor affects the interfacial tensions value.

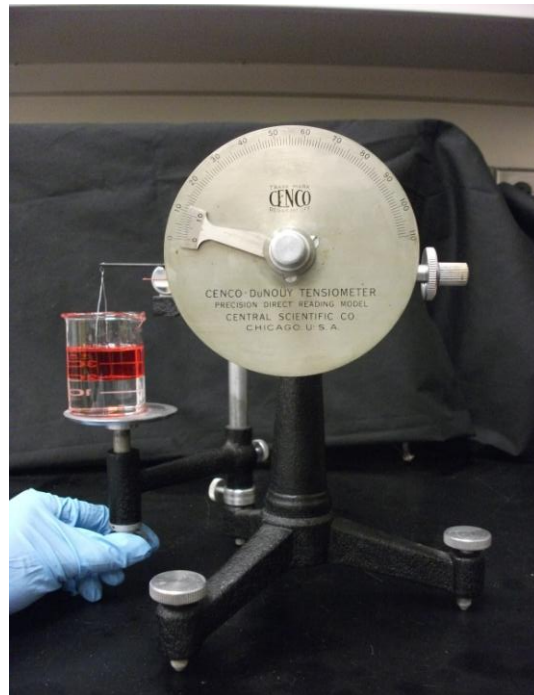


Figure 4.1 CENCO-DuNOÜY TENSIOMETER

4.1.2 Entry Pressure Scaling Method

The theoretical basis of this method is to derive the unknown $P_c - S_w$ relationship of the Glycerol-water/Soltrol 220 system from the existing $P_c - S_w$ relationship of the water/air system

by using displacement head ratio of the Glycerol-water/Soltrol 220 to water/air system. The entry pressure method resembles Leverett scaling except it uses the displacement pressure head instead of using the interfacial tensions. The assumption is made that the $P_c - S_w$ curve of the Glycerol-water/Soltrol 220 system will follow the same shape as the water/air system except the value of the displacement pressure head. The Glycerol-water/Soltrol 220 system has a low displacement head compared to the water/air phase, so the curve shifts downward. This method also can be applicable to different fluid combinations. By multiplying the $P_c - S_w$ curve of the water/air system by the ratio of the displacement pressure head of the water/air system and the Glycerol-water/Soltrol 220 system, the $P_c - S_w$ curve of the Glycerol-water/Soltrol 220 system can be demonstrated. Also, the purpose to conduct this method is to validate Leverett scaling by contrasting the scaling factors and prove the interfacial tension value which determined from CENCO-DuNOÜY TENSIOMETER can be used to measure the $P_c - S_w$ relationships for the test sands and fluids. Moreover, this method is the fundamental study for the dielectric sensor method to ensure $P_c - S_w$ relationships can be obtained using Glycerol-water/Soltrol 220 system.

To measure the displacement pressure head of the Glycerol-water/Soltrol 220 system, an experimental set up was constructed to have three identical columns located in parallel. The Glycerol-water mixture saturated sand was tightly packed to a height of 15 cm of each column. The bottom of the sand column was connected to an external constant-head device which has the same height as the saturated sand. A Mariotte's bottle supplied changes in Soltrol 220 (dyed in sudan IV) pressure with increment of 0.5 cm every 12 hours. As the Soltrol 220 entered the sand, the Glycerol-water mixture was displaced. The displacement pressure head was identified from the outflow mass of the Glycerol-water mixture. At the certain height of the Soltrol 220, the outflow of the Glycerol-water mixture increases significantly and this height of the Soltrol 220 is assumed as the displacement pressure head of the Glycerol-water/Soltrol 220 system. The experiments were conducted for five Accusands. The displacement pressure heads of the water-air system for the five Accusands were reported by *Smits and Limsuwat*, [2009]. Using this data, the scaling factors of the water/air to the Glycerol-water/Soltrol 220 system were obtained and the $P_c - S_w$ relationships for the Glycerol-water mixture/Soltrol 220 for the five Accusands were presented. The experiment was performed at room temperature (approximately 20°C). To convert the measured displacement pressure heads to the displacement pressures, the pressure can be

calculated from the equation of $P_d = \rho_{nw}gH_{nw}$, where H is the displacement pressure head which corresponds to the displacement of the Soltrol 220.

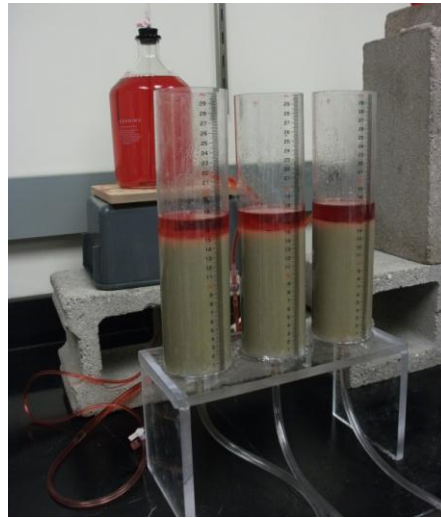


Figure 4.2 Entry Pressure Method

4.1.3 Dielectric Sensor Method

By using Leverett scaling and the entry pressure method, the scaling factors were obtained for the five Accusands to convert the $P_c - S_w$ curve of the water/air system to the Glycerol-water/Soltrol 220 system. However, the accuracy of the irreducible and residual saturation is still unknown. To obtain the irreducible and residual saturation, third method was adopted to measure the irreducible and residual saturation of the Glycerol-water mixture, as well as intermediate S_w values.

In this method, the saturation of the Glycerol-water mixture was measured rather in more direct manner using the dielectric soil moisture sensors. The dielectric property of soil depends strongly on the dielectric permittivity of the volumetric fraction of the fluids. Fortunately, the dielectric property of the Soltrol 220 is similar to that of air and the Glycerol is significantly higher than that of the Soltrol 220. The dielectric property of the Soltrol 220 is 2, and the Glycerol is 42 [Capaccioli, 2000]. This resembles the dielectric property of water-air systems in which water has a higher dielectric property compared to air. Therefore, the assumption is made that the dielectric sensors can be used to estimate the saturation of the Glycerol-water mixture.

In this study, the ECH₂O EC-5 soil moisture sensors (Decagon Devices, Inc. Pullman WA) were utilized to measure the saturation of the Glycerol-water mixture. The sensor is 5 cm long with a 0.3 L measurement volume. The frequency is 79MHz. First, the ECH₂O EC-5 soil moisture sensor was calibrated. The method to calibrate the sensor was to place the sensor in the sand which has the pre-determined saturation by changing the height of interface between the Glycerol-water mixture and the Soltrol 220. The sensor reading was recorded each saturation. The sensor is assumed to measure an average saturation along the length of sensor. The results were compared to the two-point α -mixing model developed by *Sakaki et al.* [2008; 2011] and the fitting parameter of the α was determined for the Glycerol-water/Soltrol220 system .

The two-point a-mixing model:

$$S_w = \frac{X^\alpha - X_{Soltrol}^\alpha}{X_{Glycerol}^\alpha - X_{Soltrol}^\alpha} \quad (4.1)$$

where, S_w is the saturation of wetting phase fluids which is the Glycerol-water mixture in this case, X is the sensor reading, $X_{Soltrol}$ is the sensor reading in the Soltrol 220-saturated soil, $X_{Glycerol}$ is the sensor reading in the Glycerol-water mixture saturated soil, and α is the fitting parameter which is 2.5 from *Sakaki et al.* [2008; 2011] for air/water system.

To test the sensor sensitivity and the methodology to measure the $P_c - S_w$ relationship of the Glycerol-water mixture and the Soltrol 220, the column tests were done for all five different sieve-sized sands by using ECH₂O EC-5 soil moisture sensors to measure the saturation of the Glycerol-water mixture.

Figure 4.4 shows the experimental setup of the column. The saturation of the Glycerol water mixture and the Soltrol 220 system was measured at 5 and 10 cm from the top of a 50 cm tall column. The Teflon cap was placed at the top of the column which contained a solvent resistance O-ring for preventing leakage. The Glycerol-water mixture saturated sand was tightly packed into the entire column. For the drainage process, the external constant-head device was connected at the bottom of the column. At the top of the column, Mariotte's bottle was connected which was filled with the Soltrol 220. The heights of the constant-head device and the Mariotte's bottle were initially set at the same value. By lowering the constant-head device in a stepwise manner, the Soltrol 220 was started to move into the column and simultaneously the same amount of volume of the Glycerol-water mixture was extracted from the constant-head device.

The height of the constant-head device was changed in increments of 2 – 4 cm every 12 hours and the outflow of the Glycerol-water mixture was measured. The capillary pressure was calculated from the height difference between the external constant head device and Mariotte’s bottle.

$$P_c = P_{nw} - P_w = \rho_{nw}gh_{nw} - \rho_wgh_w \quad (4.2)$$

where, P_{nw} is the pressure of the non-wetting fluids which is the pressure of Mariotte’s bottle and P_w is the pressure of the wetting fluids which is the pressure of the constant-head device. The capillary pressure needs to be measured at the location of each soil moisture sensor; therefore, the pressure of the Mariotte’s bottle and the constant-head device were calculated by using the height from the each sensor. Figure 4.5 shows the methodology to calculate the capillary pressure from 10 cm at the top of the column where the soil moisture sensor is located.

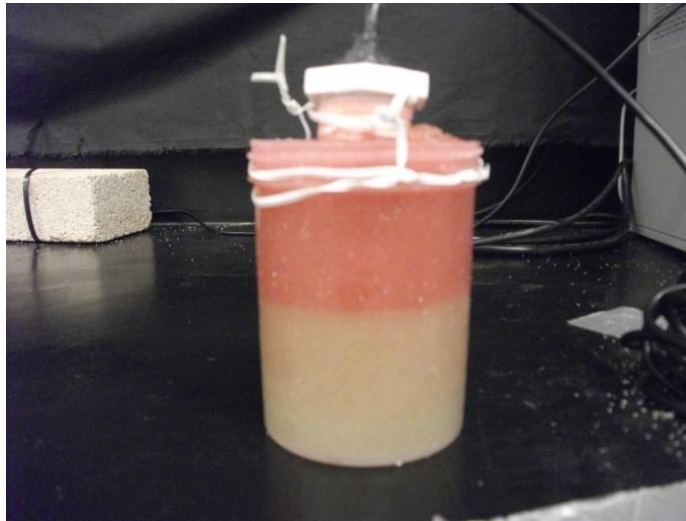


Figure 4.3 Calibration of sensor

The imbibitions process was measured after ECH₂O EC-5 sensors were completely covered with the Soltrol 220 visually and sensor readings were stabilized. To begin the imbibition processes, Mariotte’s bottle was filled with Glycerol-water mixture and was connected at the bottom of the column at the height where the drainage process stopped. The constant-head device was connected at the top of the column at the same height as the top of the column. By raising Mariotte’s bottle, the Glycerol-water mixture began to replace the Soltrol 220. The experiment was stopped before the Glycerol-water mixture reaches the tube connected at the top of the column.



Figure 4.4 Experimental setup of dielectric sensor method

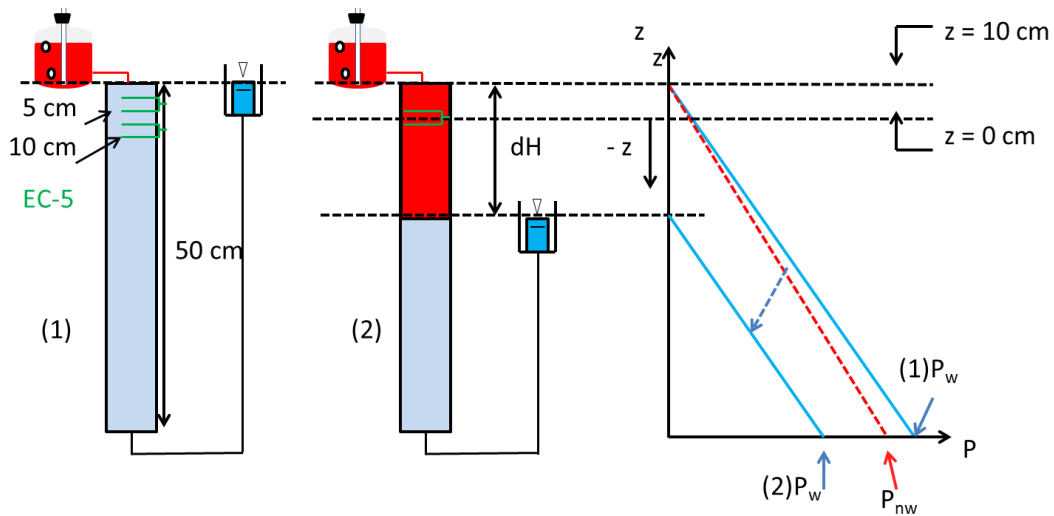


Figure 4.5 Methodology to calculate the capillary pressure

4.2 Experimental results of the $P_c - S_w$ relationship

The $P_c - S_w$ relationships were obtained for five different Accusands with varying grain sizes by using Leverett scaling, the entry pressure scaling method, and the dielectric sensor method. All of the methods were investigated as to whether or not they can be used to characterize $P_c - S_w$ relationships for the test fluids and sands. The results are described and compared below.

4.2.1 Leverett Scaling results

The interfacial tensions between the Glycerol-water mixture and the Soltrol 220 were measured by using CENCO-DuNOüY TENSIOMETER. During the measurements of the interfacial tensions, it needs to wait for about 1min to stabilize the interface of the two fluids. Moreover, the DyNOüY ring has to be clean with alcohol each time when taking the measurement to remove the non-wetting phase which adheres to the ring. In order to investigate how the interfacial tension is affected by the ratio of the Glycerol-water mixture, measurements were made for a range of Glycerol-water mixtures. Moreover, the effect of the sudan IV and salinity were investigated. The following table shows the list of the interfacial tensions between the different combinations of two fluids. The brackets (80:20) corresponds to the Glycerol and water mixture which mixed 8:2 ratio by weight and (50:50) corresponds to the mixture of 5:5 ratio by weight. (100 %) means pure Glycerol. Also, the bracket of (without sudanIV) refers to Soltrol 220 is not dyed with sudanIV.

From Table 4.1, no interfacial tension differences were observed between air/water and air/seawater, whereas Soltrol 220 (without sudanIV)/water and Soltrol 220 (without sudanIV)/seawater show significant differences. Therefore, an assumption was made that the salinity of water affects the interfacial tensions between the two fluid systems. Soltrol 220 (without sudanIV)/Glycerol (100%) has the value of 27.6, and it has significant differences compared to Soltrol 220 (without sudanIV)/Glycerol-seawater (80:20) which has the interfacial tension of 32.0. The interfacial tensions of Soltrol 220/Glycerol-water (80:20) cannot be estimated from these data; although it can be assumed it might be somewhere close to these values. Moreover, the study shows there are no significant differences between the interfacial tensions from adding the sudanIV into Soltrol 220.

The experimental result from the CENCO-DuNOüY TENSIOMETER show that the interfacial tension of Soltrol 220/Glycerol-water (80:20) is 17.3 dyne/cm at 19.0 °C and 21.0 dyn/cm at 18.0 °C. The interfacial tension values were slightly smaller than the assumption from the literature review and the result shows that the interfacial tension is highly sensitive to temperature changes. In this case, 17.3 dyne/cm was taken for the interfacial tension of Soltrol 220/Glycerol-water (80:20) because most of the experiments were conducted around 20.0 °C. Moreover, the interesting result was obtained between Soltrol 220/Glycerol-water (80:20) and

Soltrol 220/Glycerol-water (50:50) that there is not huge difference was observed between the interfacial tensions by changing the ratio of the mixture from 80:20 to 50:50.

Table 4.1 Interfacial Tensions

	Interfacial Tension [dyn/cm]	Temperature [°C]
Air/Soltrol 220 (without sudanIV)¹⁾	25.9	20.0
Soltrol 220 (without sudanIV)/water²⁾	36.4	20.0
Air/water³⁾	73.0	17.6
Soltrol 220 (without sudanIV)/seawater⁴⁾	50.4	20.0
Soltrol 220 (without sudanIV)/Glycerol(100%)⁴⁾	27.6	20.0
Soltrol 220 (without sudanIV)/Glycerol-seawater (80:20)⁴⁾	32.0	20.0
Air/brine⁴⁾	72.8	20.0
Air/Glycerol(100%)⁴⁾	63.8	20.0
Air/Soltrol 220³⁾	24.0	22.0
Air/Glycerol-water (80:20)³⁾	66.0	19.0
Soltrol 220 (without sudanIV)/Glycerol-water (80:20)³⁾	16.7	17.7
Soltrol 220/Glycerol-water (80:20)³⁾	17.3	19.0
Soltrol 220/Glycerol-water (80:20)³⁾	21.0	18.0
Soltrol 220/Glycerol-water (50:50)³⁾	20.4	18.0

¹⁾Chen et al. [1999], ²⁾Schroth et al. [1995], ³⁾Independently measured by CENCO-DuNOüY TENSIO METER, and ⁴⁾Fisher and Morrow [2006]

Based on the interfacial tension values of air/water and Soltrol 220/Glycerol-water (80:20), the scaling factor was found to be 0.24. This will be used to convert the $P_c - S_w$ relationships for the air/water system to the Soltrol 220/Glycerol-water system.

4.2.2 Entry pressure scaling results

The entry pressure head (h_d) of the Soltrol 220 to the Glycerol-water mixture was obtained for each Accusand. In order to convert the displacement pressure head of Soltrol 220 to the water head, the displacement pressure head of Soltrol 220 was multiplied by the density of Soltrol and divided by the density of water.

$$h_d (\text{Soltrol, water head}) = h_d (\text{Soltrol, Soltrol head}) \times \frac{\rho_{\text{Soltrol}}}{\rho_{\text{water}}} \quad (4.3)$$

Also, the scaling factors were obtained for each Accusands to scale the $P_c - S_w$ relationships of air/water to Soltrol 220/Glycerol-water system. The scaling factor was calculated by dividing the displacement pressure head of Soltrol in water head by the displacement pressure head of water. The obtained scaling factors are summarized in Table 4.2.

$$\text{scaling factor} = \frac{h_d (\text{Soltrol, water head})}{h_d (\text{water, water head})} \quad (4.4)$$

Table 4.2 Summary of results obtained with entry pressure scaling method

Accusand	h_d of Soltrol in Soltrol head [cm]	h_d of Soltrol in water head [cm]	h_d of water [cm]	Scaling factor [-]
#12/20	2.4	1.9	7.9	0.24
#20/30	5.0	4.0	12.0	0.33
#30/40	6.5	5.2	16.1	0.32
#40/50	9.2	7.3	19.4	0.38
#50/70	10.1	8.0	34.0	0.24

The scaling factors were in the range of 0.24 – 0.38 for five Accusand samples. #12/20 and #50/70 yielded the same scaling factors as those obtained with Leverett scaling. When measuring the displacement head of the Soltrol 220 to the Glycerol-water mixture, there are differences between the actual displacement head pressure obtained from the outflow mass of Glycerol-water mixture and the one assumed from the picture of the column taken from a camera. The picture illustrates the small amount of the Soltrol 220 starts to intrude inside the sands and at this height of the Soltrol 220 assumed to be the displacement head. Table 4.3 represents the difference between the two.

In most cases, the entry pressure head measurement conducted by the mass outflow is higher than the one observed from the picture which taken. Assumption is made that the porosity between the sand and the surface of the column is larger than that of inside the sand; therefore, Soltrol 220 is likely to inject the surface of the column and it does not inject inside the sand. This finding suggests that it is important to be aware that the visual and the actual entry pressure will

be different and the measurement should not just rely only on the visual observation.

Table 4.3 The difference between entry pressure measurement from out mass and visual determination

Accusand	Soltrol 220 Entry Pressure measurement (out mass) [cm]	Soltrol 220 Entry Pressure measurement (Visual) [cm]
#12/20	2.4	1.0
#20/30	5.0	2.4
#30/40	6.5	5.5
#40/50	9.2	6.0
#50/70	10.1	5.0-6.0

4.2.3 Dielectric sensor results

Figure 4.6 shows the result of the sensor calibration. Equation (4.1) is used to fit the measured and averaged measured values of the saturation of the sensors by changing the value of α . From the EC-5 sensor calibration, the fitting parameter α for the two-point α -mixing model was found to be 2.5, which is the same value as that for the air/water system obtained by *Sakaki et al.* [2008; 2011].

By using this fitting parameter, the Glycerol-water mixture saturation was determined from the ECH₂O EC-5 sensors. Table 4.4 lists the irreducible saturation S_i and residual saturation S_r which were obtained from the dielectric sensor method for Soltrol 220/Glycerol-water system and compared these results with one obtained for the air/water system from *Smits and Limsuwat* [2009].

In addition to the S_i and S_r values, SOLVER EXCEL 2007 was utilized to estimate the fitting parameters of van Genuchten model α , n , and m from the $P_c - S_w$ data, which was obtained from the dielectric sensor method to represent the $P_c - S_w$ curve of the van Genuchten model. The fitting parameters of α , n , and m were estimated for both drainage and imbibitions processes. Also, the maximum water content and the residual water content from the Soltrol

220/Glycerol-water mixture system were used to estimate the fitting parameters. Table 4.5 shows the result of the van Genuchten parameter for the both drainage and imbibitions processes.

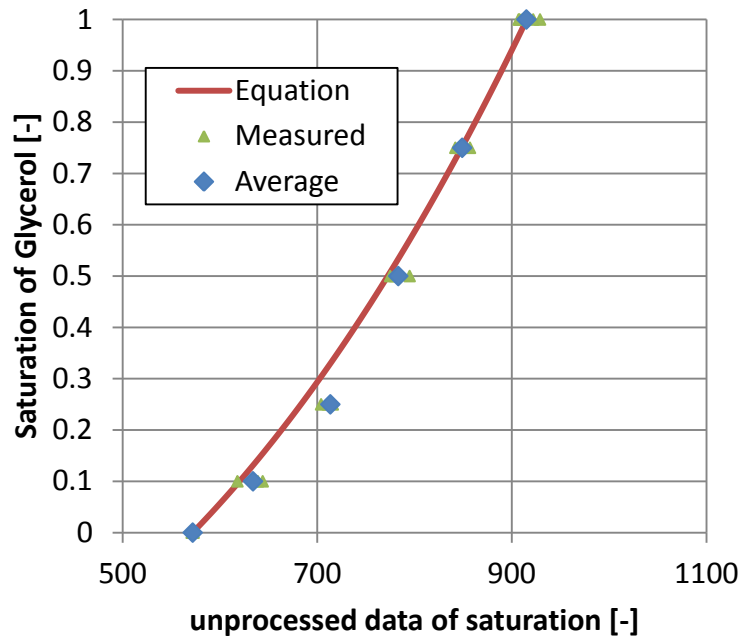


Figure 4.6 α -mixing model compared with the experimental data

Table 4.4 Comparison of S_i and S_r value between air/water and Soltrol 220/Glycerol-water system

Accusand		air/water	Soltrol 220/Glycerol-water
#12/20	S_i	0.054	0.104
	S_r	0.827	0.857
#20/30	S_i	0.082	0.056
	S_r	0.712	0.734
#30/40	S_i	0.084	0.076
	S_r	0.725	0.739
#40/50	S_i	0.087	0.040
	S_r	0.812	0.836
#50/70	S_i	0.079	0.088
	S_r	0.703	0.703

The limitation for the dielectric sensor method is it cannot take many measurement points to represent the shape of the curve. This is because that the sensor has the measurements influence to the volume of 0.3 L and the capillary pressure between the Glycerol-water mixture and Soltrol 220 can be only adjusted by increasing the head for a cm. Therefore, the experimental apparatus is not suitable to measure the small differences in capillary pressure, especially the uniform sands like Accusand has a flat slope for the $P_c - S_w$ curve so the saturation reaches the irreducible saturation in 200 – 400 Pa after it passes the displacement head pressure and only 3 – 5 points were able to measure to characterize the slope of the curve. Besides the dielectric sensor measured the residual saturation and irreducible saturation of the test fluids and sands, successfully.

4.2.4 Discussion of the $P_c - S_w$ relationships obtained with different methods

From Leverett scaling and the entry pressure scaling, the $P_c - S_w$ relationships were determined. However, the concern for these scaling methods was that the scaling factor can only scale the $P_c - S_w$ relationships in the vertical scale (along the Y-axis). Thus, the residual saturation and irreducible saturation may not be accurately determined using this scaling factor. Therefore, the dielectric sensor method was applied in order to measure these two saturations. In Appendix A, the $P_c - S_w$ relationship, which obtained from three different methodologies are shown, and the van Genuchten model is demonstrated by using the parameters in Table 4.5.

In addition, Table 4.6 represents the van Genuchten parameters for $P_c - S_w$ relationships Soltrol 220/Glycerol-water mixture system except it used the residual and irreducible saturation obtained from the air/water phase.

For the irreducible and residual saturation, slight differences were observed between the air/water and Soltrol 220/Glycerol-water mixture. Table 4.4 indicates the value of the irreducible saturation and the residual saturation for both the air/water and Soltrol 220/Glycerol-water systems. By comparing the results of all five Accusands, the irreducible saturation had more differences compared to the residual saturation. The irreducible saturation was one of the parameters which need to be provided to simulate the numerical model; therefore, it is important to incorporate these differences. Also, the results of the differences in irreducible and residual

saturation for the two systems express that Leverett scaling and the entry pressure scaling method did not provide all the data needed to simulate the behavior of scCO₂.

Table 4.5 Fitted van Genuchten parameters for the P_c - S_w relationships for the Soltrol 220/Glycerol-water mixture system

Accusand		Residual Water Content [-]	Maximum Water Content [-]	α [1/cm]	n [-]	m [-]
#12/20	drain	0.033	0.318	0.29	20.24	0.95
	imbibition	0.033	0.272	0.85	15.54	0.94
#20/30	drain	0.018	0.320	0.29	6.61	0.85
	imbibition	0.018	0.235	2.03	2.45	0.59
#30/40	drain	0.025	0.325	0.21	6.56	0.85
	imbibition	0.025	0.240	0.60	4.59	0.78
#40/50	drain	0.013	0.334	0.17	4.47	0.78
	imbibition	0.013	0.279	0.36	3.50	0.71
#50/70	drain	0.030	0.340	0.10	5.05	0.80
	imbibition	0.030	0.239	0.54	3.03	0.67

Comparing the van Genuchten parameter listed in Table 4.5 and 4.6, slight differences can be seen, although both represent the similar curve except the irreducible saturation and residual saturation points.

The result shows Leverett scaling have potential for obtaining the P_c – S_w relationships for scCO₂/brine system. However, the irreducible saturation and the residual saturation may need to be separately addresses and measured to obtain better P_c – S_w curve. Above findings were obtained under limited condition (fluid combination, sandy material). For evaluating the methods applicability for actual scCO₂ and brine system, further study is needed.

Table 4.6 Fitted van Genuchten parameters for the P_c - S_w relationships for the Soltrol 220/Glycerol-water mixture system by using the residual/irreducible saturation obtained from the air/water system

Accusand		Residual Water Content [-]	Maximum Water Content [-]	α [1/cm]	n [-]	m [-]
#12/20	drain	0.017	0.312	0.25	357.45	1.00
	imbibition	0.017	0.258	1.45	2.46	0.59
#20/30	drain	0.027	0.330	0.29	7.30	0.86
	imbibition	0.027	0.235	48.42	2.01	0.50
#30/40	drain	0.028	0.334	0.21	6.77	0.85
	imbibition	0.028	0.242	0.59	4.91	0.80
#40/50	drain	0.029	0.335	0.17	5.08	0.80
	imbibition	0.029	0.272	0.35	4.23	0.76

CHAPTER5 – DETERMINATION OF $K_R - S_w$ RELATIONSHIPS

The van-Genuchten and Mualem model is one of the most popular models to characterize the $k_r - S_w$ relationship. However, based on the literature review, the van-Genuchten and Mualem model was developed for the agricultural soils and its applicability to the test sands used in this study is still unclear. Moreover, taking measurements of the relative permeability curve is difficult because it requires complex experimental setup and time consuming. Most of the previous studies were conducted to measure the $k_r - S_w$ relationship with the water-air system and neglected the air phase flow. So, they did not show any $k_r - S_w$ relationship of the non-wetting phase. The preliminary modeling results from *Cihan et al.* [2011] used the experimental data of tank experiment suggest that these estimated relative permeability relationships did not represent the observed $scCO_2$ behavior in the tank experiment.

5.1 Description of $k_r - S_w$ measurement

This study investigated the two-phase flow of the Glycerol-water mixture and Soltrol 220, so the non-wetting phase relative permeability curve cannot be neglected. The purpose of measuring the $k_r - S_w$ relationship independently from the van-Genuchten and Mualem model was to observe whether there are any differences between the van-Genuchten and Mualem model and the experimental results and to investigate the hysteresis of the $k_r - S_w$ curve.

5.1.1 The van-Genuchten – Mualem Model

Table 2-1 shows the equations for van-Genuchten and Mualem model and often 0.5 is used for η value. The van Genuchten – Mualem model was fitted to five Accusand samples by using the van Genuchten parameter of m from Table 4.5. The parameter m for drainage and imbibitions process was used respectively, in order to demonstrate the hysteresis of the $k_r - S_w$ relationship.

5.1.2 The Long Column Method

The long column method was developed by *Corey* [2002] to demonstrate the k_r-S_w relationships for the wetting phase. The experiment was established for the homogeneous packing of the long vertical column. The concept of this method is to have a steady downward flow with uniform capillary pressure and saturation. Therefore, the experimental method is assumed to have a uniform hydraulic gradient which is $dh/dL = 1$, and a hydraulic conductivity is equal to the flux flow. The relative permeability is measured from the outflow rate of fluid by substituting the outflow rate into equation 2.4 for the wetting phase and equation 2.5 for the non-wetting phase. The requirement of the long column method is that the whole column has to be homogeneous.

Figure 5.1 shows the experimental setup of the long column experiment. The long-column experimental setup [*Corey*, 2002] consisted of a 95-cm-long acrylic pipe with two ECH₂O EC-5 soil moisture sensors and two tensiometers, which were hydrophilic and only measured wetting fluid pressure head. The EC-5 soil moisture sensors were located a 40 cm apart while tensiometers were located at 30 cm and 70 cm from a bottom of the column. The tensiometers and EC-5 sensors were applied to obtain the precise data of the head differences and the saturation in the system. The top of column is open to the atmosphere and the bottom of the column is connected to the constant-head device. The height of the constant-head device is at the same level where the end of the column is. The glycerol-water mixture saturated sand was tightly packed uniformly throughout the column and at the top and bottom of the column had about 5 cm of gravel layer in order to distribute the both fluids uniformly. The Glycerol-water mixture saturated sand was packed into the 80 cm column. Both the wetting and non-wetting phases were injected from the top of the column by the Mariotte's bottles. The injection rates of both fluids were adjusted by using needles which were connected to the Mariotte's bottle. In the beginning of the experiment, in order to get the intrinsic permeability k_i of the system, only the Glycerol-water mixture was applied to measure the outflow rate of the Glycerol-water mixture. Darcy's law was used in order to get the saturated hydraulic conductivity K_s value using the head difference measurements from the tensiometers and calculated the k_i using equation 5.1.

$$K_s = \frac{k_i \rho_{glycerol-water} g}{\mu_{glycerol-water}} \quad (5.1)$$

where subscripts shows the Glycerol-water mixture.

The k_i is the unique value of the porous medium and it is not dependent on the fluid combinations. The estimated k_i values were compared with the one calculated from the hydraulic conductivity of the air-water system [Smits and Limsuwat, 2009] which is indicated in Table 3.4 to evaluate a packing of long column is tight enough to get similar k_i values. In order to examine the hysteresis behavior of the relative permeability curve, a larger ratio of the Glycerol-water mixture to the Soltrol 200 was applied at the top of the column and was increased incrementally by the amount of the Soltrol 200 until only the Soltrol 200 was injected into the column for the drainage process. Once the column was saturated with Soltrol 200, the imbibitions process started increasing the fraction of Glycerol-water mixture to Soltrol 200 until only the Glycerol-water mixture was injected into the column. During the experiment, the saturation and the head difference between the two tensiometers were measured simultaneously to see the constant head gradient and the uniform saturation was maintained inside the column.

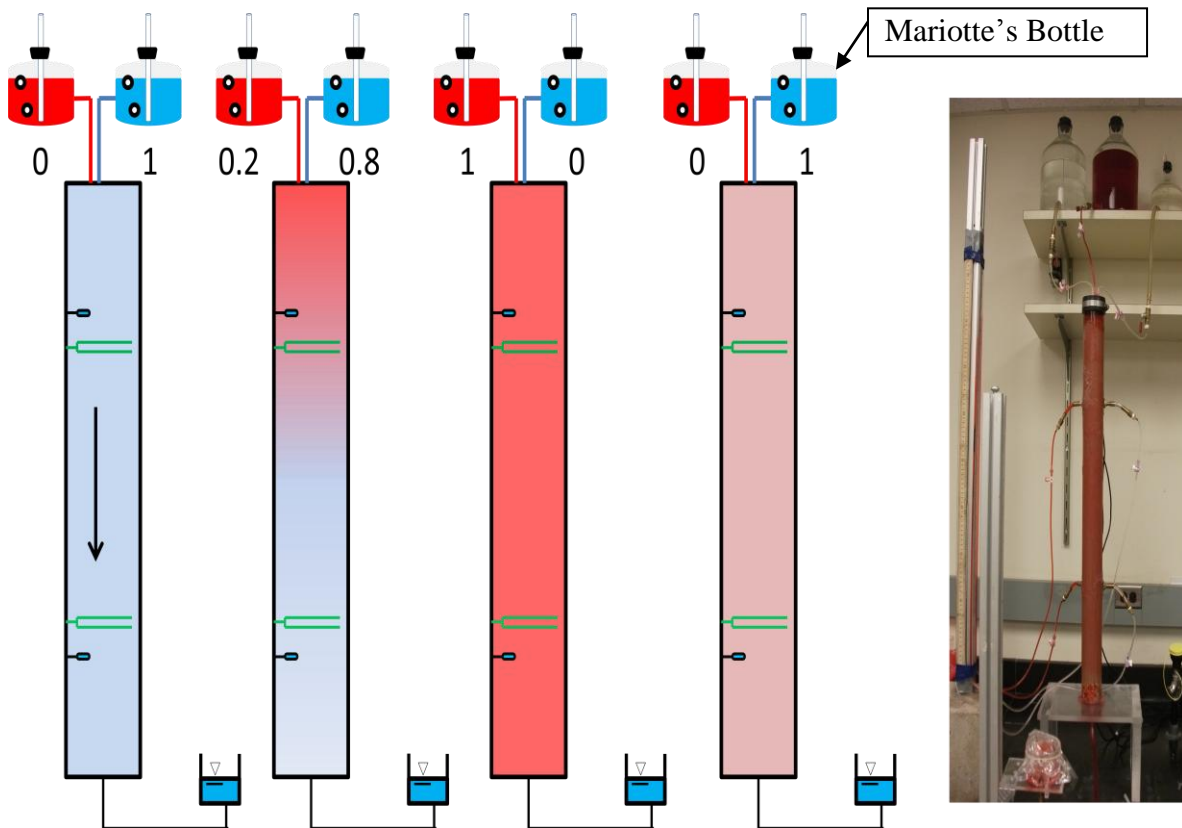


Figure 5.1 Experimental setup of Long Column Experiment

5.1.3 Hydrostatic Method

Dane et al. [1998] developed a new methodology to measure the non-wetting phase relative permeability. The theory of the method is to conduct an experiment in a hydrostatic condition so that a vertical steady state flow is maintained in the entire porous medium and the column has the uniform capillary pressure throughout the domain. Therefore, when the wetting phase is at hydrostatic and the capillary pressure of the non-wetting phase is constant, the driving force of the non-wetting phase is the density differences between the two fluids. The limitation of this theory is that it cannot use liquids which have similar densities. The proposed method which they have used to measure the relative permeability for the non-wetting phase is shown in the following paragraph.

The flow equations for the wetting and non-wetting phase are

$$q_w = -\frac{k_w}{\mu_w} \frac{\partial P_w^*}{\partial z} = -\frac{k_w}{\mu_w} \frac{\partial}{\partial z} [P_w + \rho_w g h] \quad (5.2)$$

$$q_{nw} = -\frac{k_{nw}}{\mu_{nw}} \frac{\partial P_{nw}^*}{\partial z} = -\frac{k_{nw}}{\mu_{nw}} \frac{\partial}{\partial z} [P_{nw} + \rho_{nw} g h] \quad (5.3)$$

where q is flux [cm/s], k is effective permeability [cm²], μ is viscosity [Pa s], P is pressure [Pa], z is vertical coordinate [cm], P^* is piezometric pressure [Pa], ρ is density [g/cm³], and g is gravity [m/s²].

The experiment was conducted under the hydrostatic condition for the wetting phase and the vertical steady state flow was maintained for the non-wetting phase; therefore, steady P_c and saturation S values were expected throughout the sample. At the steady state flow, the top and bottom of the column has the same P_c ; therefore,

$$\left. \frac{\partial P_{nw}^*}{\partial z} \right|_{top} = \left. \frac{\partial P_{nw}^*}{\partial z} \right|_{Bottom} \quad (5.4)$$

Also, the wetting phase is hydrostatic:

$$\frac{d}{dz} [P_w + \rho_w g h] = 0 \Leftrightarrow \frac{dP_w}{dz} = -\rho_w g \quad (5.5)$$

The capillary pressure is defined as $P_c = P_{nw} - P_w$, so

$$\frac{dP_c}{dz} = \frac{dP_{nw}}{dz} - \frac{dP_w}{dz} \quad (5.6)$$

And the P_c is steady at the top and bottom of the column; therefore,

$$\left. \frac{dP_c}{dz} \right|_{top} = \left. \frac{dP_c}{dz} \right|_{Bottom} \quad (5.7)$$

By substituting the above equation into the non-wetting phase equation,

$$q_{nw} = -\frac{k_{nw}}{\mu_{nw}} \left[\frac{dP_c}{dz} + (\rho_{nw} - \rho_w)g \right] \quad (5.8)$$

where, q_{nw} is constant when $\frac{dP_c}{dz} = 0$, so

$$q_{nw} = -\frac{k_{nw}}{\mu_{nw}} (\rho_{nw} - \rho_w)g \quad (5.9)$$

From this equation, the driving force of the non-wetting phase is only the density differences between the two fluids when the wetting phase is hydrostatic and the capillary pressure of the non-wetting phase is at constant.

Figure 5.2 shows the experimental setup of the hydrostatic method. A 6cm tall Ceramic cylinder was glued to both end ridges of the 6.5 cm tall Teflon cylinder. The ceramic cylinder was hydrophilic and impermeable to the non-wetting fluid. The Teflon/Ceramic cylinder was closed with Teflon caps which had threads rods and wind nuts. Both caps had the O-rings which prevent fluids from leaking. Both top and bottom cap had the meshes to prevent the sand from going through the tubing. The cavity between the Teflon/Ceramic cylinders was filled with the wetting fluids and the P_w was changed by altering the height of the constant-head device which connected to the cavity. The non-wetting fluid was introduced to the column from the bottom to the top by using a Mariotte's bottle at the constant head. The non-wetting fluid outflow rate was measured from the column.

Figure 5.2 shows the experimental setup of the hydrostatic method with the corresponding heights. The non-wetting phase entered from the bottom of the column and drained from the top of the column. By estimating the pressure at the top of the column for both the wetting and non-wetting phase:

$$P_{nw}(Z = B) = \rho_{nw}gH_1 \quad (5.10)$$

$$P_w(Z = B) = -\rho_wgx \quad (5.11)$$

So, the capillary pressure is,

$$P_c(Z = B) = P_{nw} - P_w = \rho_wgH_1 + \rho_wgx \quad (5.12)$$

Also, the bottom of the porous column is calculated:

$$P_{nw}(Z = A) = (6.5 - y)\rho_{nw}g \quad (5.13)$$

$$P_w(Z = A) = -(x - 6.5)\rho_wg \quad (5.14)$$

Therefore,

$$P_c(Z = A) = P_{nw} - P_w = (6.5 - y)\rho_{nw}g + (x - 6.5)\rho_wg \quad (5.15)$$

From the theory, the capillary pressure of the top and bottom of the column should be equal,

$$\rho_{nw}gH_1 + \rho_wgx = (6.5 - y)\rho_{nw}g + (x - 6.5)\rho_wg \quad (5.16)$$

$$y = 6.5 \times \left(1 - \frac{\rho_w}{\rho_{nw}}\right) - H_1 \quad (5.17)$$

From the following equation, H_1 is arbitrary, so y is the function of the H_1 . In this case, the $H_1 = 1.3$ cm; therefore, $y = -4.2$ cm.

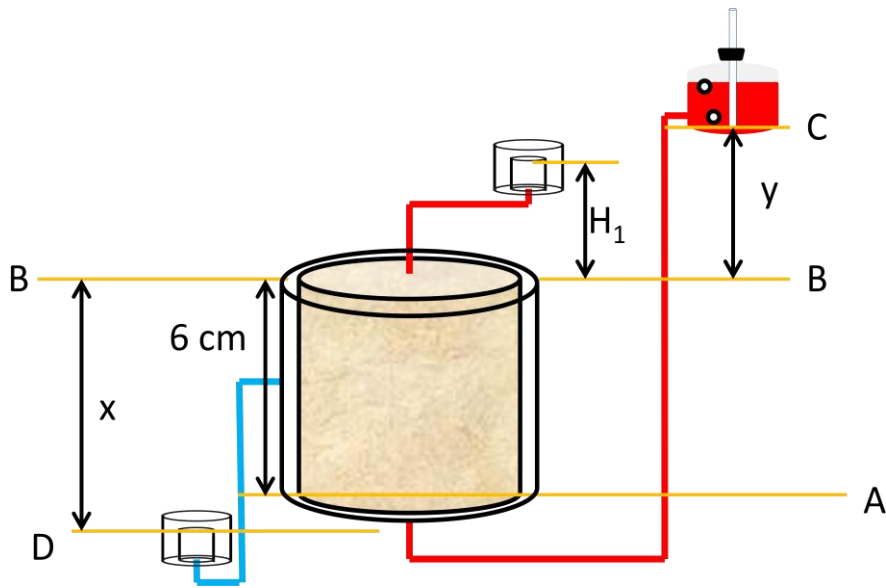


Figure 5.2 Hydrostatic Method

During the experiment, the wetting phase should not come out from the top of the column. Also, the pressure of the non-wetting phase should not exceed the pressure of the wetting phase; in other words, it has to have the positive P_c value for at all times. Moreover, the P_c was changed by alternating the elevation of the constant head device which connected to the cavity. By increasing the x value, the P_c value increased simultaneously. The saturation inside the column was measured by estimating the out mass of the wetting fluid. Also, the inflow rate of the non-wetting phase was constant throughout the column by maintaining the elevation of y and constantly supplying the non-wetting fluid from the Mariotte's bottle. The column was wet packed with Glycerol-water mixture in order to avoid the intrusion of air inside the column. The relative permeability curve was calculated from the flow rate by using the following equation:

$$q_{nw} = -\frac{k_{nw}}{\mu_{nw}}(\rho_{nw} - \rho_w)g \quad (5.5)$$

k_{nw} is the effective permeability, so the intrinsic permeability k_i has to be calculated from the saturated hydraulic conductivity equation for the air-water phase. The relative permeability for the non-wetting phase is calculated by using equation (2.8).

The column was wet packed with Glycerol-water mixture in order to avoid the intrusion of air inside the column. At the same time, the top and the bottom of the column have to be filled with Soltrol 220; this method requires some tips for packing the fluids. First, the tube which connected at the bottom of the column needs to be fully saturated with Glycerol-water mixture to fulfill the wet packing condition. After the sand is packed, the Soltrol 220 is applied for 1 ml at the top of the column and close with the cap. At this time, the cap is connected to the tube which filled with Soltrol 220. The next step, the column is flipped and the tube which is saturated with Glycerol-water mixture has to be disconnected then the column is again connected to the tube which comes out from the Mariotte's bottle filled with Soltrol 220. When connecting the tube, it needs to avoid the air entry. At last, the column is flipped back to the same position and the experiment can be started.

5.2 The results of the $k_r - S_w$ relationship

For the measurement of $k_r - S_w$ relationships, Glycerol-water mixture of 5:5 by weight is applied instead of an 8:2 ratio by weight. By changing the concentration of the Glycerol-water mixture, the viscosity drops by an order of magnitude, and it makes the flow rate faster; therefore, the column reaches the steady state condition faster than using the Glycerol-water mixture 8:2 by weight. Table 5.1 shows the property of the Glycerol-water mixture 5:5 and 8:2 by weight.

Table 5.1 Properties of Glycerol-water mixture

	Density [g/cm^3]	Viscosity [Pa s]	σ [dyn/cm]
Glycerol-water (8:2)	1.21	0.06086	21.0
Glycerol-water (5:5)	1.13	0.00600	20.4

The reason that Glycerol-water mixture of 5:5 can be used instead of 8:2 is that the saturation, porous medium, temperature, interfacial tension, and capillary number are the factors which characterize the relative permeability curve for the two phase flow system [Fulcher *et al.*, 1985; Kumar *et al.*, 1985; Brooks and Purcell, 1952; Shen *et al.*, 2006]. Shen *et al.* [2006] indicated that the interfacial tension has an impact on the relative permeability, and they observed the characteristics of the relative permeability changes significantly with different interfacial tensions. From Table 5.1, the interfacial tension is almost the same between Soltrol 220/Glycerol-water (8:2) and Soltrol 220/Glycerol-water (5:5), so this study can eliminate the impact from the interfacial tensions.

Table 5.2 Capillary Number

	Capillary Number [-]	
	Glycerol-water (8:2)	Glycerol-water (5:5)
#12/20	2.63E-07	2.46E-07
#20/30	1.61E-07	1.50E-07
#30/40	7.42E-08	6.93E-08
#40/50	3.64E-08	3.40E-08
#50/70	2.03E-08	1.90E-08

In addition, the capillary number is listed in Table 5.2 for five Accusands with the Glycerol-water mixture of 8:2 and 5:5. The saturated hydraulic conductivity of the wetting fluid was used to calculate Capillary number. By contrasting the obtained data, all of them are in the same order of magnitude and have similar values. Moreover, Capillary number is the dimensionless number describing which forces dominate in porous media. According to *Krevor et al.* [2012] capillary number N_c which has a larger value than 10^{-6} has an impact on the relative permeability curves. Table 5.2 shows $N_c \ll 10^{-6}$; therefore, the assumption was made that the relative permeability curves for the Glycerol-water mixture of 8:2 and 5:5 by weight do not show any differences.

5.2.1 The results of the long column method

Due to the limitation of the experimental setup, the long column experiment is not applicable for the coarse sands; therefore, the relative permeability of Accusand #12/20 and #20/30 for the Glycerol-water mixture cannot be measured. This is because the flow rate is too fast and the supply from Mariotte's bottle cannot be adjusted to fulfill this flow rate. Also, the long column method is not applicable to measure the high Glycerol-water saturation range because the Soltrol 220 is not continuous inside the column and it never reaches the steady state condition. In the earlier stage of the experiment, the long column was also intended to measure the relative permeability for the non-wetting phase, however, it was failed because the non-wetting phase was not continuous inside of the tube which connects the column and the constant head device and it proves that it cannot apply the Darcy's law.

To present the applicability of the Glycerol-water mixture of 5:5 for this study, the long column experiments were conducted for both Soltrol 220/Glycerol-water (8:2) and Soltrol 220/Glycerol-water (5:5) system. Figure 5.3 displays the obtained relative permeability data for both Glycerol-water mixture of 8:2 and 5:5 for Accusand #30/40. Also, the van Genuchten – Mualem model was demonstrated for both drainage and imbibitions by using the van Genuchten parameter which is listed in Table 4.5.

Figure 5.3 shows that both fluids have nearly the same trends of the curve. These experimental data prove that when the fluid has the same porous medium, interfacial tension, and

capillary number less than 10^{-6} , it will show the similar relative permeability curves. As shown in Figure 5.3, there are differences between the van Genuchten – Mualem model and the experimental data. The van Genuchten – Mualem and Brooks and Corey – Burdine models are developed for the agricultural soils; therefore, the Brooks and Corey – Burdine and van Genuchten – Mualem models might not represent the characteristic of the relative permeability for the sands materials. From the report of *Irmay* [1954] and *Hausenberg and Zaslavsky* [1963], the relative permeability curve for the uniform pore-size sand grains shifts the relative permeability curve to the left and Figure 5.3 represents the same trend by comparing the experimental data with the drainage curve of the van Genuchten – Mualem model. So it can be said that the long column measures the relative permeability curve appropriately and the van Genuchten – Mualem model is not applicable to represents the $k_r - S_w$ relationships of test sands and fluids which used in this project.

Hysteresis behavior was not able to see from Figure 5.3. The van Genuchten – Mualem model also did not represent any hysteresis; therefore, the wetting phase relative permeability did not need to consider the hysteresis behavior. Moreover, the irreducible saturation and residual saturation values did not match with the one obtained from the dielectric sensor method. Often, the long column underestimated the residual saturation value. This is due to the experimental setup that the column takes too long time to reach the residual saturation.

5.2.2 The result of the hydrostatic method

The non-wetting phase relative permeability of Accusand #30/40, #40/50, and #50/70 were measured using the hydrostatic method. *Irmay* [1954] only suggested the relative permeability curve of the wetting phase because he only considered the air-water system. However, this study focuses on the two phase flow system of Glycerol-water mixture and Soltrol 220; therefore, it is important to determine the relative permeability of Soltrol 220 to understand the behavior of the $scCO_2$. Figure 5.4 shows the non-wetting phase relative permeability of Accusand #30/40.

The figure represents that the experimental data has the significant difference compared to the van Genuchten – Mualem model. Therefore, the van Genuchten – Mualem model cannot be used to propose the relative permeability for the numerical model.

The measurements from the hydrostatic method did not well represent the hysteresis behavior of the non-wetting phase relative permeability. Especially, it was difficult to measure the imbibitions process from this experimental method due to the complex behavior of the two-phase flow system and moreover, the experiments took a long time to reach the steady state condition. Therefore, some of the data were missing for the imbibitions process due to the time limitation.

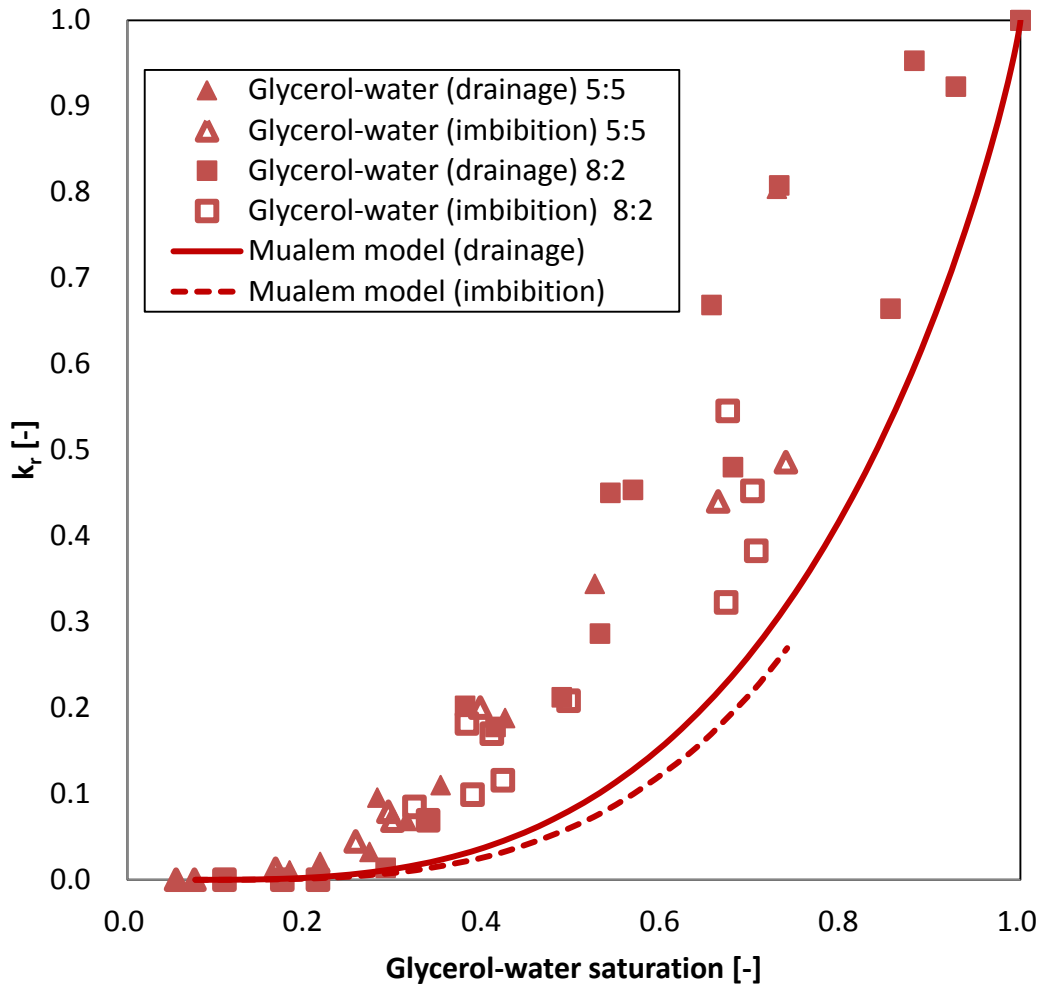


Figure 5.3 Comparison of the relative permeability for Glycerol-water mixture of 8:2 and 5:5 for Accusand #30/40

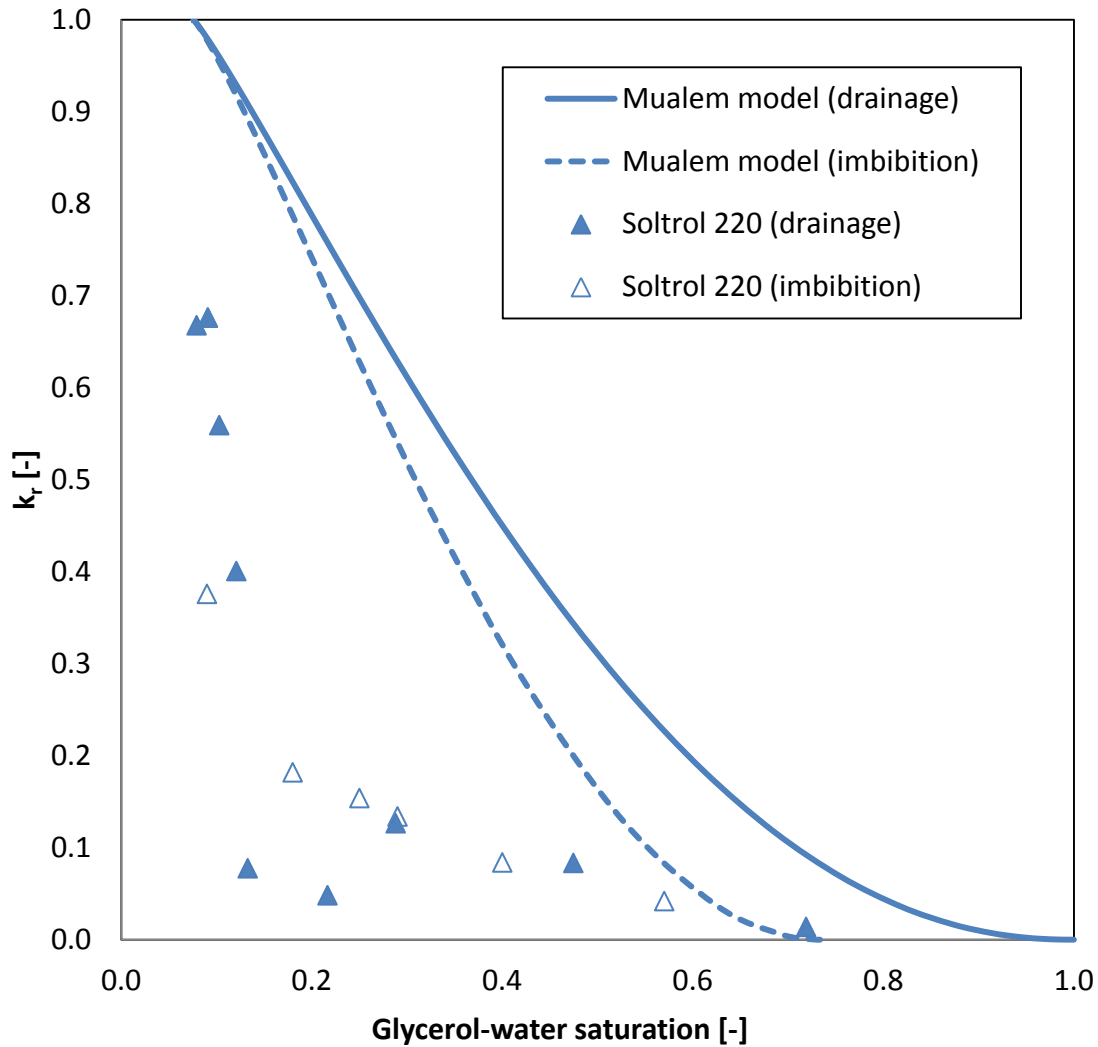


Figure 5.4 The non-wetting phase relative permeability for Accusand #30/40

5.2.3 Discussion of the $k_r - S_w$ relationship derived from two different methods

The $k_r - S_w$ relationships of Accusand #30/40, #40/50, and #50/70 were measured from the long column method and the hydrostatic method. The results of the long column method and the hydrostatic method show that the van Genuchten – Mualem model is not applicable to represent $k_r - S_w$ relationships and indicate that it is important to derive the relative permeability independently from the constitutive models. Furthermore, the relative permeability results concluded that there is no significant hysteresis behavior was found for both relative permeability curves. To propose the actual site investigation of $scCO_2$ /brine system, it is

essential to measure the relative permeability, although, the measurements for the imbibitions process can be neglected. Appendix B represents the relative permeability curve for the #40/50 and #50/70 sands.

In addition, the experimentally obtained relative permeability for both wetting non-wetting phase were compared with the actual relative permeability data of liquid CO₂/brine which was obtained from *Bennion and Bachu 2005*. They have measured several rock samples from the Wabamun Lake area, Alberta basin in Canada. From all these samples, Wabamun high permeable carbonate rock was picked to compare with the experimental data because it has high permeability compared to other rocks and it also had similar viscosity ratio to the surrogate fluid system. The figure 5.5 shows the comparison between Accusand Glycerol/water system and carbonate rock liquid CO₂/brine system.

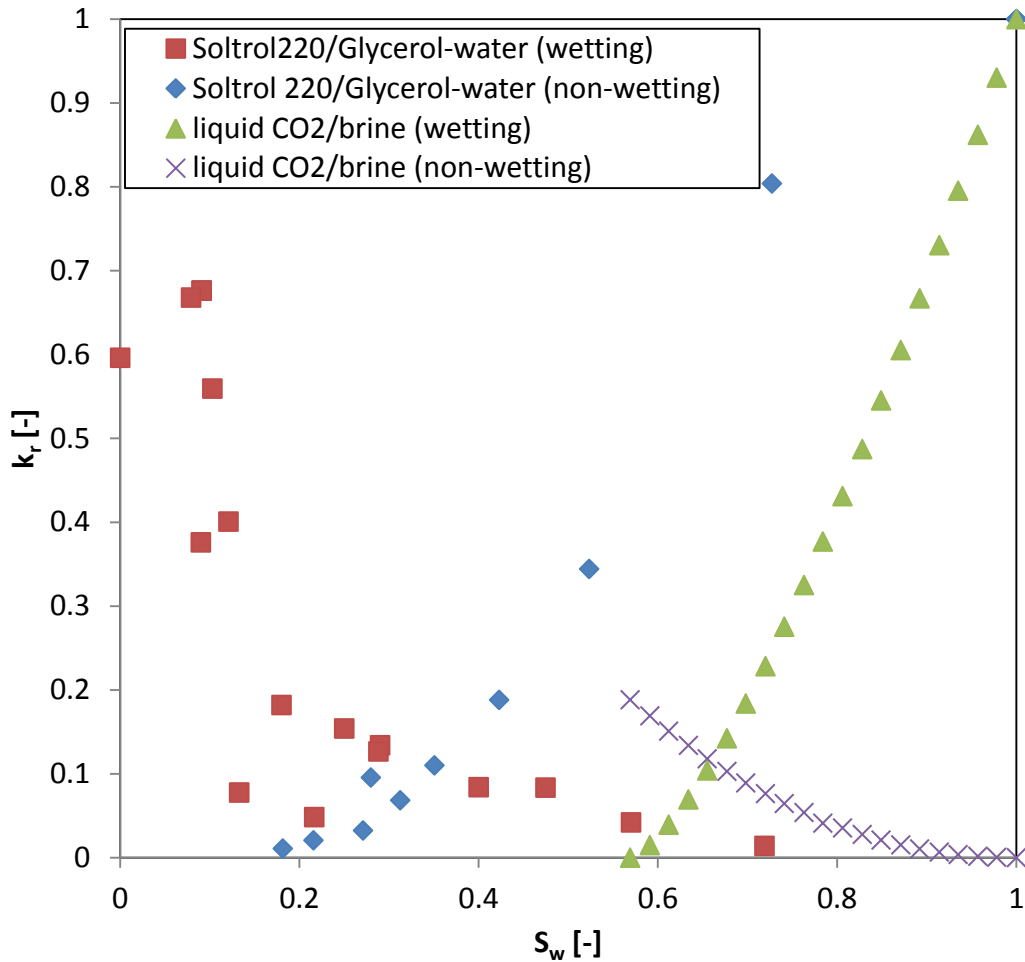


Figure 5.5 Comparison between the relative permeability data of Soltrol 220/Glycerol-water and liquid CO₂/brine systems

Comparing the two systems, it shows that the liquid CO₂/brine system has reached to k_r equals to 0 at very high saturation compared to the Soltrol 220/Glycerol-water system. This is because the core sample of carbonate rock has low permeability and porosity compared to Accusands. The relative permeability of carbonate rock was measured by laboratory coreflood experiment [*Bennion and Bachu, 2005*].

CHAPTER 6 – MODELING

The $P_c - S_w$ and the $k_r - S_w$ relationships were obtained from the experimental methods presented in the previous chapters for the test sands and fluids. In order to investigate the applicability of measured constitutive relationships, they were used as the material parameters as inputs to the numerical model and the model were used to simulate the tank experiment. The motivation for the model analysis is to investigate the applicability of the constitutive relationships obtained from the experiments to a tank experiment and to examine the impact of constitutive relationships on the two-phase flow system. In addition, the applicability of the constitutive models for the test sands and fluids were also examined.

6.1 The constitutive relationships in TOUGH2 T2VOC

TOUGH2 T2VOC was selected as the test code to simulate the tank experiment. The TOUGH2 T2VOC model was applied to the Glycerol-water phase by changing the hydraulic properties of the aqueous phase. Also, the hydraulic properties for the Soltrol 220 were used for the volatile organic compound in the model. Since Soltrol 220 is a non-volatile organic compound, the non-aqueous phase was treated as a non-volatile liquid. The model has the ability to use constitutive models for the capillary pressure – saturation and relative permeability – saturation relationships as inputs.

From the previous chapter, it was found that neither the wetting nor non-wetting fluid relative permeability derived from the van Genuchten – Mualem model fit the experimental data. Moreover, the column experiments showed that the irreducible and residual saturations in the test sands and fluids showed significant differences compared to the air/water system. Therefore, it is important to obtain these residual values separately.

Instead of using the van Genuchten – Mualem Model, the experimentally obtained $k_r - S_w$ data were used in the model simulations. The following equation shows the fitted curves for the $k_r - S_w$ relationships from the experimental data for both the wetting and non-wetting phase relative permeability.

$$k_r = 0.6436 \times S_w^2 + 0.48416 \times S_w - 0.12353 \quad (6.1)$$

$$k_{rn} = \frac{\left(\frac{1 - S_w}{1 - 0.076}\right)^{5.3}}{1.6} \quad (6.2)$$

T2VOC is a module to calculate the air, aqueous, and VOC phase. In this study, there is no gas phase; therefore, the relative permeability for the gas phase was considered to be 0 at all time.

Figure 6.1 shows the comparison between the fitted relative permeability curves and experimentally obtained data using Accusand #30/40. The figure shows both the wetting and non-wetting relative permeability data obtained from the long column method and the hydrostatic method for the drainage process. Also, the van Genuchten – Mualem model and the fitted relative permeability curves for both phases were compared. To draw the curve for the van Genuchten – Mualem model, the van Genuchten parameters were used. These parameters were obtained from the van Genuchten model, which was fitted to the results from the dielectric sensor method.

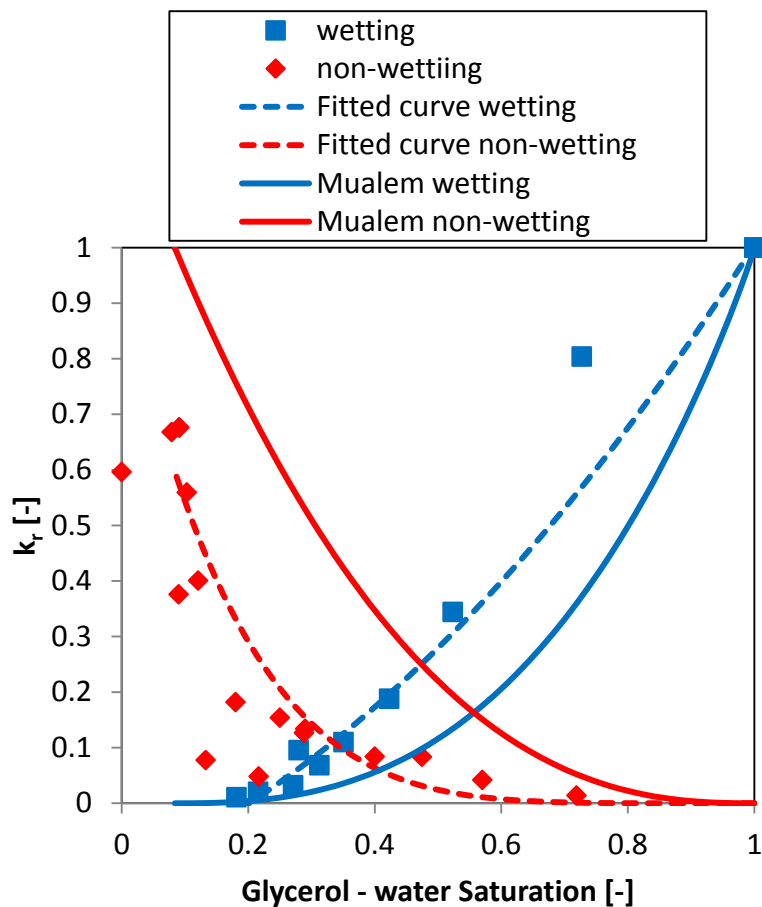


Figure 6.1 Comparison between fitted curve and van Genuchten – Mualem model

6.2 Tank experiment

This section describes the experimental design of the tank experiment. Also, TOUGH2 T2VOC was used to simulate this tank experiment using the constitutive relationships which obtained from the constitutive models and the column experiments. The tank experiment was not conducted by the author of this thesis. The data was generated by *Trevisan et al.* [2013]. More details of the experiments can be found in *Trevisan et al.* [2013]. All experimental methods were developed by him and the data he generated was used in the model comparison.

6.2.1 Design of tank experiment

The tank experiment was designed by *Trevisan et al.* [2013]. The tank has its dimensions 5.6 cm, by 90.0 cm, by 60.0 cm in the x, y, and z axis, respectively. The well is located at the left corner of the tank and it is a cylinder of 3.2 cm diameter and 12.3 cm height. The right bottom of the tank was connected to an external constant-head device to maintain the Glycerol-water mixture at a predetermined head. Accusand #30/40 homogeneous case experiment was conducted. At first the tank was wet packed with Glycerol-water mixture. Accusand #30/40 was packed inside of the tank about 16.5 cm thick and #110 sand was packed at the top of Accusand for about 30 cm thick to replicate the cap rock condition. The dip angle of the interface between Accusand #30/40 and #110 sand was 2.0° . Gravel was packed to fill the space between Accusand and the end walls of the tank. Also, #110 sand was placed at the left side of the well to prevent Soltrol 220 from migrating to the left end of the tank. Figure 6.2 shows the design of tank experiment.

An X-ray system was used to measure the saturation of the non-wetting fluids in the tank. 480 points were picked to measure the saturation in the Accusand #30/40. Figure 6.3 shows the points where the saturation measurements were taken from the X-ray system.

Marriotte's bottle is connected at the bottom of the well and it was located above 45 cm of wet-packed sands. The bottle is filled with Soltrol 220. The weight of the fluid in the Mariotte's bottle was measured as a function of time using electronic balance and, the outflow mass of Glycerol-water mixture was measured. The average injection rate of Soltrol 220 was

$1.17 \cdot 10^{-8} \text{ m}^3/\text{s}$ and the injection was stopped after 5.5 hours. The cumulative volume of injected Soltrol was about 240 ml.

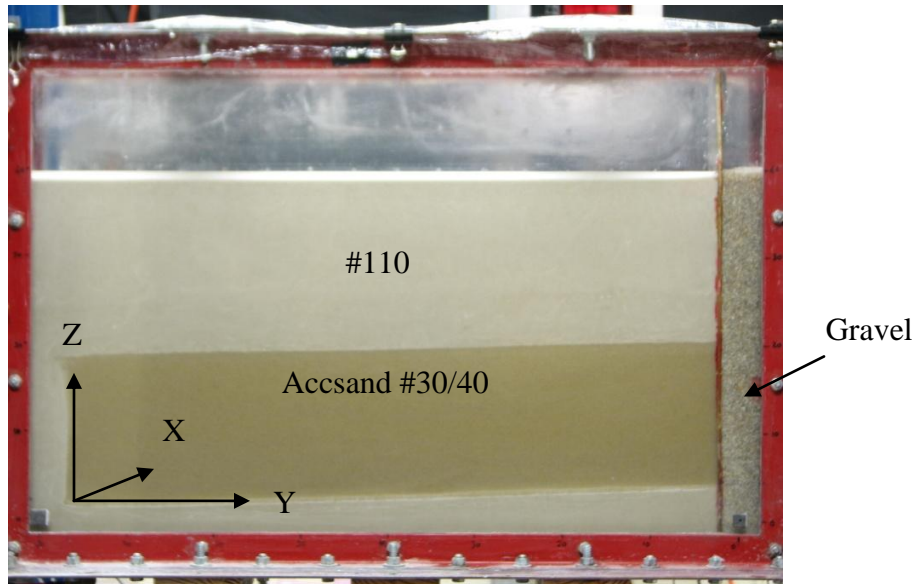


Figure 6.2 Design of the tank [Trevisan *et al.*, 2013]

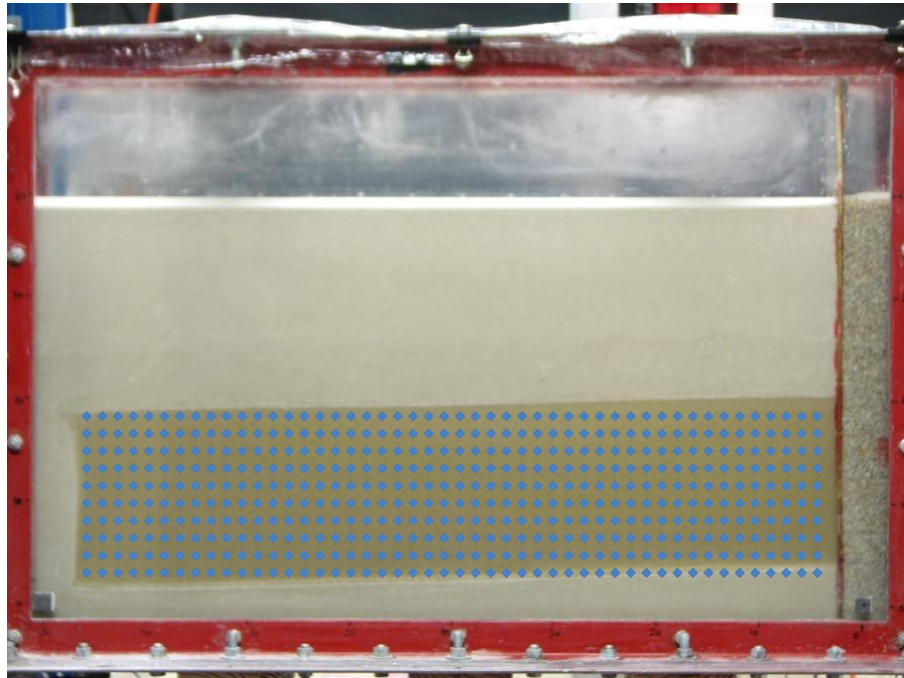


Figure 6.3 Saturation points taken from X-ray system [Trevisan *et al.*, 2013]

6.2.2 Numerical modeling of tank experiment

TOUGH2 T2VOC model was used to simulate the tank experiment with Accusand #30/40 packed in a homogeneous configuration. Codes MESHMAKER and AssignROCK were used to make the model grid. The model only made the grid for Accusand #30/40 because the #110 sand conditions can be made only to assign the properties of the top and bottom of the sand to be no-flow. Each grid block was designed to have dimensions 5.6 cm, by 1.0 cm, by 1.0 cm. In addition, at the top and bottom of the grid block of the tank was made to have no-flow to prevent Soltrol 220 to go out from the tank domain and replicate the cap rock. The grid has 1276 elements and 2458 connections. The schematic and dimensions of tank is given in Figure 6.4 and 6.5.

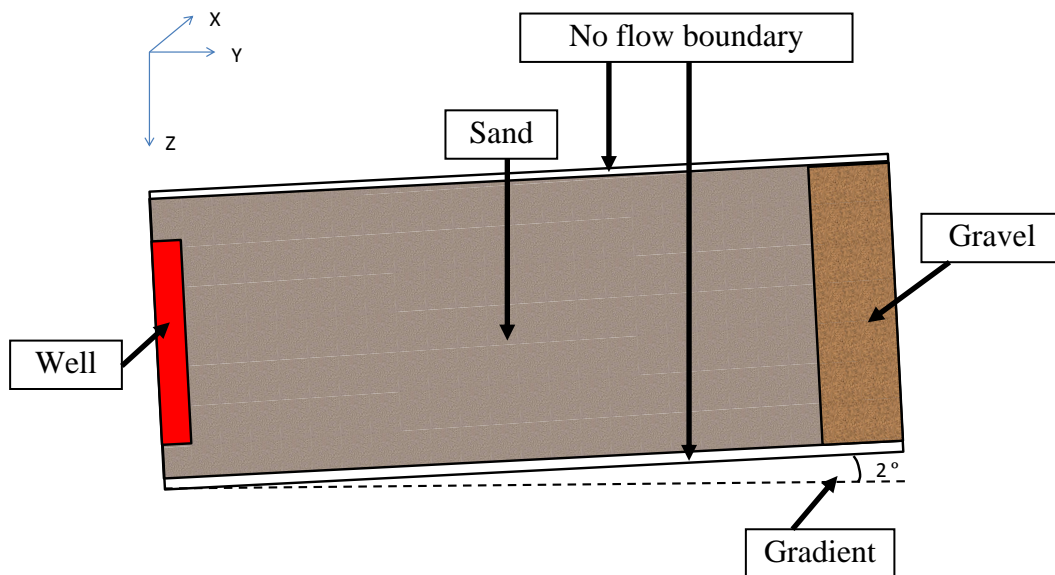


Figure 6.4 Schematic of the tank

First, the plume propagation in the tank experiment was simulated using the numerical model until the propagation stopped. The atmospheric pressure for 101,590 Pa at an elevation of 1767 m (Denver area) and gravitational acceleration of 9.7960 g/m² were used in the simulations. The tank experiment had #110 sand on top of Accusand #30/40 for 30 cm to replicate the cap rock. Therefore, the numerical model needed to consider the height of #110 when calculating the hydrostatic pressure of the tank. In order to create the hydrostatic pressure distribution, the top and the bottom of the Accusand #30/40 were calculated to have the pressure of 104,400 Pa and

106,300 Pa, respectively. The hydraulic properties of the Glycerol-water mixture and Soltrol 220 were provided as inputs to TOUGH2 T2VOC model.

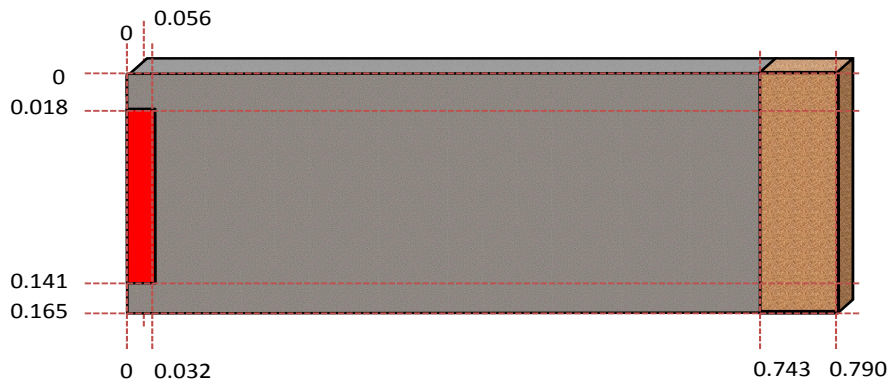


Figure 6.5 Extent of the tank

After the model obtained the steady state condition which is the condition that no longer the primary variables of pressure, saturation, mole fraction, and temperature is changed, Soltrol 220 was started to inject at the flow rate of $1.17 \times 10^{-8} \text{ m}^3/\text{s}$ for 5.5 hours. Soltrol 220 was injected into only the top grid of the well. This is because that Soltrol 220 is lighter than the Glycerol-water mixture and during the actual i tank experiment; the injected Soltrol 220 seems to be only coming out from the top of the well due to the density differences. The initial condition of this simulation was employed the last step of the steady state condition before injecting the Soltrol 220. The table 6.1 shows the parameters of the sand properties and van Genuchten parameters of the constitutive models. The reason that the $k_r - S_w$ relationships for the column experiment do not have the parameters is because they are not depending on the van Genuchten parameters. The $k_r - S_w$ relationships for the column experiment have fitted curves which shown in equation 6.1 and 6.2.

During the simulation of Soltrol 220 injection, the constitutive relationships of the $P_c - S_w$ and $k_r - S_w$ were applied as the material parameters. **Simulation 1** used the constitutive

relationships obtained from the column experiments for the test fluids and sands. The simulation used the van Genuchten parameters obtained from the dielectric sensor method fitted to the van Genuchten model for the $P_c - S_w$ relationships. For the $k_r - S_w$ relationships, the curve was fitted to the experimentally obtained data. **Simulation 2** used the van Genuchten model to present the $P_c - S_w$ relationships with the S_i and S_r value for the air/water system. Also, for the $k_r - S_w$ relationships, it uses the van Genuchten – Mualem model.

The simulation results were compared to the actual tank experiment results and investigated which simulation captured the experimental observation better.

Table 6.1 Material parameters for the model

	$P_c - S_w$			
	S_m [-]	n [-]	α_{gn} [1/m]	α_{nw} [1/m]
Accusand #30/40 from column experiments	0.076	6.56	1.00	21.00
Accusand #30/40 from constitutive models	0.084	6.77	1.00	21.00
#110	0.116	12.49	1.06	2.12
Gravel	0.006	9.03	12.52	25.04
Well	0.070	6.57	4.93	9.86
	$k_r - S_w$			
	S_{wr} [-]	S_{nr} [-]	S_{gr} [-]	n [-]
Accusand #30/40 from column experiments				
	S_m [-]	n [-]		
Accusand #30/40 from constitutive models	0.084	6.77		
#110	0.116	12.49		
Gravel	0.006	9.03		
Well	0.070	6.57		
	ϕ [-]	k_i [m ²]		
Accusand #30/40	0.33	1.08E-10		
#110	0.34	4.24E-12		
Gravel	0.35	1.55E-09		
Well	0.60	1.18E-10		

6.3 Modeling results and discussions

This section shows comparison between the simulation results and the experimental results. The accuracy of the constitutive relationships was investigated as well as the impact of the constitutive relationships on the two-phase flow system.

6.3.1 Result of steady state condition

The model reached steady state condition at simulation time of 0.54×10^9 seconds. At the bottom left grid of gravel to have a volume of $1.0 \times 10^3 \text{ m}^3$ this grid block is assigned to be the sink and source.

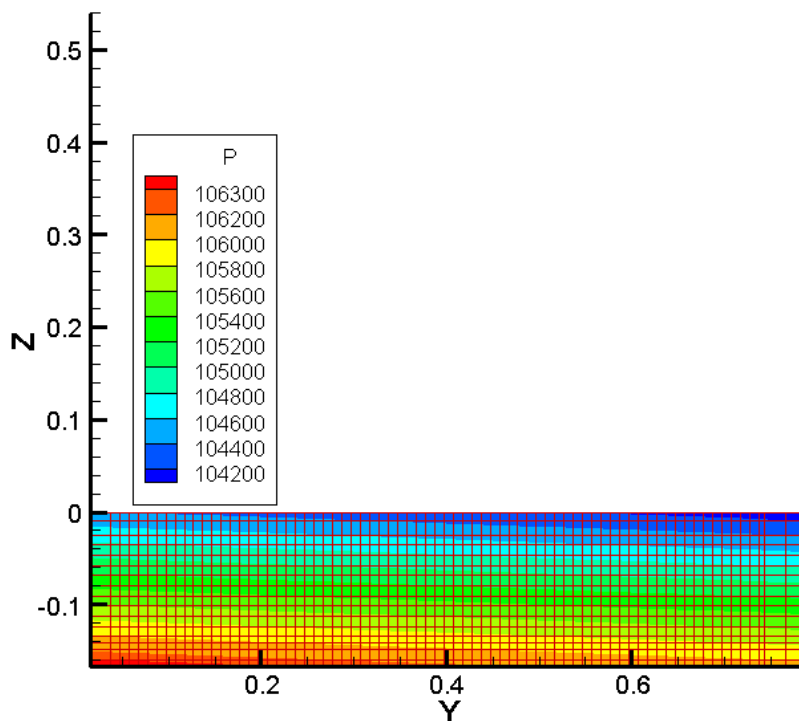


Figure 6.6 Steady state conditions

Figure 6.6 shows the steady state condition of the tank simulation. P represents the pressure [Pa] inside of the tank. This steady state condition was used as the initial condition for the simulation of Soltrol 220 injection models. The pressure distribution is showing slight slope because Accusand was made to have the dip angle of 2.0° .

6.3.2 The simulation results of Soltrol 220 injection

The results of TOUGH2 T2VOC models and the tank experiments were compared. The letters A, B, C, D, and E on Figure 6.7 represents the saturation points which were taken from X-ray system. Figure 6.8 through Figure 6.12 are comparing the saturation with time obtained from the tank experiments and the two model simulations (Simulation 1 and Simulation 2). In appendix C, the schematic of experimental and simulation results are shown to represent evolution of Soltrol 220 during the injection period.

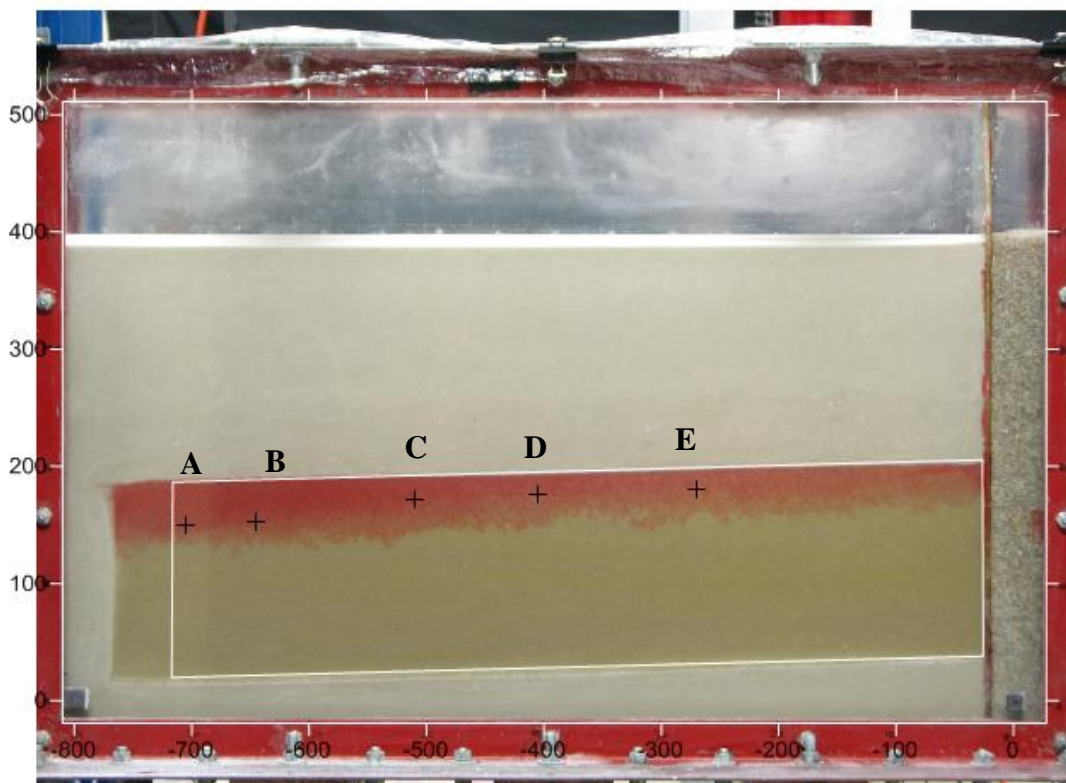


Figure 6.7 Representative saturation points of X-ray system

The pictures in the Appendix C show that simulation 2 better represents the tank experiment than simulation 1 from the contour map of saturation. Although, the contour from the tank experiment does not represent any quantitative data of saturation; therefore, it is important to investigate which simulation matched with the tank experiment using the saturation data measured from the X-ray system. By looking at Figure 6.8 through Figure 6.12, these figures indicate that overall, simulation 1 represents the actual tank experiment better than simulation 2.

The results showed that the constitutive relationships which obtained from the experimental data represents better than Mualem model and the S_i and S_r data from the scaling method. Therefore, the results show that the van Genuchten – Mualem model is not applicable to the test sands and fluids and for the scaling methods; they required to have additional experiments to measure the irreducible and residual saturations. Also, these figures show that saturation data obtained from the simulation better represent the tank experiment where it close to the well, although differences still remained between the tank result and the simulation result at the front of the plume.

X-ray system measured saturation for 480 points. Using these saturation values, the total mass of injected Soltrol 220 into the tank was calculated and compared with the total mass of injected Soltrol 220 measured using the scale. The Mariotte's bottle was placed on the scale to record changes in weight with time. The scale measured a cumulative volume of 240 ml of Soltrol 220 was injected during the injection period. Multiplying by the density of Soltrol 220, the total mass of injected Soltrol 220 was found to be 0.1896 kg. While the total volume V_n [L³] of injected Soltrol 220 from X-ray system was calculated by using the spatial integral of plume length l_n across the tank [Fagerlund *et al.*, 2007]. The saturation points measured by X-ray system were about 1.5 cm apart from each point and the width of the tank is 5.6 cm; therefore,

$$V_n(t) = \int_0^{1.5} \int_0^{1.5} l_n(x, z, t) dx dz \quad (6.3)$$

l_n can be defined as,

$$l_n(x, z, t) = \int_0^{5.6} \phi(x, y, z, t) S_n(x, y, z, t) dx \quad (6.4)$$

Multiplying the density of Soltrol 220 to V_n , the total mass of injected Soltrol 220 was 0.1849 kg. The total mass of injected Soltrol 220 calculated from the saturation taken by X-ray system are similar to the one measured from the scale. Therefore, this result shows that the wall effect can be neglected in this tank experiment. This is because if there were wall effect, the saturation in the front of the plume will be overestimated and the calculated total mass of injected Soltrol 220 from the X-ray saturation data will be higher than that of actual injected total amount of Soltrol 220.

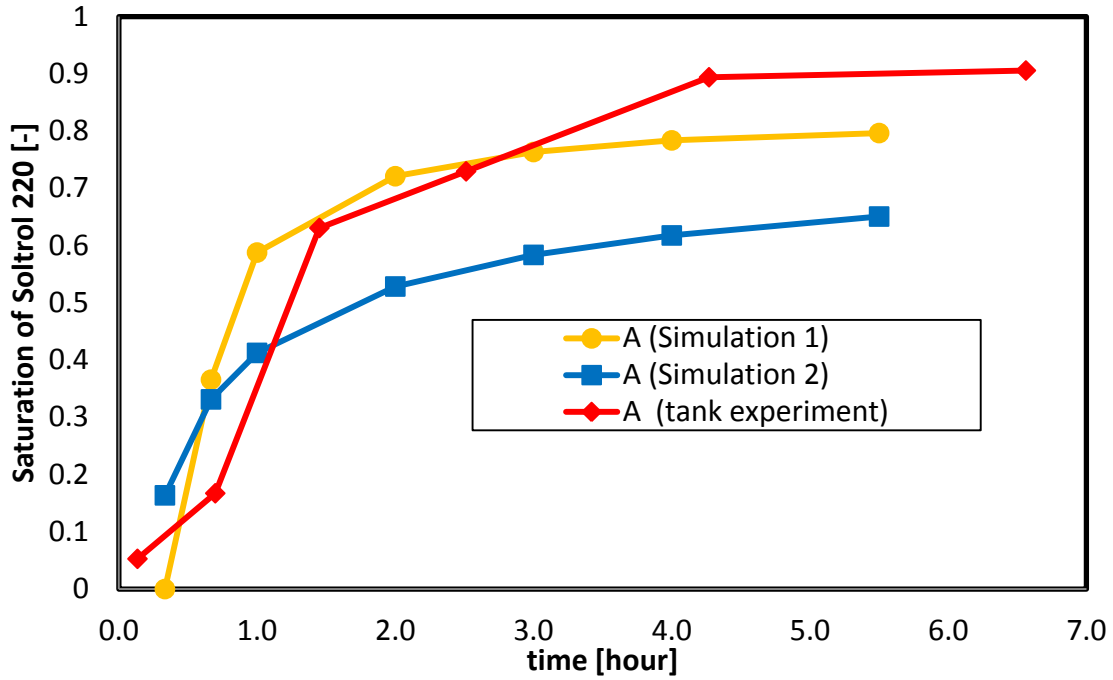


Figure 6.8 Result of saturation point A

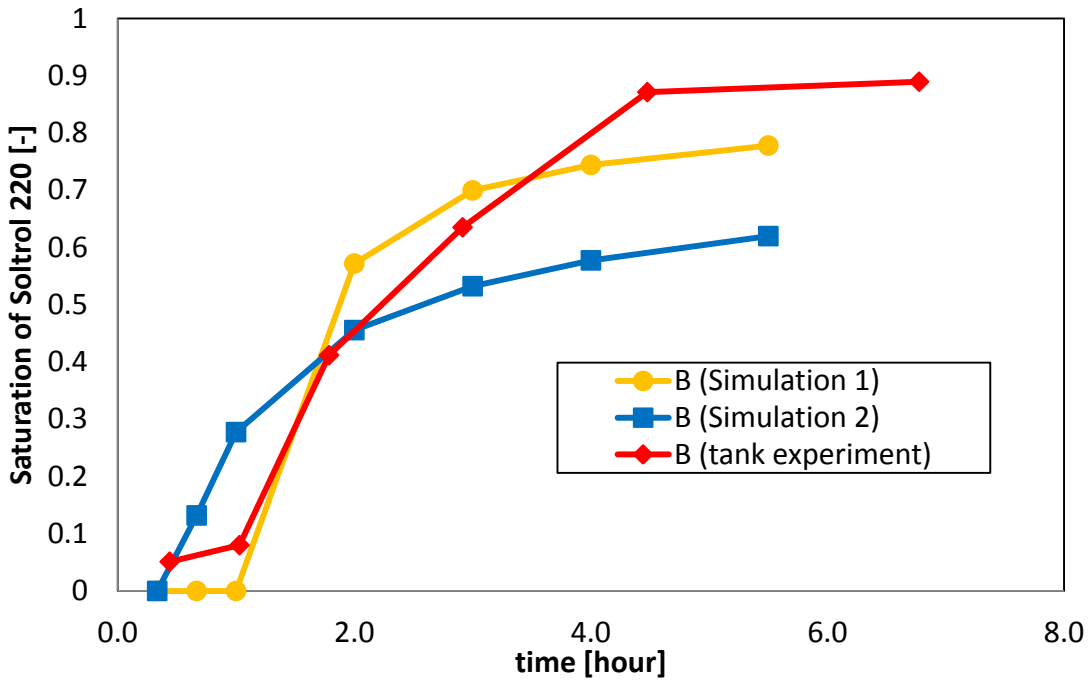


Figure 6.9 Result of saturation point B

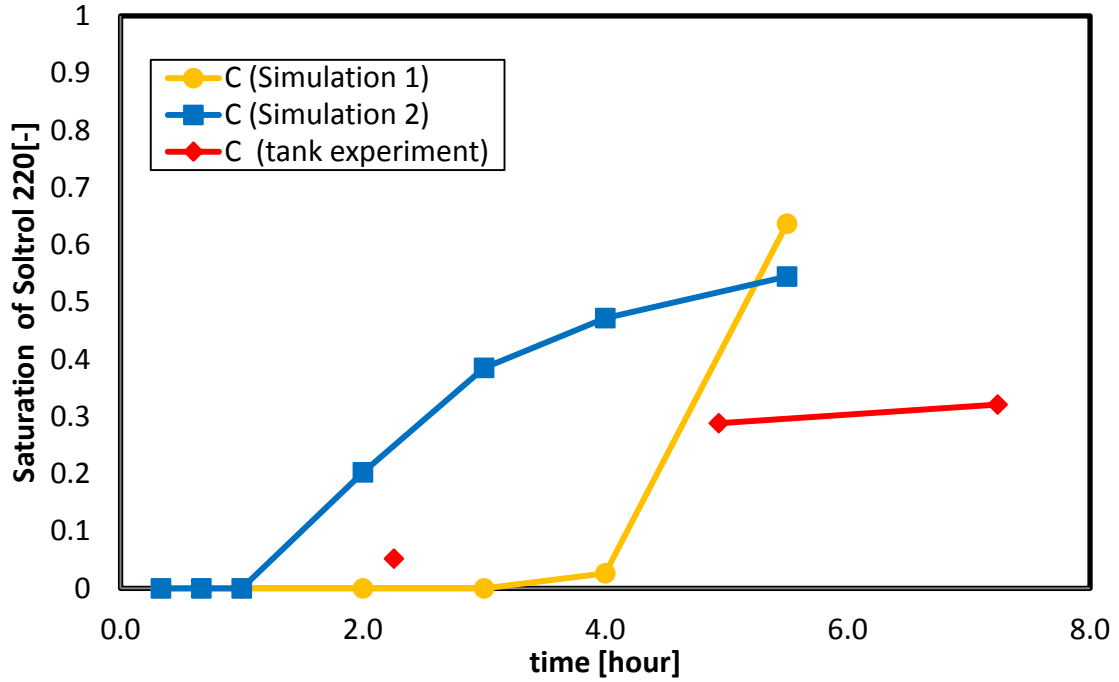


Figure 6.10 Result of saturation point C

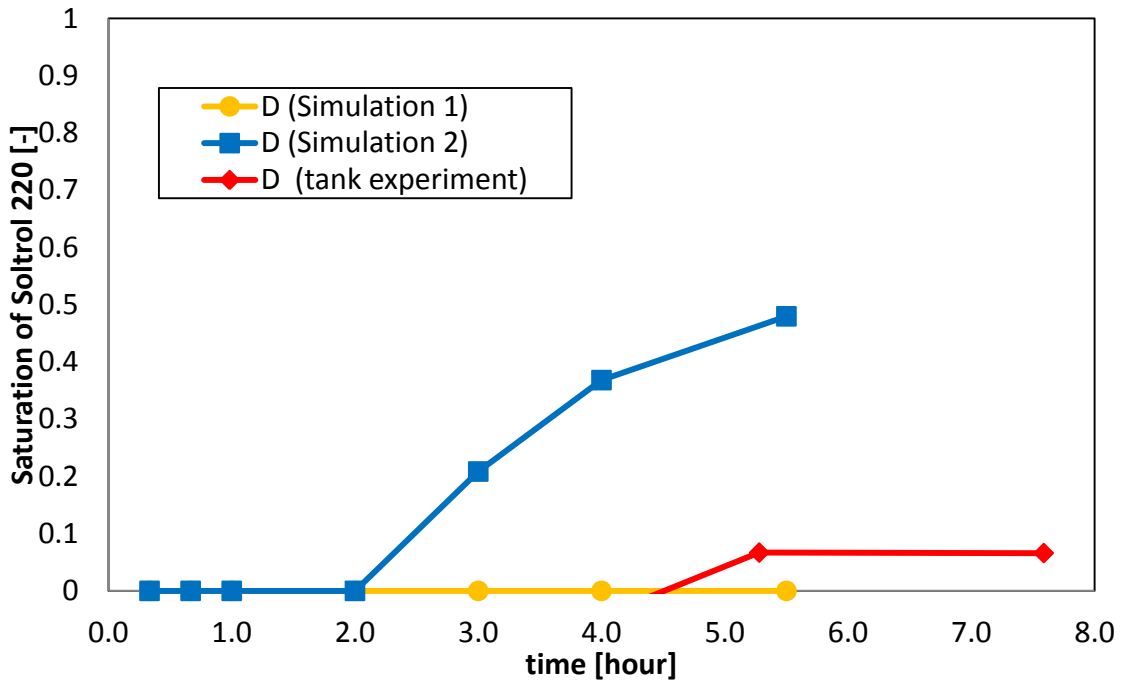


Figure 6.11 Result of saturation point D

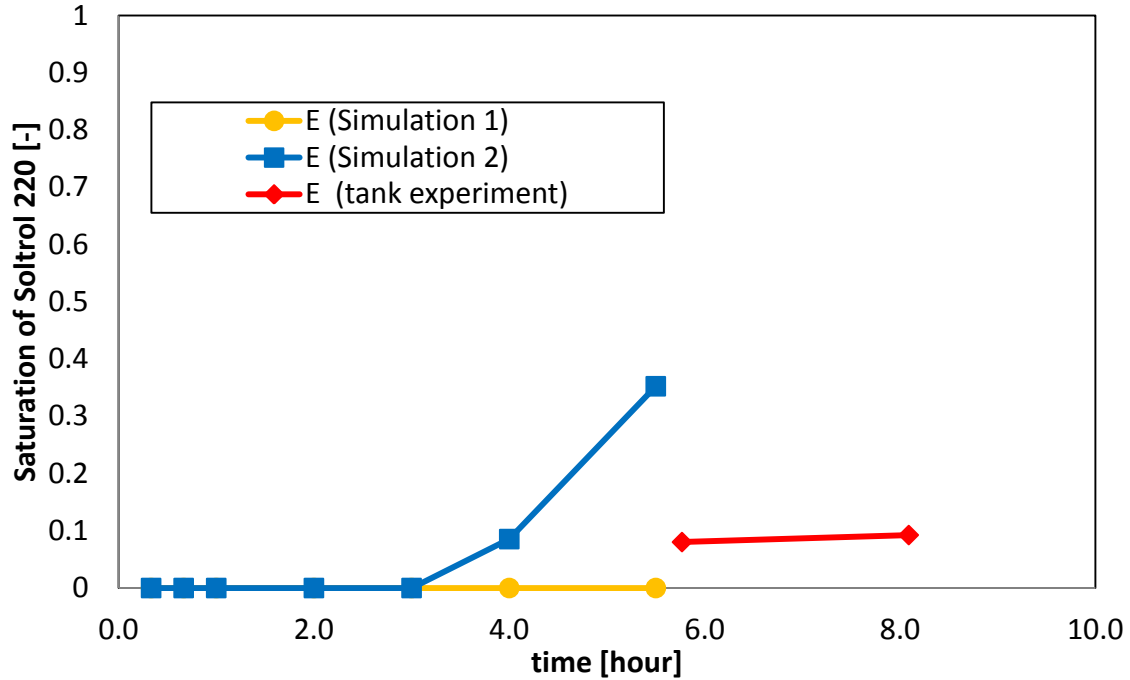


Figure 6.12 Result of saturation point E

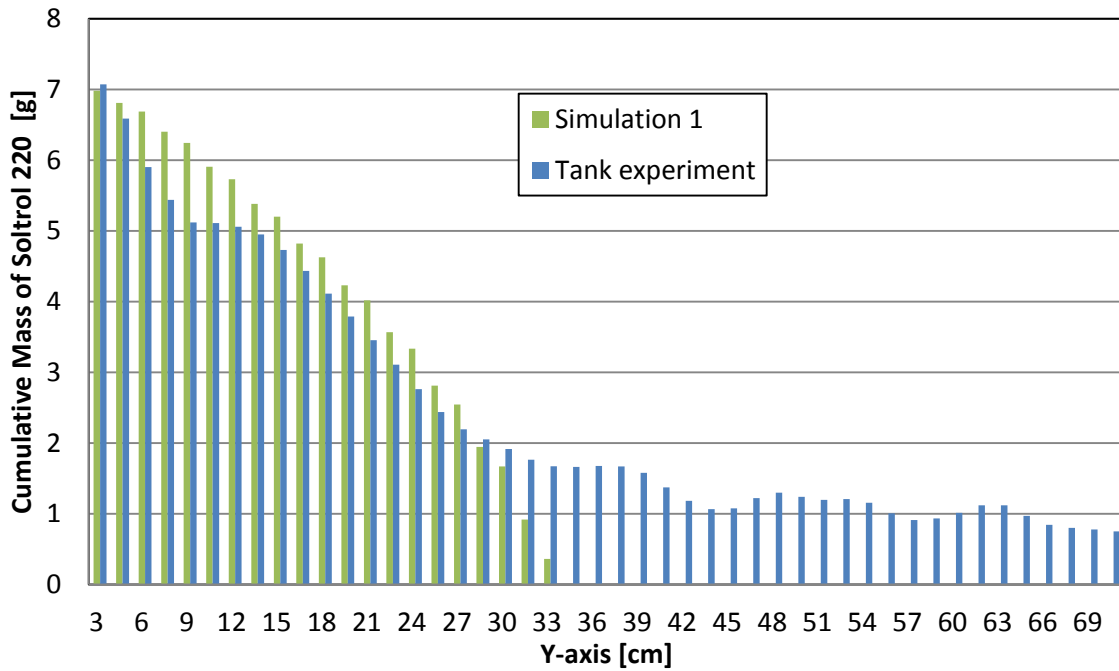


Figure 6.13 Cumulative mass of Soltrol 220

Figure 6.13 shows the cumulative mass of Soltrol 220 vs. horizontal coordinate of the tank at 5.5 hours after the injection. This figure also shows the difference between Simulation 1 and the tank experiment. The result of Simulation 1 matched the total mass of Soltrol 220 of the

tank experiment better where it closes to the well. However, in the front of the plume, the result reveals a significant difference between Simulation 1 and the tank experiments. In addition, comparing the results of Simulation 1 and the tank experiment in the figures presented in Appendix C, the tank experiment shows the plume to be evolved upward from the well, and it starts to migrate along the boundaries of the Accusand and #110 sand. While, the Simulation 1 predicts that the plume will spread out more from the side of the well. One possible explanation is that the $P_c - S_w$ relationships were based on a lower entry pressure value for the tank experiment than what was used in Simulation 1. With a lower entry pressure, the Soltrol 220 would be injected into the sand much faster than what Simulation 1 assumes, and it would migrate faster along the boundary of #110 and Accusand #30/40.

CHAPTER 7 – CONCLUSIONS AND RECOMMENDATIONS

This chapter summarizes the findings of this investigation and recommendations for future studies. The chapter also includes the contributions to the actual onsite investigation of carbon sequestration studies.

7.1 Summary

The objectives of this project were to investigate the applicability of the constitutive models, to examine the impacts on the two-flow system by changing the $P_c - S_w$ and $k_r - S_w$ relationships, and to provide suggestions how the findings contribute to investigation of $scCO_2$ behavior in the saline aquifers. To have the reliable constitutive relationships are one of the most important factors to simulate, characterize, and understand the two-phase flow system. Recently, the constitutive models become one of the popular methods to derive the constitutive relationships, although the applicability of the constitutive models to our test fluids and sands are still uncertain. Therefore, it is necessary to have the accurate constitutive relationships and to investigate the applicability of the constitutive models in order to understand the mechanisms of the two-phase flow system of $scCO_2$ and brine.

Chapter 3 describes the sands and fluids which used to perform the experiments. According to the papers of *Shook et al.* [1992] and *Gharbi et al.* [1998], they have identified that capillary number, bond number, viscosity ratio, and density ratio can be used to characterize two immiscible flows in similar porous medium. According to these dimensionless numbers, the surrogate fluids of $scCO_2$ and brine were selected to be Glycerol-water mixture of 8:2 by weight and Soltrol 220 dyed with sudan IV, respectively. In addition, the test sands properties were mostly obtained from the previous studies and the summary of the test sand properties were listed.

The experimental methods and results of the $P_c - S_w$ relationships were mentioned in Chapter 4. Three different approaches such as Leverett scaling, the entry pressure scaling method, and the dielectric sensor method were applied to obtain the $P_c - S_w$ relationships of the test sands and fluids. Each method was used to measure the $P_c - S_w$ relationships for five different Accusands. All the methods show the similar $P_c - S_w$ curves, although the irreducible and residual

saturation values were found to be slightly different between the two scaling methods and the dielectric sensor method.

The experimental methods and results of the k_r-S_w relationships were described in Chapter 5. The long column method was applied to measure the relative permeability of the wetting phase and the hydrostatic methods was used to measure for the non-wetting phase. The long column method was not the sufficient method to measure the relative permeability at the high saturation. This is because that the saturation of the column did not reach the steady state condition. Moreover, the long column method cannot be used for measuring the non-wetting phase relative permeability because the non-wetting phase fluid is not continuous in side of tube which connects the column and the constant head device so it cannot apply Darcy's law. Also, the hydrostatic method requires a long time to reaches the steady state and moreover, it cannot see the condition of the fluids inside of the column; therefore, it is difficult to determine the accuracy of the data sets. The results show that it has a significant differences compared to van Genuchten – Mualem model and most of the data shifts from the curve to the left.

Chapter 6 represents the simulations of the tank experiment and comparison with the actual tank experiment. The tank experiment was designed to have the homogeneous packing of Accusand #30/40. Soltrol 220 was injected for a certain time and observed the migration of the plume. X-ray system was implemented to measure the saturation inside of the tank. TOUGH2 T2VOC was used to simulate this tank experiment. Two simulations were conducted that the one used the constitutive relationships obtained from the column experiments and the other one used from constitutive models. As a result, the numerical model which used the constitutive relationships from the column experiments matched with the tank experiments better than the one used constitutive models. However, the numerical model could not precisely capture Soltrol 220 behavior.

7.2 Findings of the applicability of the constitutive relationships

Many lessons were obtained from the experimental results of P_c-S_w and k_r-S_w relationships. For the measurements of the P_c-S_w relationships, three different methods were able to represents the P_c-S_w curve for the test fluids and sand. In below, the list of advantages and disadvantages are described for each method.

Leverett scaling : Leverett scaling uses the theory of the interfacial curvature multiplied by a factor that is the property of the porous media corresponding to the dimensionless function $J_{(S_{ew})}$. This dimensionless function can be expressed as the relationships between the two arbitrary systems. Experimental results show that Leverett Scaling is applicable for our test sands and fluids to scale the $P_c - S_w$ curve. Although, the limitations of Leverett Scaling is that they have a same irreducible and residual saturations as the fluids combinations they were scaled from. However, these values varied depends on the fluids and experimental conditions so another experimental study is needed to obtain the accurate irreducible and residual saturation values for the test fluids and sands. Also, when measuring the interfacial tensions with tensiometers, one needs to be aware that the temperature should be at the same as the experimental conditions because the interfacial tensions are sensitive to temperature.

Entry pressure scaling method : This scaling method can scale the $P_c - S_w$ curve by using the differences between displacement head of the unknown $P_c - S_w$ curve and the displacement head of known $P_c - S_w$ curve. The displacement head has to be measured by the outflow mass of the Glycerol-water mixture because the visually obtained displacement head does not represents the actual displacement head because of the wall effect. Entry pressure scaling method also has the same disadvantages as the Leverett scaling that it has to measure irreducible and residual saturations. The displacement head obtained from this method has the highest value compared to other two methods.

Dielectric sensor methods : This method uses the EC-5 sensors to measure the saturation inside of the column and the capillary pressure from the differences in the head of the Glycerol-water and Soltrol 220. This method can measure the irreducible saturation and the residual saturation of the test fluids and sands and the multiple plots of the $P_c - S_w$ relationships. Although, the capillary pressure can only change by a centimeter; therefore, the measurements cannot take many points between the irreducible and residual saturations of the test sands and fluids. Mainly, the dielectric sensor methods obtained the displacement head about the same as the Leverett scaling and smaller than the entry pressure scaling mehod.

The results from these methods show that all the methods can be applicable to measure the $P_c - S_w$ relationships. However, for the two scaling methods did not show the same irreducible and residual saturations value obtained from the dielectric sensor method. Therefore,

to have the reliable sets of the $P_c - S_w$ relationships, it needs to measure these saturation values independently from the scaling methods.

Two different methods were modified to characterize the $k_r - S_w$ relationships. In the following paragraph represents the advantages and the limitations of the each method.

Long column method : The long column method was implemented to measure the wetting phase relative permeability. In theory, it is noted that the column has uniform saturation and it has the uniform hydraulic gradient of one. In this project, the method was modified to have two hydrophilic tensiometers which can measure the hydraulic pressure and EC-5 sensors that can measure the saturation inside of the column to have more precise data. The relative permeability of the Accusand #30/40, #40/50, and #50/70 were obtained successfully, although Accusand #12/20 and #20/30 were not able to measure from this method. This is because the hydraulic conductivity of the sand is too high and the supply from the Mariotte's bottle cannot be adjusted that high flow rate. Also, the relative permeability points at the high Glycerol-water saturation were not able to measure because the non-wetting phase were not continuous inside of the column so the column did not reach the steady state condition.

Hydrostatic method : Hydrostatic method was applied to characterize the non-wetting phase relative permeability. This method can be used to measure all five different Accusands, but it was used to measure only for Accusand #30/40, #40/50, and #50/70 because there are no data for the wetting phase relative permeability of Accusand #12/20 and #20/30 from the long column method. The disadvantages of this method are that it takes too long time to reach the steady state and also it is difficult to define when the experiment reaches the steady state condition. From the theory, this method can be used to measure the imbibitions process of the relative permeability measurements; although for the imbibitions process, only the data of Accusand #30/40 was obtained. According to the result obtained from Accusand #30/40, the non-wetting relative permeability does not represent any hysteresis.

The results of these two methods indicate that during the $k_r - S_w$ relationships measurements, the hysteresis can be neglected. Also, the experimental data show the significant differences between the van Genuchten – Mualem model. Therefore, it is important to measure the relative permeability independently from the constitutive models.

7.3 Findings of the constitutive relationships impacts on the two-phase flow system

From the simulations of TOUGH2 T2VOC models which used the constitutive relationships from the experiments and the constitutive models show interesting results. By comparing these simulation results with the tank experiments, the model which used the constitutive relationships from the experimental data shows better match. Especially, at the high saturation range of the Glycerol-water mixture, Simulation 1 represents the tank experiment fairly well. However, differences in saturation are still remained especially in the low saturation range of the Glycerol-water mixture. One possible explanation is that the $P_c - S_w$ relationships were based on a lower entry pressure value for the tank experiment than what was used in Simulation 1. By having the smaller entry pressure head, the Sotlrol 220 should get inside of the sand faster and it will migrated faster than what it is shown in the simulation now. The sensitivity analysis is required to see the impact of the entry pressure to the tank simulation. The results suggested that the constitutive relationships have a huge impact on the two-phase flow system and to have the applicable constitutive relationships will improve the quality of models.

7.4 Contribution to the onsite investigations

The methods developed to characterize the $P_c - S_w$ and $k_r - S_w$ relationships were for surrogate fluids and they were not for the actual scCO₂ and brine system. From the results of the $P_c - S_w$ measurement, it can be said that Leverett scaling is successful method to scale the $P_c - S_w$ relationships. Leverett scaling can be used to scale the $P_c - S_w$ relationships for the scCO₂/brine system. This scaling method is feasible to measure the $P_c - S_w$ relationships for the scCO₂/brine system because Leverett scaling only requires measuring the interfacial tensions and there are many literatures which indicate the interfacial tensions of scCO₂ and brine at various conditions. However, the residual and irreducible saturations are still needed to measure separately from the scaling method. Especially, the residuals saturation of scCO₂ is an important parameter to investigate the capillary trapping mechanisms of scCO₂.

There are no hysteresis behavior was observed from the experimentally obtained $k_r - S_w$ relationships. Therefore, the relative permeability measurements do not required to consider the hysteresis effect. Also, it might be better to run one test to see whether the van Genuchten – Mualem model is applicable for the test sample or not.

7.5 Recommendation to the future study

This project is a fundamental study to understand the effective capillary trapping mechanisms of scCO₂ in saline aquifers. The study proves that having the accurate constitutive models improve the quality of the numerical models and the obtained result of the constitutive relationships can be used as the fundamental properties of test sands and fluids. However, the simulation result did not reproduce the tank experiment; therefore, many improvements are needed to understand the physics of the carbon sequestrations. Recommendations for future works follow,

Homogeneous tank experiment: First of all, the constitutive relationships of $P_c - S_w$ needs to implement to have high displacement head value and see whether the model represents the tank experiments better than the one mentioned in this thesis. Moreover, another experiment is needed to be run with other sand to see whether measured constitutive relationships represents the tank experiment.

Heterogeneous tank experiment: Heterogeneous case should be run for at least one time to see the impact of the constitutive relationships and examine is there any suggestion that can give to investigate the actual scCO₂ and brine system.

Entry pressure head: The simulation result did not replicate the actual tank experiment, especially the behavior at the front of the plume. An assumption was made that an inaccurate entry pressure might have caused this problem. A sensitivity analysis is necessary to understand the impact of the entry pressure value on the simulation results and also to determine which entry pressure best fits the actual tank experiment.

Imbibition Process: In this project, the constitutive relationships were only compared with the drainage process of the tank experiments. Therefore, it might be interesting to see how the constitutive relationships will affects two-phase flow behavior in imbibitions process. Moreover, it will be important to compare the residual saturation of Soltrol 220 in the simulation and the tank experiments to contribute the understanding of the trapping mechanisms of scCO₂.

CHAPTER 8 – REFERENCES

- Aminzadeh-goharrizi, B., DiCarlo, D., Hyun Chung, D. O. O., Roberts, M., Bryant, S., and Huh, C. (2012, April). Effect of Spontaneous Formation of Nanoparticle Stabilized Emulsion on the Stability of a Displacement. In *SPE Improved Oil Recovery Symposium*.
- Bachu, S., W. D. Gunther, and E. H. Perkins (1994), Aquifer disposal of CO₂: Hydrodynamic and mineral trapping, *Energy Convers. Manage.*, 35(4), 269-279.
- Bachu, S., and Bennion, B. (2008). Effects of in-situ conditions on relative permeability characteristics of CO₂-brine systems. *Environmental Geology*, 54(8), 1707-1722.
- Bachu, S., and Bennion, D. B. (2009). Experimental assessment of brine and/or CO₂ leakage through well cements at reservoir conditions. *International Journal of Greenhouse Gas Control*, 3(4), 494-501.
- Bennion, B., and Bachu, S. (2005, October). Relative Permeability Characteristics for Supercritical CO₂ Displacing Water in a Variety of Potential Sequestration Zones. In *SPE Annual Technical Conference and Exhibition*.
- Bennion, D., and Bachu, S. (2006, September). Dependence on temperature, pressure, and salinity of the IFT and relative permeability displacement characteristics of CO₂ injected in deep saline aquifers. In *SPE Annual Technical Conference and Exhibition*.
- Benson, M. S., and Surles, T. (2006). Carbon dioxide capture and storage: an overview with emphasis on capture and storage in deep geological formations. *Proceedings of the IEEE*, 94(10), 1795-1805.
- Benson, S. M., and Cole, D. R. (2008). CO₂ sequestration in deep sedimentary formations. *Elements*, 4(5), 325-331.
- Brooks, R. H., and Corey, A. T. (1964). Hydraulic properties of porous media. *Hydrology Papers, Colorado State University*, (March).
- Brooks, C. S., & Purcell, W. R. (1952, October). Surface area measurements on sedimentary rocks. In *Fall Meeting of the Petroleum Branch of AIME*.
- Burdine, N. T. (1953). Relative permeability calculations from pore size distribution data. *Journal of Petroleum Technology*, 5(3), 71-78.
- Busby, R. D., Lenhard, R. J., and Rolston, D. E. (1995). An Investigation of Saturation-Capillary Pressure Relations in Two-and Three-Fluid Systems for Several NAPLs in Different Porous Media. *Ground Water*, 33(4), 570-578.
- Cary, J. W., Simmons, C. S., and McBride, J. F. (1989). Predicting oil infiltration and redistribution in unsaturated soils. *Soil Science Society of America Journal*, 53(2), 335-342.
- Chadwick, R. A., Williams, G. A., Williams, J. D. O., & Noy, D. J. (2012). Measuring pressure performance of a large saline aquifer during industrial-scale CO₂ injection: The Utsira Sand, Norwegian North Sea. *International Journal of Greenhouse Gas Control*, 10, 374-388.

- Chalbaud, C., Robin, M., Lombard, J. M., Martin, F., Egermann, P., & Bertin, H. (2009). Interfacial tension measurements and wettability evaluation for geological CO₂ storage. *Advances in Water Resources*, 32(1), 98-109.
- Chen, J., Hopmans, J. W., and Grismer, M. E. (1999). Parameter estimation of two-fluid capillary pressure–saturation and permeability functions. *Advances in Water Resources*, 22(5), 479–493.
- Cheng, N. S. (2008). “Formula for viscosity of glycerol-water mixture.” *Industrial and Engineering Chemistry Research*, 47, 3285–3288.
- Cihan, A., Tyner, J. S., and Perfect, E. (2009). Predicting relative permeability from water retention: A direct approach based on fractal geometry. *Water Resources Research*, 45(4), W04404.
- Corey, A. T. (1994). *Mechanics of immiscible fluids in porous media*. Water Resources Publication.
- Corey, A.T. (2002). *Methods of soil analysis: physical methods*. Part 4. SSSA book series no. 5. SSSA, Madison, Wis. 899–903
- Craig, F. F. (1971). The reservoir engineering aspects of waterflooding, in *SPE Monograph Series 3*, 142 pp. Society of Petroleum Engineers, New York.
- Crain, R.E. (2013). Available at: <http://www.spec2000.net/09-wettability.htm>
- Dane, J. H., C. Hofstee, and A. T. Corey (1998), Simultaneous measurement of capillary pressure, saturation, and effective permeability of immiscible liquids in porous media, *Water Resour. Res.*, 34(12), 3687–3692, doi:10.1029/1998WR900026
- Demond, A. H., and Roberts, P. V. (1991). Effect of interfacial forces on two-phase capillary pressure—saturation relationships. *Water Resources Research*, 27(3), 423–437.
- Demond, A. H., and Roberts, P. V. (1993). Estimation of two-phase relative permeability relationships for organic liquid contaminants. *Water resources research*, 29(4), 1081–1090.
- Doughty, C., and Pruess, K. (2004). Modeling supercritical carbon dioxide injection in heterogeneous porous media. *Vadose Zone Journal*, 3(3), 837–847.
- Dullien, F. A. L. (1992), *Porous Media Fluid Transport and Pore Structure*, Academic, San Diego.
- Elliot, T. R., and Celia, M. A. (2012). Potential Restrictions for CO₂ Sequestration Sites Due to Shale and Tight Gas Production. *Environmental science & technology*, 46(7), 4223-4227.
- Espinoza, D. N., & Santamarina, J. C. (2010). Water-CO₂-mineral systems: Interfacial tension, contact angle, and diffusion—Implications to CO₂ geological storage. *Water resources research*, 46(7), W07537.
- Fagerlund, F., Illangasekare, T. H., & Niemi, A. (2007). Nonaqueous-phase liquid infiltration and immobilization in heterogeneous media: 2. Application to stochastically heterogeneous formations. *Vadose Zone Journal*, 6(3), 483-495.
- Falta, R. W., Pruess, K., Finsterle, S., and Battistelli, A. (1995). T2VOC users guide.

- Fetter, C. W. (1999). *Contaminant hydrogeology (2nd edn.)*. Upper Saddle River, New Jersey: Prentice hall.
- Fischer, U., & Celia, M. A. (1999). Prediction of relative and absolute permeabilities for gas and water from soil water retention curves using a pore-scale network model. *Water Resources Research*, 35(4), 1089-1100.
- Flett, M., R. Gurton, and I. Taggart (2004), The function of gas–water relative permeability hysteresis in the sequestration of carbon dioxide in saline formations, *SPE Pap. 88485–MS*, Soc. of Pet. Eng., Richardson, Tex.,
- Friedmann, S. J. (2013). CO₂ Capture and Sequestration. In *Fossil Energy* (pp. 597-617). Springer New York.
- Fulcher, R. A., Ertekin, T., and Stahl, C. D. (1985). Effect of capillary number and its constituents on two-phase relative permeability curves. *Journal of petroleum technology*, 37(2), 249-260.
- Garmeh, G., & Johns, R. (2010). Upscaling of Miscible Floods in Heterogeneous Reservoirs Considering Reservoir Mixing. *SPE Reservoir Evaluation & Engineering*, 13(5), 747-763.
- Gharbi, R., E. Peters, and A. Elkamel, (1998). Scaling Miscible Fluid Displacement in Porous Media. *Energy and Fuels*, 12, 801–811.
- Hauzenberg, I. and Zaslavsky, D. (1963). The effect of size of water stable aggregates on field capacity. Department of Civil Engineering, Technion, Haifa, P.H., Vol.35 as quoted by Bear (1972). 483–487.
- Hesse, M. A., Orr, F. M., and Tchelepi, H. A. (2008). Gravity currents with residual trapping. *Journal of Fluid Mechanics*, 611(1), 35–60.
- Hofstee, C., Dane, J. H., and Hill, W. E. (1997). Three-fluid retention in porous media involving water, PCE and air. *Journal of contaminant hydrology*, 25(3), 235-247.
- Hovorka, S. D., C. Doughty, and M. H. Holtz (2004), Testing efficiency of storage in the subsurface: Frio brine pilot experiment, paper presented at International Conference on Greenhouse Gas Control Technologies (GHGT-7), Int. Energy Agency, Vancouver, B. C., Canada.
- IPCC, 2005. In: Metz, B., Davidson, O., de Coninck, H.C., Loos, M., Meyer, L.A. (Eds.), IPCC Special Report on Carbon Dioxide Capture and Storage. Prepared by Working Group III of the Intergovernmental Panel on Climate Change. Cambridge University Press, Cambridge, UK, New York, NY.
- IPCC (Intergovernmental Panel on Climate Change). *Climate Change 2007: The Physical Science Basis*. Cambridge, UK: Cambridge University Press, 2007.
- Irmay, S. (1954). On the hydraulic conductivity of unsaturated soils. *Transactions, American Geophysical Union*, 35, 463-467.
- Juanes, R., E. J. Spiteri, F. M. Orr Jr., and M. J. Blunt (2006). Impact of relative permeability hysteresis on geological CO₂ storage, *Water Resour. Res.*, 42, W12418, doi:10.1029/2005WR004806.

- Kamaruddin, S. A., Sulaiman, W. N. A., Rahman, N. A., Zakaria, M. P., Mustaffar, M., & Saari, R. (2011). A Review of Laboratory and Numerical Simulations of Hydrocarbons Migration in Subsurface Environments. *Journal of Environmental Science and Technology*, 4(3), 191-214.
- Klute, A., & Dirksen, C. (1986). Conductivities and diffusivities of unsaturated soils. *Methods of soil analysis. Part, 1*, 687-734.
- Kosugi, K. (2007). Reviewing classical studies in soil physics "A new model for predicting the hydraulic conductivity of unsaturated porous media" By Y. Mualem *Water Resources Research*, Vol.12, NO.3, 513-522 (1976) and "A closed-form equation for predicting the hydraulic conductivity of unsaturated soils" By M. Th. van Genuchten *Soil Science Society of America Journal*, Vol.44, NO.5, 892-898 (1980), *J. Jpn. Soc. Soil Phys.* 106, 47-60
- Krevor, S. C. M., R.Pini, L.Zuo, and S. M.Benson (2012). Relative permeability and trapping of CO₂ and water in sandstone rocks at reservoir conditions, *Water Resour. Res.*, 48, W02532, doi:10.1029/2011WR010859.
- Kumar, S., Torabzadeh, S. J., & Handy, L. L. (1985, March). Relative permeability functions for high-and low-tension systems at elevated temperatures. In *SPE California Regional Meeting*.
- Kumar, A., R. Ozah, M. Noh, G. A. Pope, S. Bryant, K. Sepehrnoori, and L.W.Lake (2005). Reservoir simulation of CO₂ storage in deep saline aquifers, *Soc. Pet. Eng. J.*, 10(3), 336-348.
- Lake, L. W. (1989). *Enhanced Oil Recovery*, Prentice Hall, Englewood Cliffs, NJ.
- Lenhard, R. J. (1992). Measurement and modeling of three-phase saturation-pressure hysteresis. *Journal of Contaminant Hydrology*, 9(3), 243-269.
- Lenhard, R. J., & Parker, J. C. (1987). Measurement and prediction of saturation-pressure relationships in three-phase porous media systems. *Journal of contaminant hydrology*, 1(4), 407-424.
- Lenhard, R. J., and J. C. Parker (1987). A model for hysteretic constitutive relations governing multiphase flow: 2. Permeability-saturation relations. *Water Resour. Res.*, 23(12), 2197-2206.
- Leverett, M. C. (1941). Capillary behavior in porous solids, *Trans. Am. Inst. Min. Metall. Pet. Eng.*, 142, 152-169
- Liu, N., Ghorpade, S., Harris, L., Li, L., Grigg, R., and Lee, R. (2010, October). The Effect of Pressure and Temperature on Brine-CO₂ Relative Permeability and IFT at Reservoir Conditions. In *SPE Eastern Regional Meeting*.
- Metz, B., Davidson, O., De Coninck, H., Loos, M., & Meyer, L. (2005). *IPCC special report on carbon dioxide capture and storage*. Intergovernmental Panel on Climate Change, Geneva (Switzerland). Working Group III.
- Mualem, Y. (1976). A new model for predicting the hydraulic conductivity of unsaturated porous media. *Water Resour. Res.*, 12, 513-522.

- Müller, N. (2010). Supercritical CO₂-brine relative permeability experiments in reservoir rocks—Literature review and recommendations, *Transp. Porous Media*, 87(2), 367–383.
- Nordbotten, J. M., Celia, M. A., and Bachu, S. (2005). Injection and storage of CO₂ in deep saline aquifers: Analytical solution for CO₂ plume evolution during injection. *Transport in Porous Media*, 58(3), 339-360.
- Oak, M. J. (1990), Three-phase relative permeability of water-wet Berea, *SPE Pap. 20183-MS*, Soc. of Pet. Eng., Richardson, Tex, (SPE/DOE 20183).
- Oliveira, L. I., & Demond, A. H. (2003). Estimation of primary drainage three-phase relative permeability for organic liquid transport in the vadose zone. *Journal of contaminant hydrology*, 66(3), 261-285.
- Oostrom, M., and Lenhard, R. J. (1998). Comparison of relative permeability-saturation-pressure parametric models for infiltration and redistribution of a light nonaqueous phase liquid in sandy porous media. *Advances in Water Resources*, 21(2), 145–157.
- Oostrom, M., Wietsma, T. W., Covert, M. A., and Vermeul, V. R. (2007). Zero-Valent Iron Emplacement in Permeable Porous Media Using Polymer Additions. *Ground Water Monitoring & Remediation*, 27(1), 122-130.
- Pentland, C., Itsekiri, E., Al-Mansoori, S., Iglauer, S., Bijeljic, B., and Blunt, M. (2010). Measurement of nonwetting-phase trapping in sandpacks. *Spe Journal*, 15(2), 274-281.
- Perrin, J.-C., and S. Benson (2009). An experimental study on the influence of sub-core scale heterogeneities on CO₂ distribution in reservoir rocks, *Transp. Porous Media*, 82, 93–109.
- Plasynski, S. I., Litynski, J. T., McIlvried, H. G., Vikara, D. M., & Srivastava, R. D. (2011). The critical role of monitoring, verification, and accounting for geologic carbon dioxide storage projects. *Environmental Geosciences*, 18(1), 19-34.
- Pruess, K. (2005), ECO2N: A TOUGH2 Fluid Property Module for Mixtures of Water, NaCl, and CO₂. Lawrence Berkeley Laboratory Report LBNL-57952, Berkeley, CA.
- Sakaki, T., Limsuwat, A., Smits, K. M., and Illangasekare, T. H. (2008). Empirical two-point α -mixing model for calibrating the ECH2O EC-5 soil moisture sensor in sands. *Water Resources Research*, 44(4), W00D08.
- Sakaki, T., Schulte, E. P., Cihan, A., Christ, A.J, and Illangasekare, T.H. (2011). Airflow pathway dynamics in heterogeneous subsurface influenced by land surface boundary conditions. *Vadose Zone Journal*. 11–0118.
- Schroth, M. H., J. D. Istok, S. J. Ahearn, and J. S. Selker (1995). Geometry and position of light nonaqueous phase liquid lenses in water-wetted porous media, *J. Contam. Hydrol.*, 19, 269–287.
- Schnaar, G., and Digiulio, D. C. (2009). Computational modeling of the geologic sequestration of carbon dioxide. *Vadose Zone Journal*, 8(2), 389–403.
- Shen, P., Zhu, B., Li, X. B., and Wu, Y. S. (2006). The Influence of Interfacial Tension on Water-Oil Two-Phase Relative Permeability. In *SPE/DOE Symposium on Improved Oil Recovery*.

- Shook M, Li D, and Lake LW (1992) Scaling immiscible flow through permeable media by inspectional analysis. Journal Name: *In Situ*; (United States); Journal Volume:16:4:Medium: X; Size: Pages: 311–350.
- Smits, K. M., Sakaki, T., Limsuwat, A., and Illangasekare, T. H. (2009, May). Determination of the thermal properties of sands as affected by water content, drainage/wetting, and porosity conditions for sands with different grain sizes. In *AGU Spring Meeting Abstracts* (Vol. 1, p. 05).
- Spiteri, E., Juanes, R., Blunt, M., and Orr, F. (2008). A new model of trapping and relative permeability hysteresis for all wettability characteristics. *Spe Journal*, 13(3), 277-288.
- Stone, H. L. (1970), Probability model for estimating three-phase relative permeability. *Journal of Petroleum Technology*, 22(2), 214-218.
- Torp, T. A., and Gale, J. (2004). Demonstrating storage of CO₂ in geological reservoirs: The Sleipner and SACS projects. *Energy*, 29(9), 1361–1369.
- Trevisan, L et al. (2013). In progress.
- Tuller, M., & Or, D. (2002). Unsaturated Hydraulic Conductivity of Structured Porous Media A Review of Liquid Configuration–Based Models. *Vadose Zone Journal*, 1(1), 14-37.
- van Genuchten, M. T. (1980), A closed-form equation for predicting the hydraulic conductivity of unsaturated soils. *Soil Sci. Soc. Am. J.*, 44, 892–898.
- Wildenschild, D., Armstrong, R. T., Herring, A. L., Young, I. M., and William Carey, J. (2011). Exploring capillary trapping efficiency as a function of interfacial tension, viscosity, and flow rate. *Energy Procedia*, 4, 4945–4952.
- Wilkins, M. D., Abriola, L. M., & Pennell, K. D. (1995). An experimental investigation of rate-limited nonaqueous phase liquid volatilization in unsaturated porous media: Steady state mass transfer. *Water Resources Research*, 31(9), 2159-2172.
- Young, T. (1805). An essay on the cohesion of fluids. *Philosophical Transactions of the Royal Society of London*, 95, 65–87.

APPENDIX A – THE RESULT OF CAPILLARY PRESSURE FOR ALL SANDS

Figure A.1 through A.4 represents the $P_c - S_w$ relationships of Accusand #12/20, #20/30, #30/40, #40/50, and #50/70. The figures show the comparison between Leverett scaling, the entry pressure method, the dielectric sensor method, and the van Genuchten model (VG model). The van Genuchten model used the dielectric sensor method to estimate the fitting parameters and these van Genuchten parameters are listed in Table 4.5. Also, Accusand #50/70 does not represent Leverett scaling and the entry pressure method because the data for air/water phase $P_c - S_w$ relationships are missing.

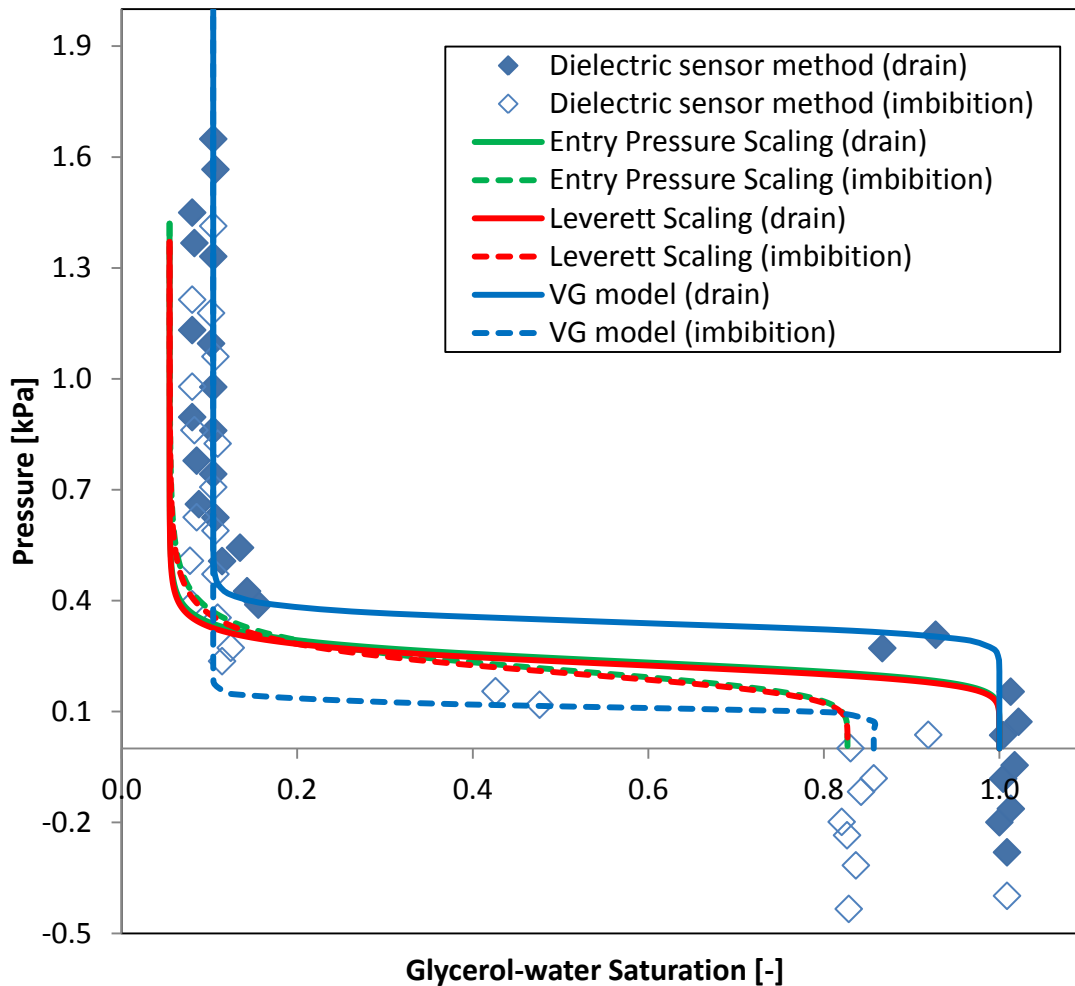


Figure A.1 Accusand #12/20

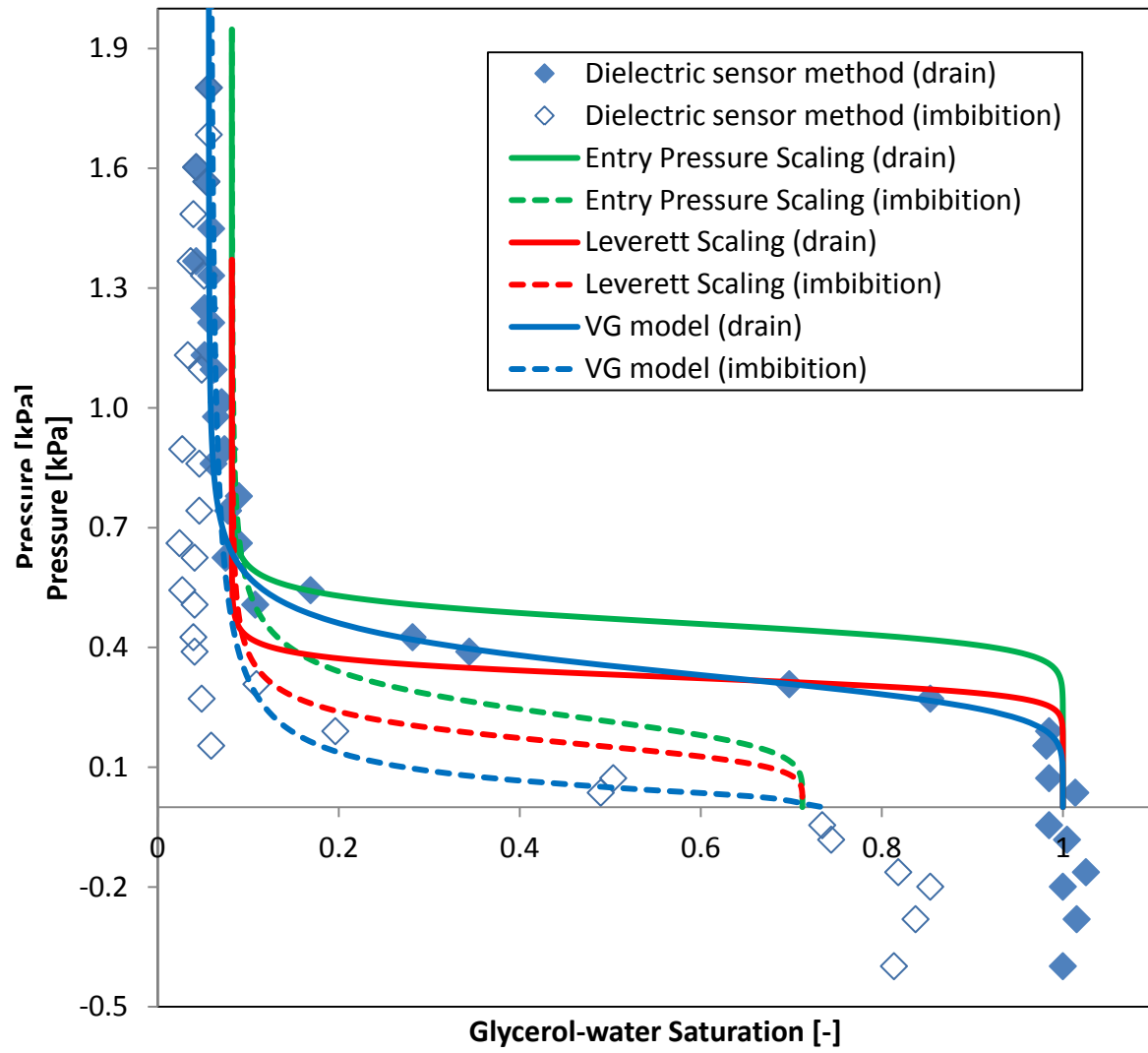


Figure A.2 Accusand #20/30

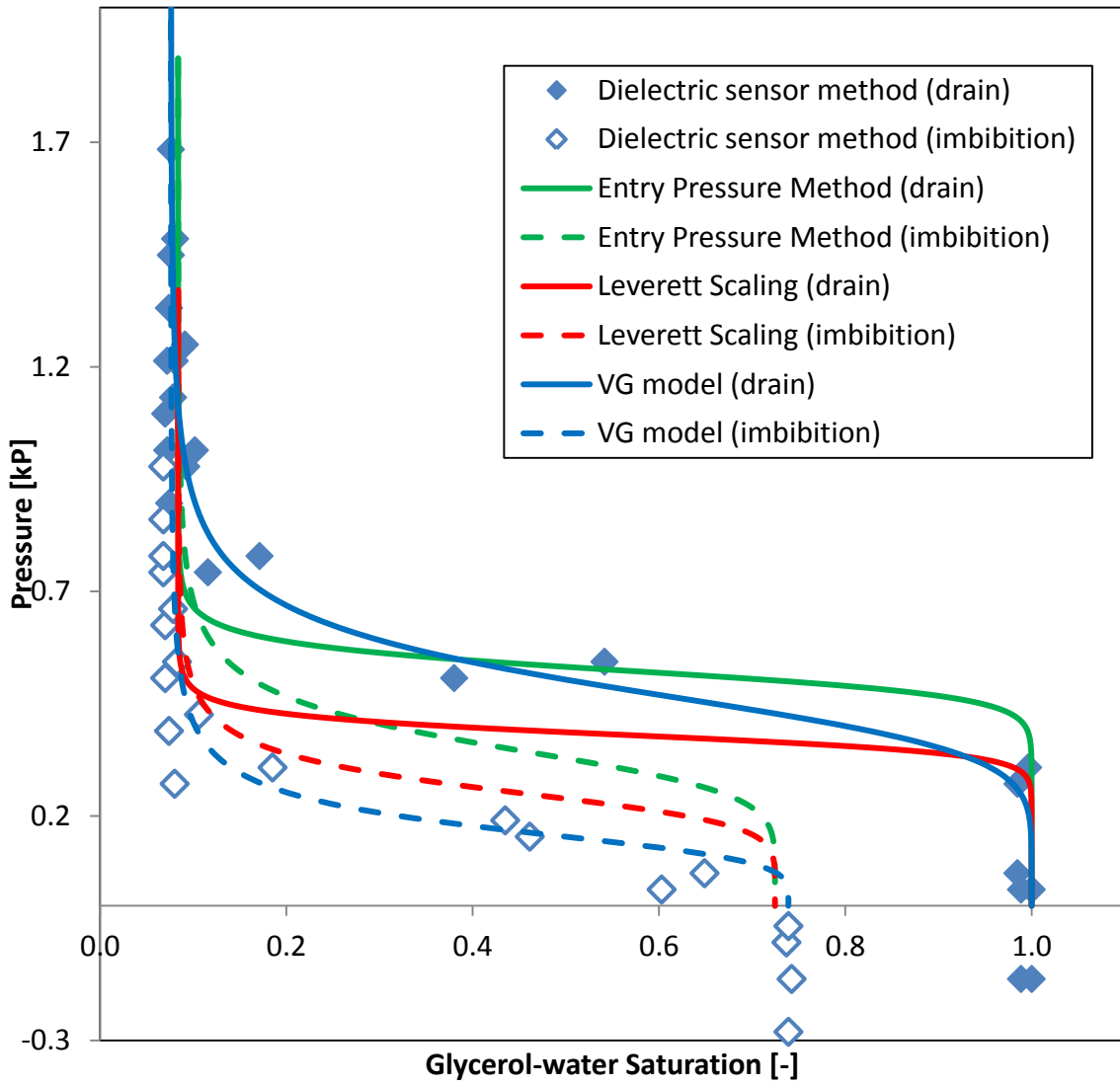


Figure A.3 Accusand #30/40

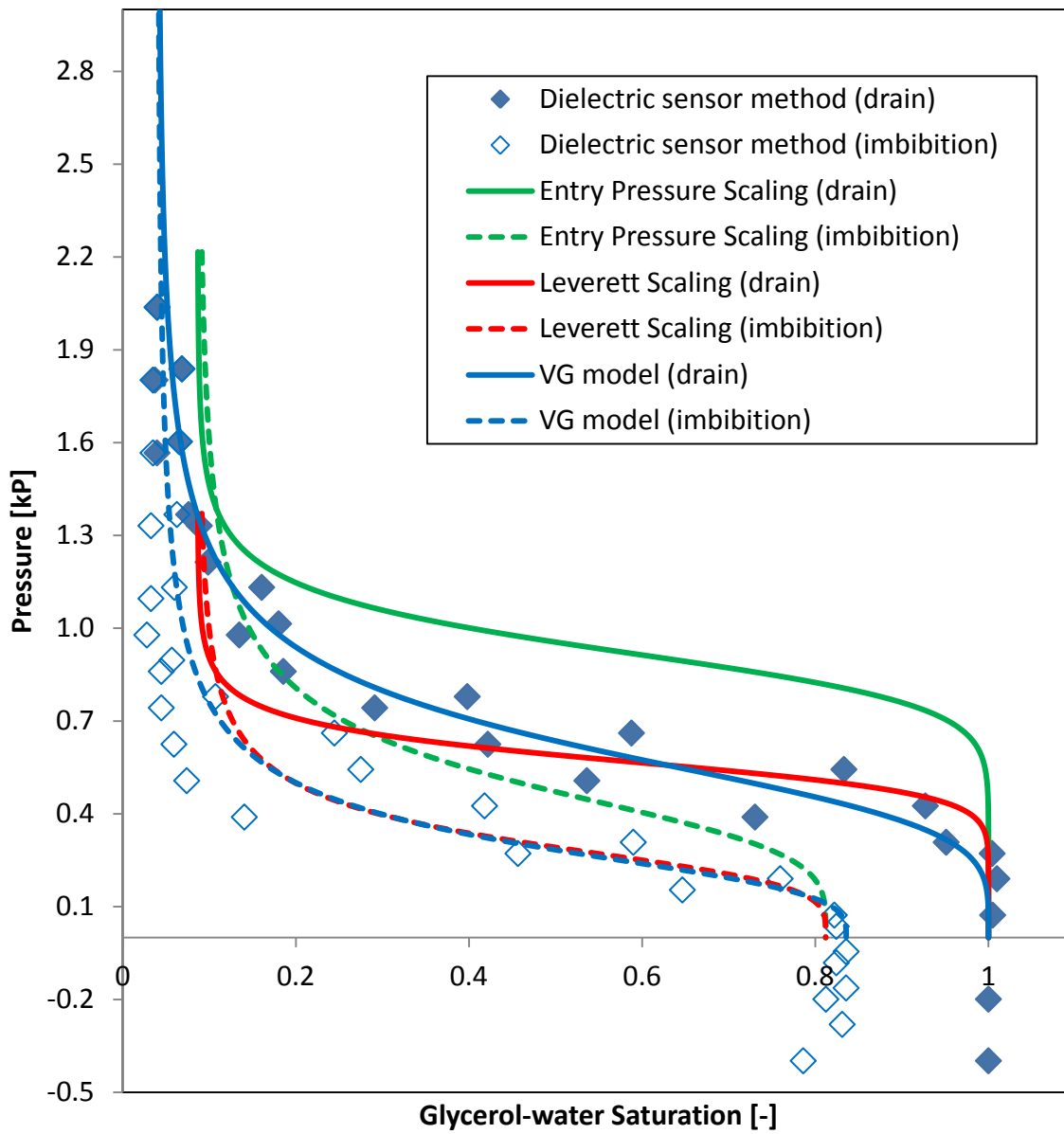


Figure A.4 Accusand #40/50

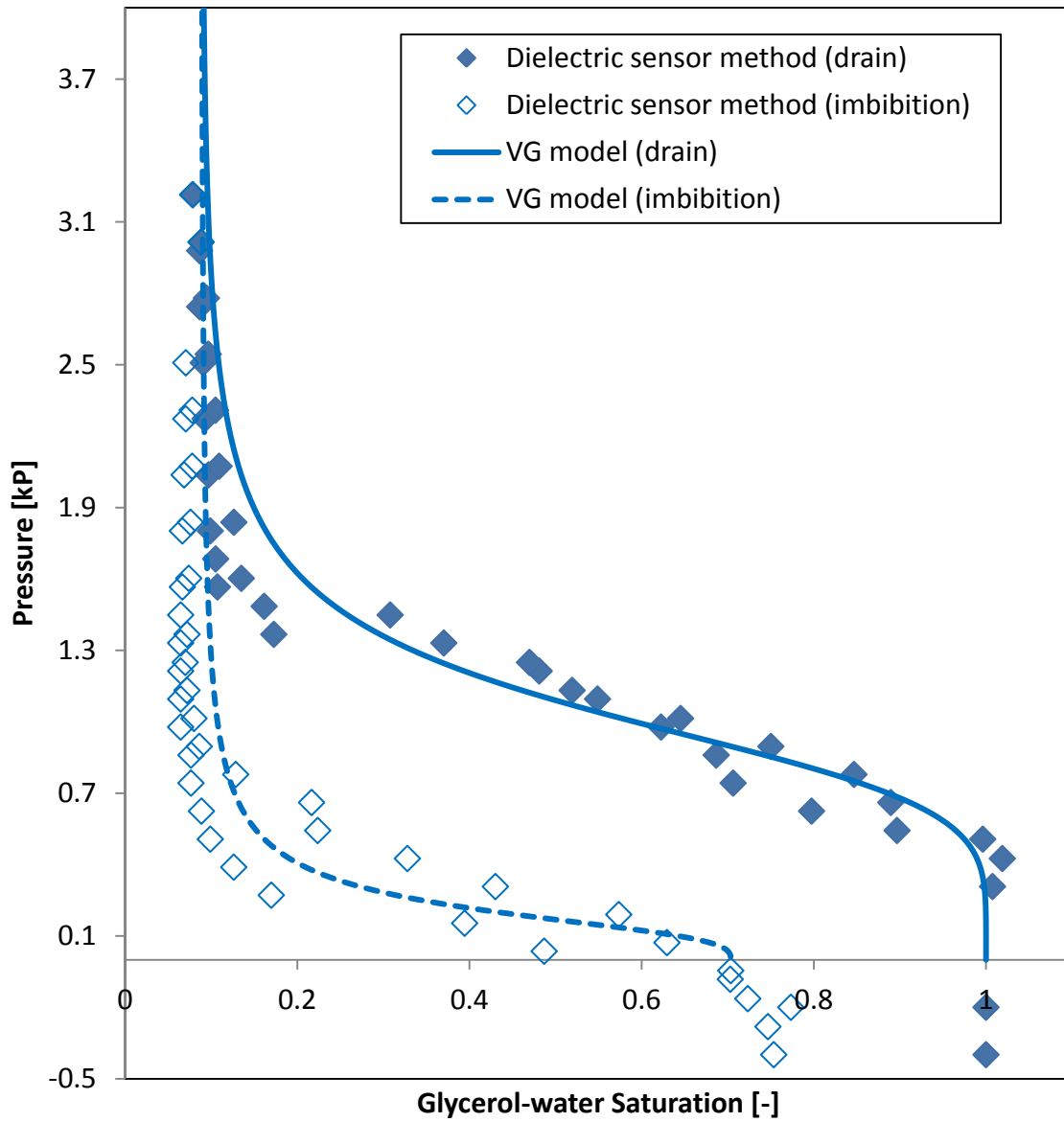


Figure A.5 Accusand #50/70

APPENDIX B – THE RESULTS OF RELATIVE PERMEABILITY TEST

Figure B.1 and B.2 shows the relative permeability curve for Accusand #40/50 and #50/70, respectively. For the wetting phase relative permeability, both sands represent the same trend as the Accusand #30/40. While the non-wetting phase relative permeability, they show slightly different trends. This is because often the few ml of Glycerol-water mixture comes out from the tube which connected at the bottom of the tube due to the displacement with Soltrol 220; therefore, the experiment cannot measure the accurate saturation measurement inside of the column.

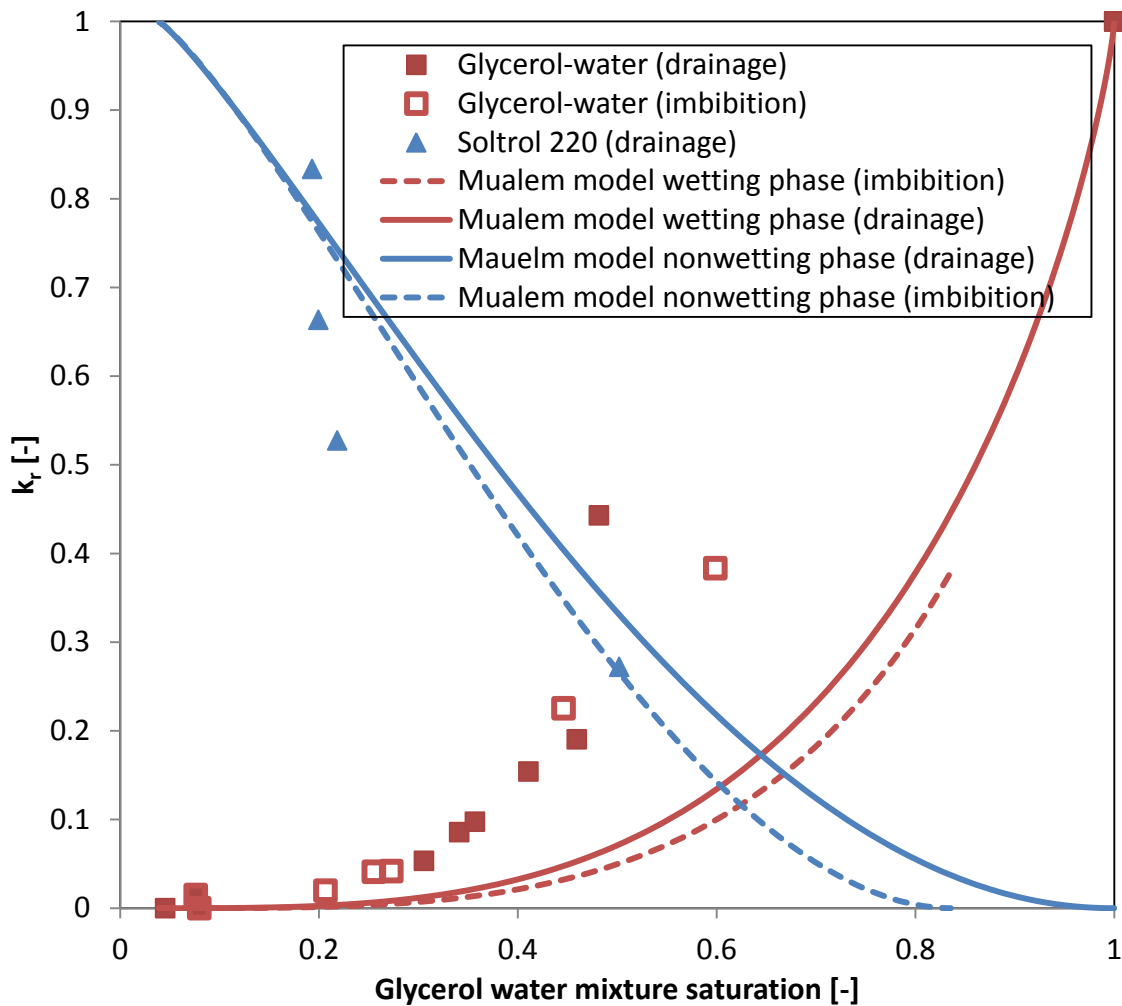


Figure B.1 Relative permeability of Accusand #40/50

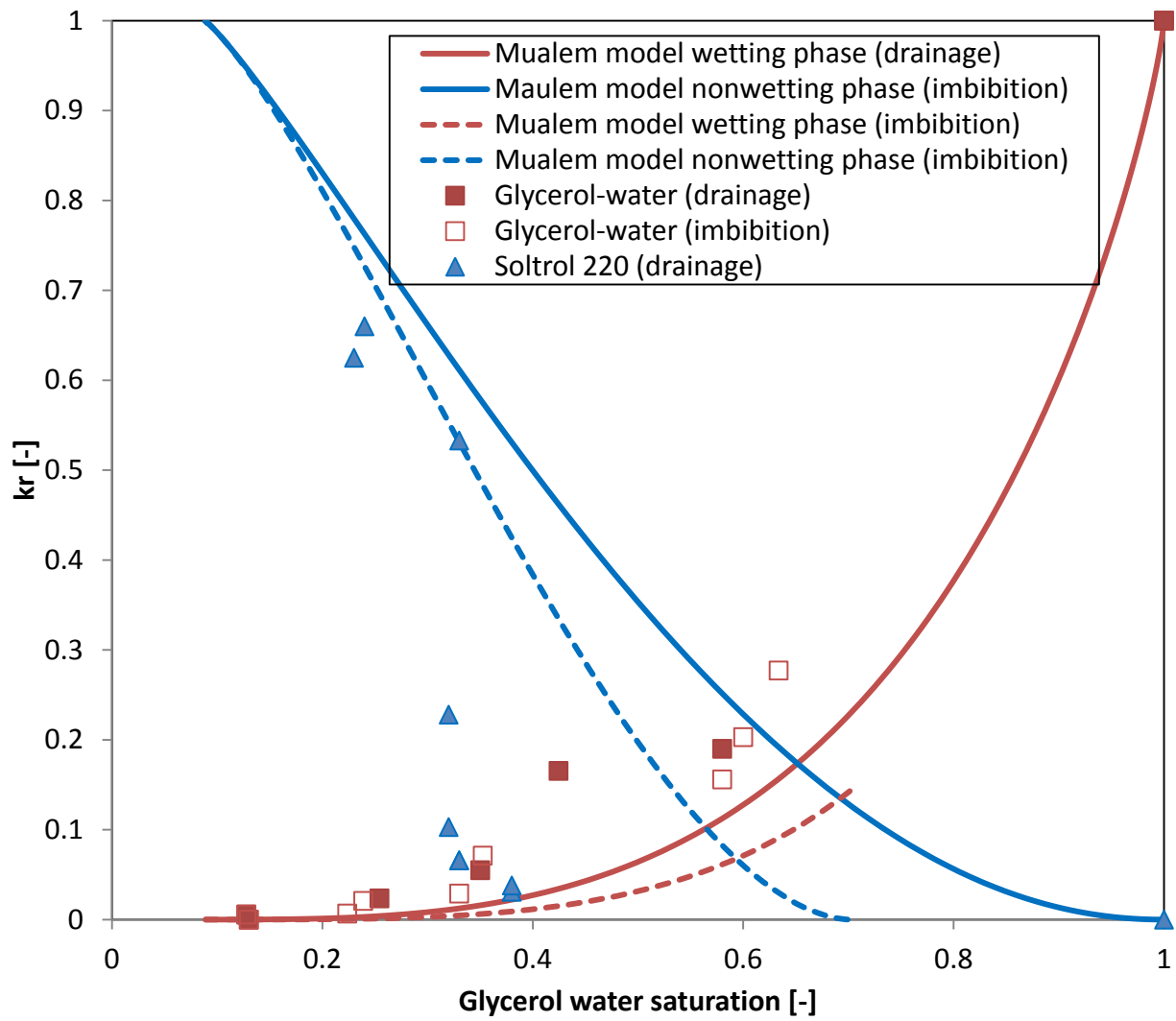


Figure B.2 Relative permeability of Accusand #50/70

APPENDIX C – THE COMPARISON OF THE CONTOUR MAPS

Figures show the evolution of Soltrol 220 with time for the case of Simulation 1, Simulation 2, and the tank experiments. Tecplot was used to visualize the TOUGH2 results.

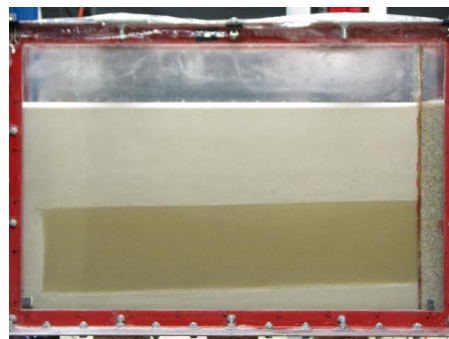
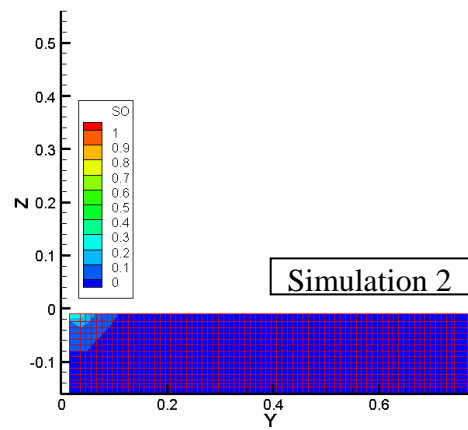
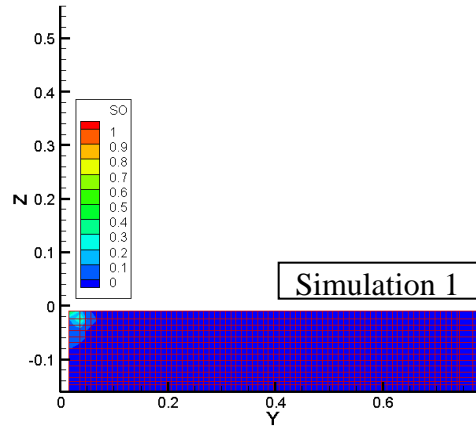


Figure C.1 0.2 hour from injection

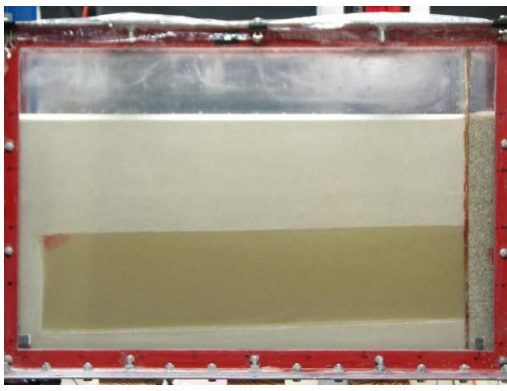
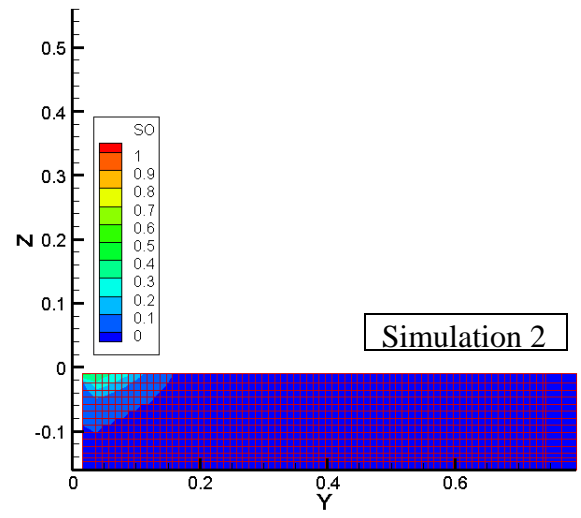
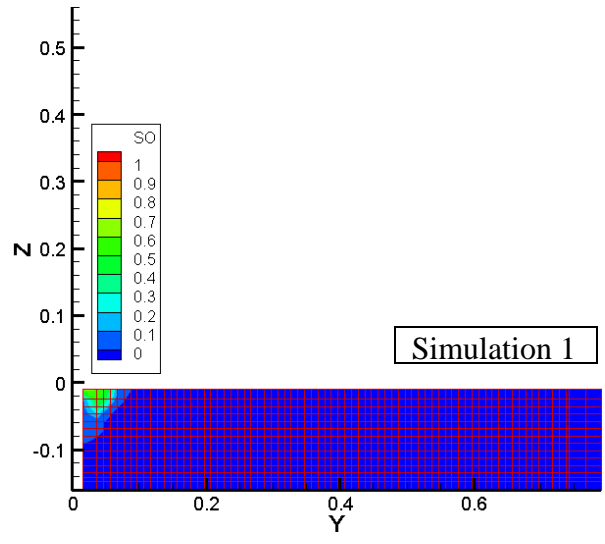


Figure C.2 0.45 hour from injection

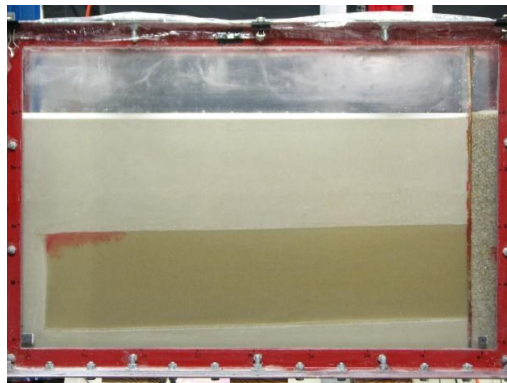
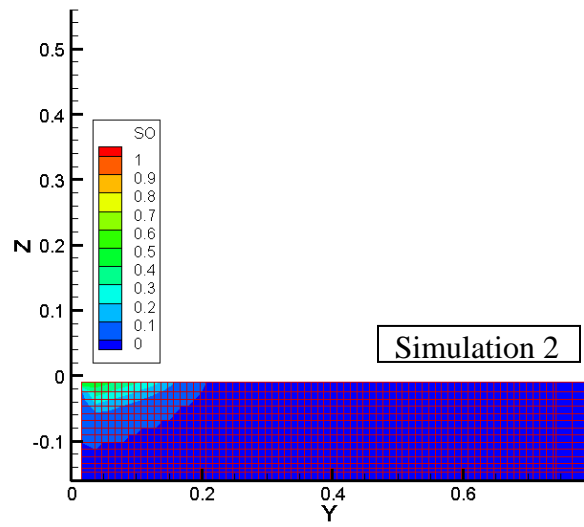
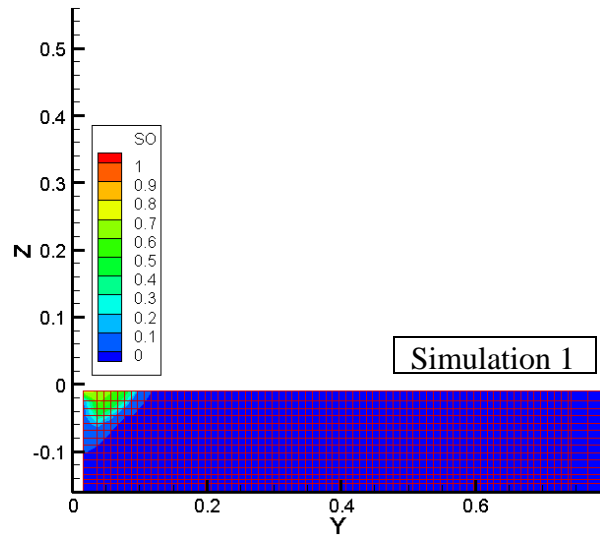


Figure C.3 0.77 hour from injection

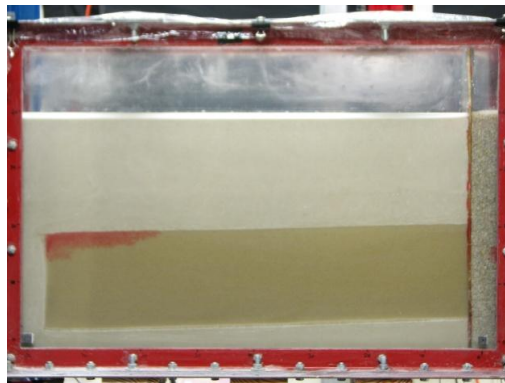
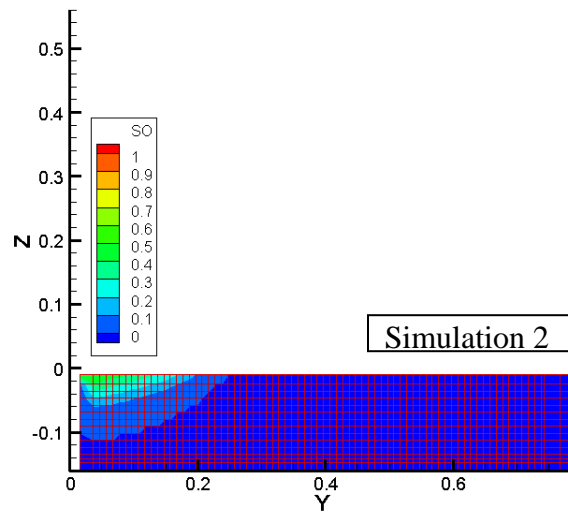
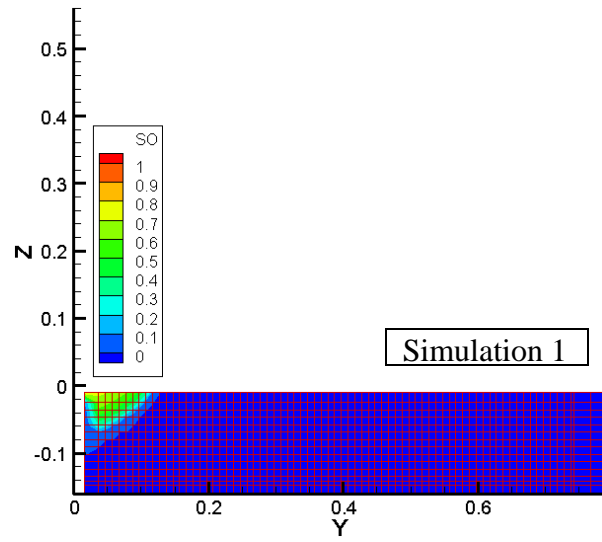


Figure C.4 1.03 hour from injection

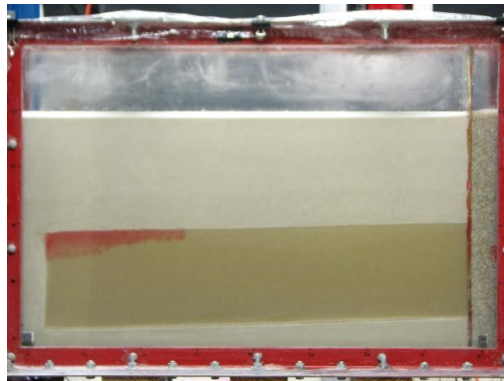
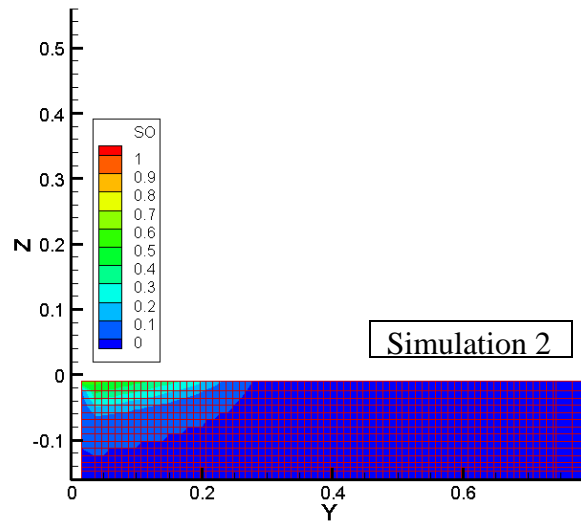
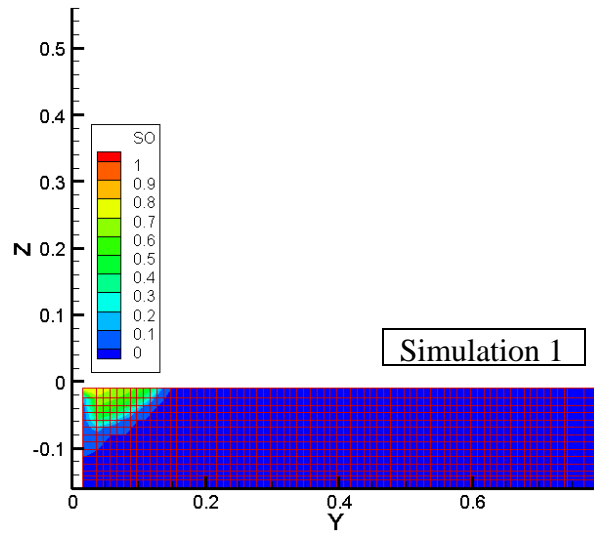


Figure C.5 1.30 hour from injection

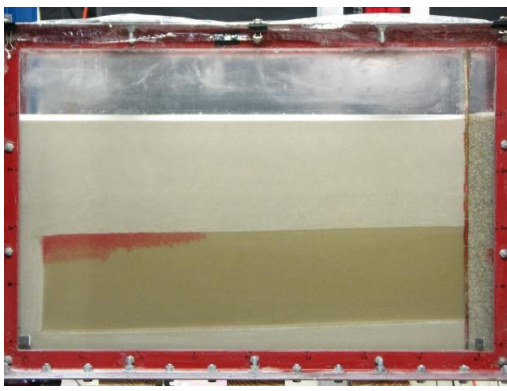
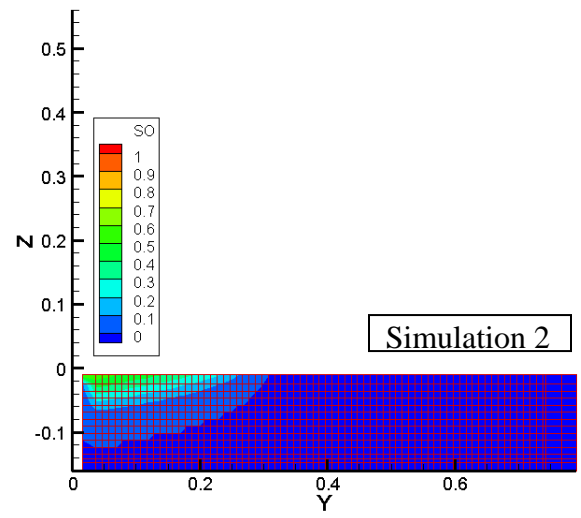
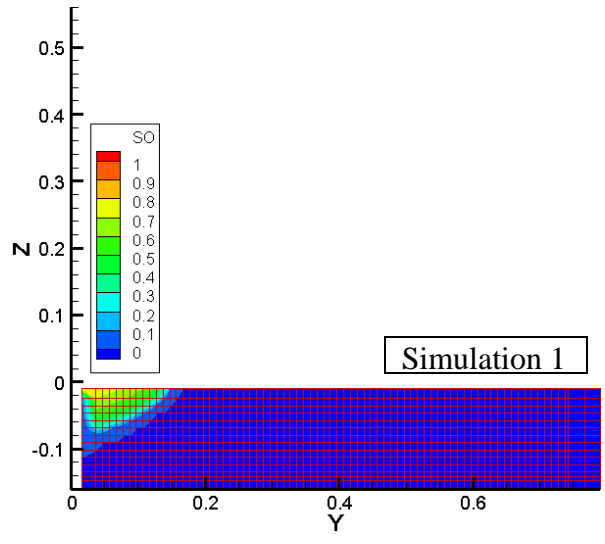


Figure C.6 1.55 hour from injection

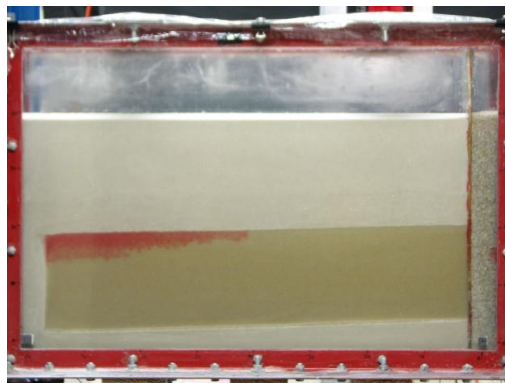
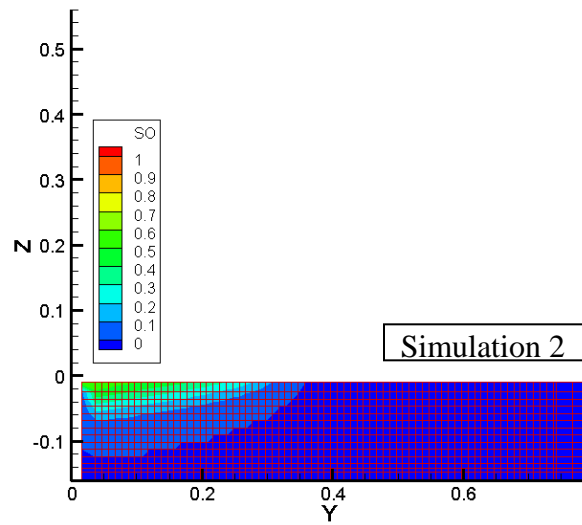
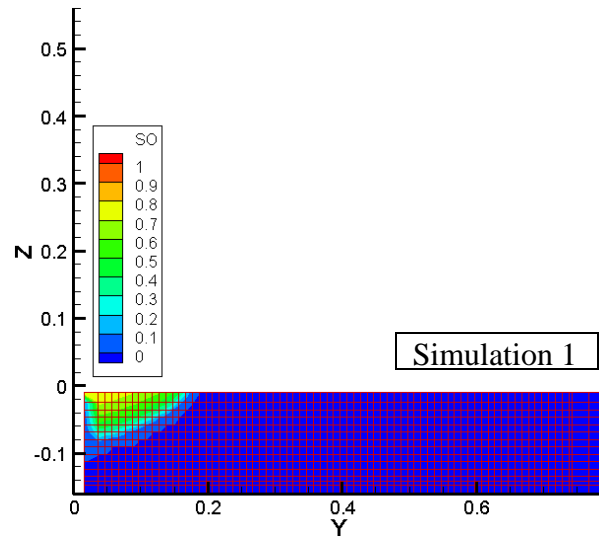


Figure C.7 1.95 hour from injection

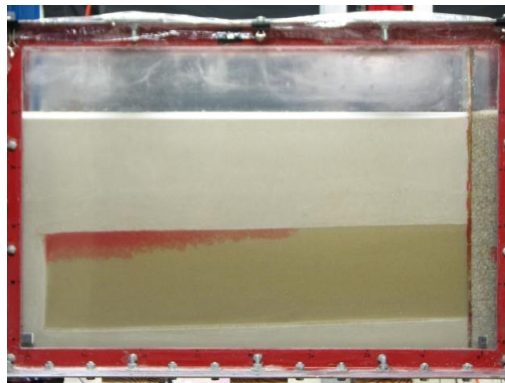
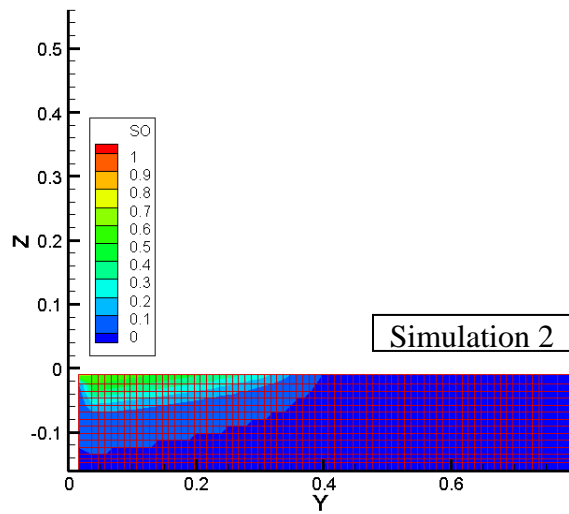
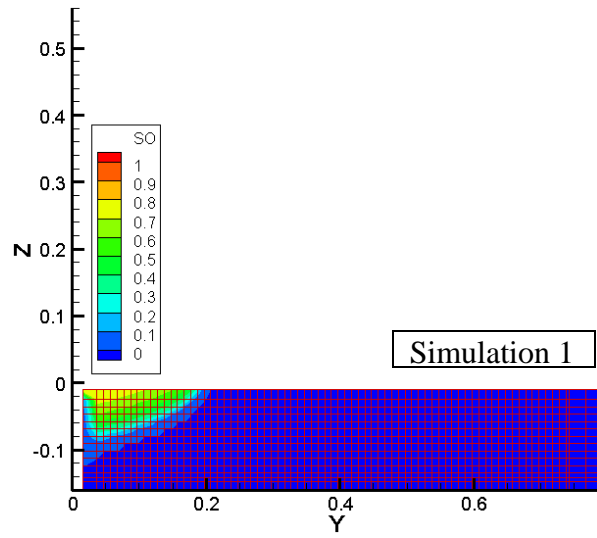


Figure C.8 2.33 hour from injection

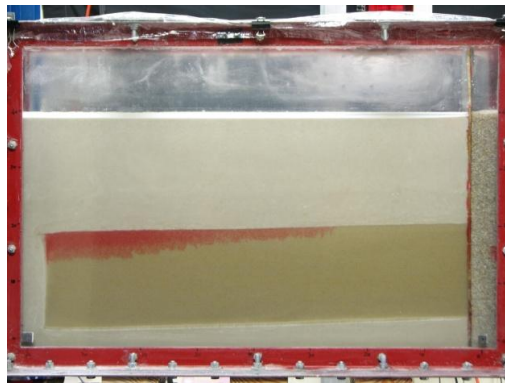
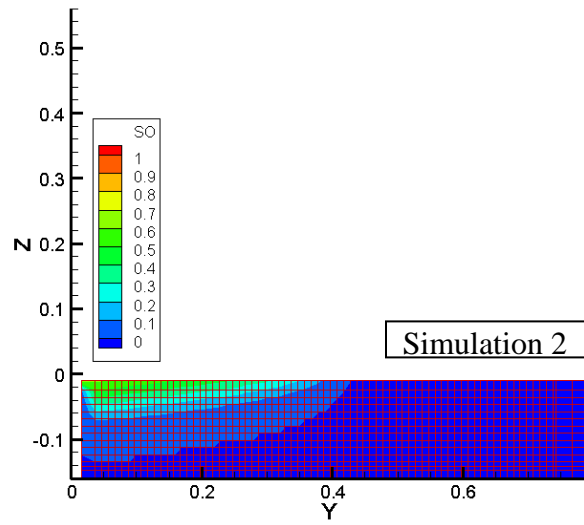
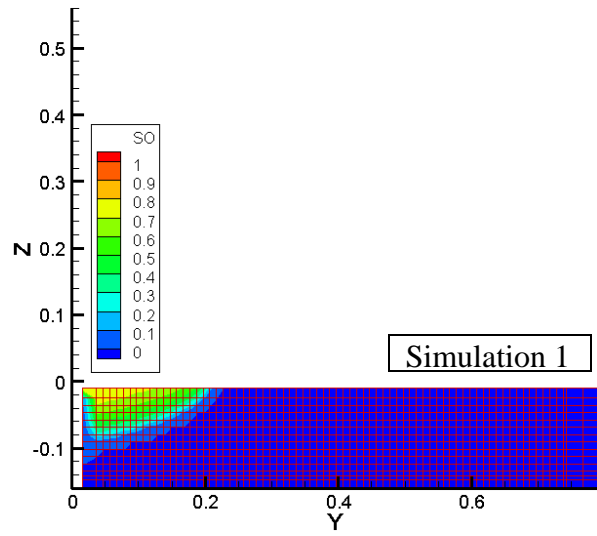


Figure C.9 2.66 hour from injection

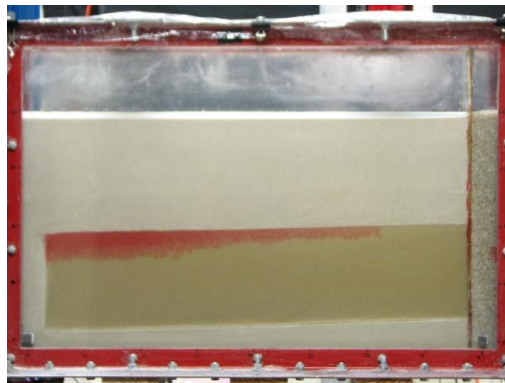
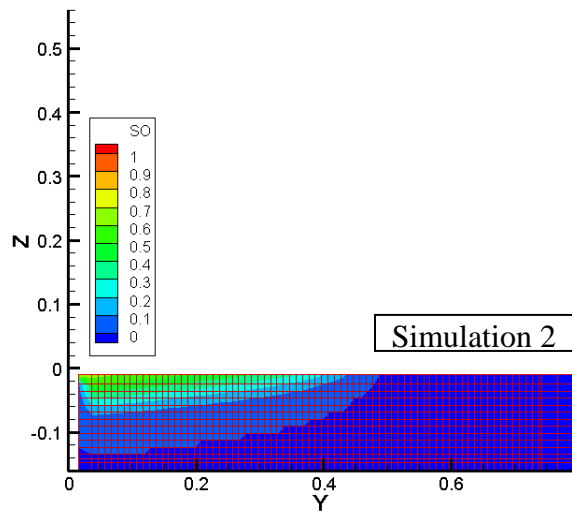
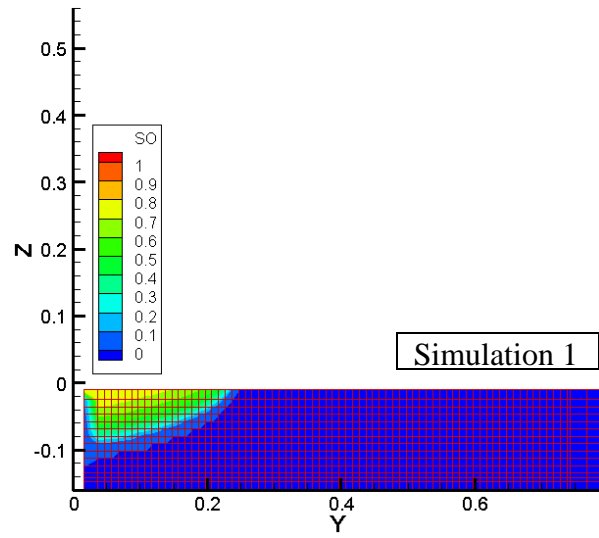


Figure C.10 3.18 hour from injection

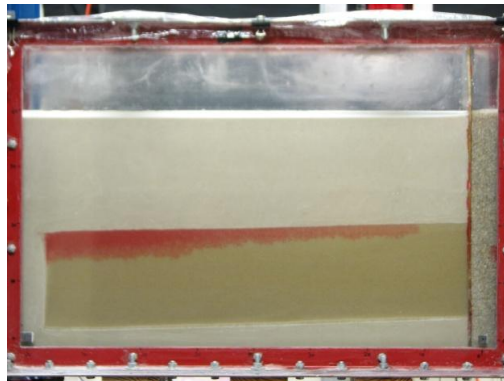
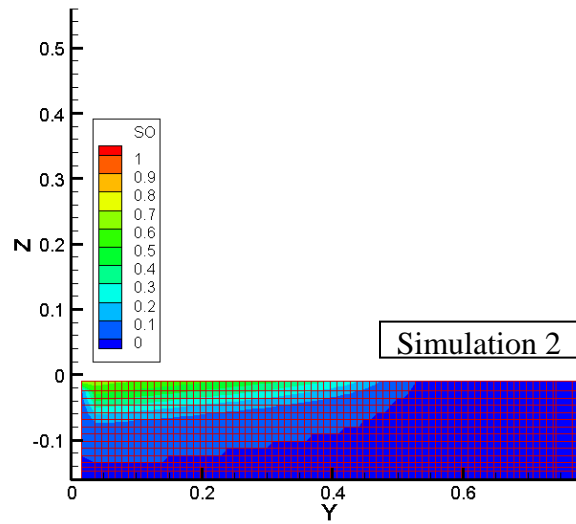
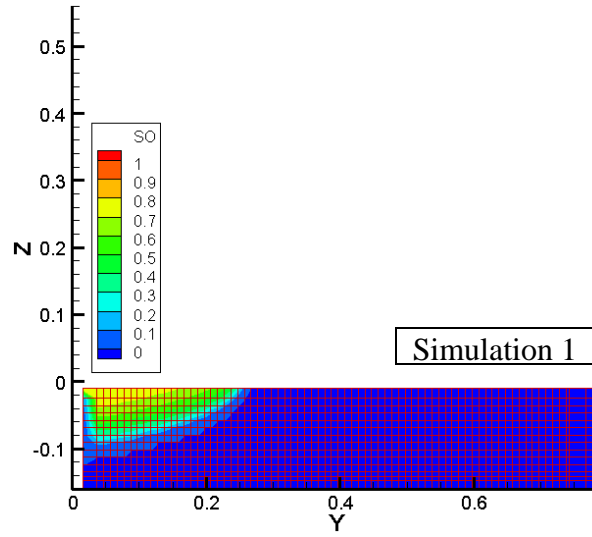


Figure C.11 3.56 hour from injection

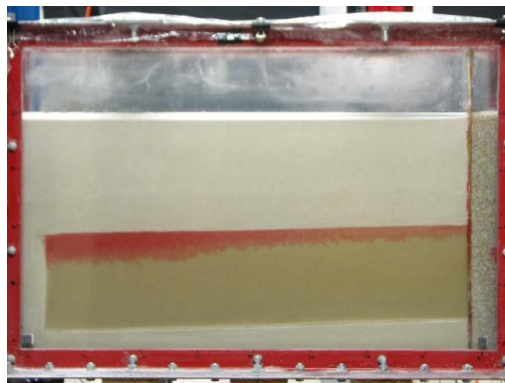
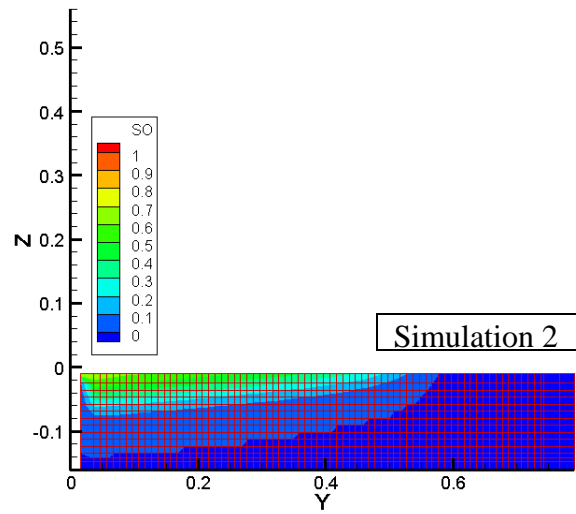
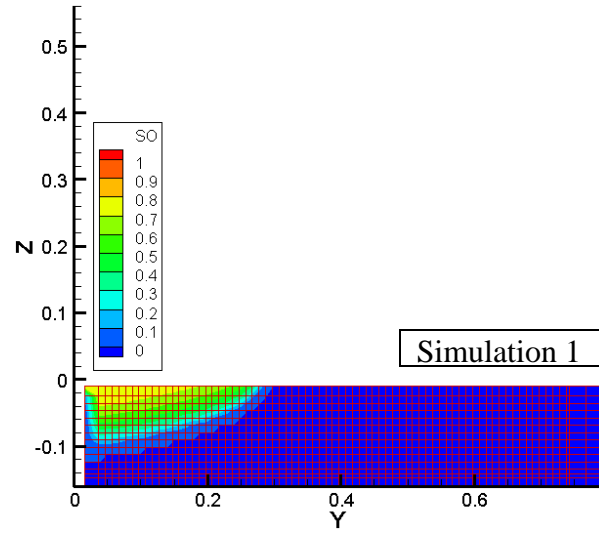


Figure C.12 4.13 hour from injection